UNIVERSITY OF CALIFORNIA, SAN DIEGO

Mechanisms Of Motor Activity Regulation In Axonal Transport

A Dissertation submitted in partial satisfaction of the

Requirements for the Degree of Doctor of Philosophy

in

Neurosciences

by

Gerald Feliz Reis

Committee in charge:

Professor Lawrence Goldstein, Chair
Professor Gaudenz Danuser
Professor Joe Gleeson
Professor Edward Koo
Professor Eliezer Masliah
Professor David Williams

2008

The Dissertation of Gerald Feliz Reis is approved, and it is acceptable in quality and form for publication on microfilm:

Chair

University of California, San Diego

2008

DEDICATION

In recognition of all those who have helped me to reach this day:

- My parents for teaching me discipline, inspiring me to seek excellence, and encouraging me to pursue my dreams
- Ethne McGehee who believed in me and gave me the initial push towards success here in the US
- Jewel Riddle who helped me during times of financial hardship in college
- Dr. Karen Parfitt, my first laboratory mentor, who instilled within me a passion for experimental science
- Dr. David Becker, Dr. Bruce Telzer, and Dr. Elaine Freund, some of my science professors at Pomona College for their excellent teaching and support
- Dr. Erin Schuman for giving me the chance to assist her in many interesting projects and contribute significantly to the experimental work in her lab
- Dr. Larry Goldstein for investing his time and resources into my scientific training. I am forever grateful for his patience and teaching during graduate school.
- My wife for her unconditional love and support
- My science and non-science friends who helped me learn how to do science and stay the course

EPIGRAPH

"Think high; feel deep"
-Elie Wiesel, Nobel Laureate and Holocaust Survivor

"Success is not the goal; it is the result"
-Kareem Abdul-Jabbar

TABLE OF CONTENTS

LIST OF ABBREVIATIONS

APP – amyloid precursor protein

APPYFP – amyloid precursor protein fused to yellow fluorescent protein

RL – run length

SV – segmental velocity

PF– pause frequency

PD – pause duration

A – anterograde axonal transport

R – retrograde axonal transport

KHC – kinesin heavy chain

KLC – kinesin light chain

DHC – dynein heavy chain

DIC – dynein intermediate chain

DLC – dynein light chain

LIST OF FIGURES

LIST OF TABLES

ACKNOWLEDGEMENTS

I would like to thank Dr. Larry Goldstein for his support and mentoring during graduate school. This thesis work would not have been possible without him. In addition, I would like to thank Dr. Gaudenz Danuser for a wonderful collaboration that led to development of the particle tracking software designed during the course of this thesis project. Furthermore, I would like to thank Dr. Ge Yang, postdoctoral fellow in the Danuser lab, for devoting copious amounts of time to the programming and designing of this software.

My thesis committee has added many helpful comments to this work. I am thankful for the time they invested in this exercise.

Lukasz Szpankowski provided much support with data analysis for which I am very grateful. In addition, Dr. Ge Yang also helped analyze data, and Dr. Sameer Shah helped with preliminary data analysis and experimental design.

I also would like to acknowledge my colleagues in the Goldstein lab who provided mentorship and support during my stay in the lab. I thank specially Dr. Kristina Schimmelpfeng Henthorn, Dr. Tomas Falzone, Dr. Angels Almenar, Dr. Carole Weaver, Dr. Jason Duncan, Dr. Shermali Gunawardena, Dr. Kristi Bache, and Cheryl Herrera.

In addition to funding provided by Dr. Larry Goldstein, my work was supported by the University of California San Diego Medical Scientist Training Program, Neurosciences Graduate Program, Merck Pharmaceuticals (which sponsored one year of graduate training), and the Ruth L. Kirschstein National Research Service Award (Fellowship #5F31AG024672).

Chapter 2 will be submitted for publication: Reis GR, Yang G, Szpankowski L, Danuser G, Goldstein LSB. "Mechanisms of motor activity regulation in axonal transport." The dissertation author was the primary author and investigator of this paper.

Chapter 3 will also be submitted for publication: Reis GR and Goldstein LSB. "Kinesin-1 overexpression and cytoplasmic dynein reduction improve transport in an APP overexpression background." The dissertation author was the primary author and investigator of this paper.

VITA

EDUCATION

University of California San Diego School of Medicine, La Jolla, CA
MD expected, estimated 2010

University of California San Diego Graduate Neurosciences Program,
La Jolla, CA
PhD in Neurosciences, 2008

Pomona College, Claremont, CA
BA in Molecular Biology, 1997

RESEARCH EXPERIENCE

June 2003 - present – thesis work in the laboratory of Dr. Larry Goldstein investigating mechanisms of motor protein activity regulation in axonal transport and strategies for rescuing transport defects induced by APP overexpression.

Summer 2002 – research rotation in the laboratory of Dr. Mark Tuszynski where I studied how the degenerating or injured adult central nervous system is responsive to signals that can promote neural regeneration. I successfully cloned the receptor *trkA* and began making a viral expression system to target *trkA* expression to regions of the central nervous system.

Winter 2002 – research rotation in the laboratory of Dr. Lawrence Goldstein where I studied the molecular mechanisms of axonal organelle transport and the role of transport dysfunction in neurodegenerative diseases. I used Western blot analysis to study the anterograde and retrograde transport of several proteins in axons of the sciatic nerve.

Summer 2001 – research rotation in the laboratory of Dr. Thomas Kipps where I studied the physiology of human B cells with the goal of applying this information to the treatment of chronic lymphocytic leukemia (CLL). During my summer rotation in his laboratory, I had the opportunity to work with gene cloning, PCR, and peptide loading assays in tissue culture. In addition, we designed peptides that induced major histocompatibility complex I (MHCI) receptor expression onto the surface of cells in culture (T2 cell line).

Summer 1997 - Summer 2001 – laboratory technician and research assistant in the laboratory of Dr. Erin Schuman, Caltech, CA, where I studied the molecular mechanisms involved in hippocampal synaptic transmission and plasticity. At Dr. Schuman's laboratory I had the opportunity to learn new techniques (e.g. confocal and 2-photon microscopy, immunohistochemistry, and adenoviral hippocampal slice

injection), perfect techniques that I had learned in college (e.g., electrophoresis, western blotting, and electrophysiology), and interact with graduate students and post-doctoral fellows. As a highlight to my research in the Schuman lab, I contributed to several of the lab's publications (please refer to list of publications).

Fall 1996 - Summer 1997 – Senior thesis experimental project, Pomona College, CA. Continued work in the laboratory of Dr. Karen Parfitt. This work led to a publication (see publications list) and a travel award for outstanding undergraduate research from the Faculty for Undergraduate Neuroscience (FUN). This award allowed me to attend the 1997 Society for Neuroscience (SFN) meeting where I presented my work.

Summer 1996 – Summer Undergraduate Research Program (SURP). Worked in the laboratory of Dr. Karen Parfitt studying synaptic plasticity and changes that accompany normal aging in the mammalian hippocampus.

MEDICAL EXPERIENCE

Fall 1995 - Summer 1996 – volunteer at Pomona Valley hospital, Pomona, CA

Fall 2000 - Summer 2001 – attended weekly neurosurgery case discussions and observed neurosurgeries, Hungtington Hospital, Pasadena, CA

TEACHING EXPERIENCE

Spring 2005 - Spring 2008 – tutor for basic neurology course at UCSD medical school. Teaching was done only during the Spring quarter. Course director: Dr. Mark Kritchevsky.

MEMBERSHIPS

1997-1998 – Society For Neuroscience (SFN)

AWARDS AND HONORS

2003-2008	UCSD Neurosciences Graduate GPA 4.0
2006	Ruth L. Kirschstein National Research Service Award
1997	Faculty for Undergraduate Neuroscience (FUN award)
1995-1997	Achievement of Excellence for Academic Merit
1994	First Generation Student Scholarship
1992	ASCC Tom Normand International Student of the Year
1992	Bailey Memorial Scholarship
1992	Shirley Vanderpool Memorial Scholarship
1991-1993	Exemplary Scholarship (4.0 GPA)

EMPLOYMENT

1997-2001	*Laboratory Technician/Research Assistant*, HHMI, PI: Dr. Erin Schuman
1997	*Laboratory Technician/Research Assistant*, Caltech, PI: Dr. Erin Schuman
1997 (winter)	*Laboratory Technician*, Pomona College, PI: Dr. Karen Parfitt
1996 (summer)	*Student Researcher*, Pomona College, PI: Dr. Karen Parfitt

PUBLICATIONS

Journal Articles

Gerald F. Reis, Michael B. Lee, Alex S. Huang, and Karen D. Parfitt (2005) Adenylate cyclase-mediated forms of neuronal plasticity in hippocampal area CA1 are reduced with aging. *J. Neurophysiol.* 93(6): 3381-9

Shao Jun Tang, Gerald Reis, Hyejin Kang, and Erin M. Schuman (2002) A rapamycin-sensitive signaling pathway contributes to long-term synaptic plasticity in the hippocampus. *PNAS* **99** (1): 467-72

Massimo D'Apuzzo[*], Georgia Mandolesi[*], Gerald Reis, and Erin M. Schuman (2001) Abundant GFP expression and long-term potentiation in hippocampal acute slices by *in vivo* injection of sindbis virus. *J Neurophysiol.* **86** (2): 1037-42

Long Ma[*], Gerald Reis[*], Luis F. Parada, and Erin M. Schuman (1999) Neuronal NT-3 is not required for synaptic transmission or long-term potentiation in area CA1 of the adult mouse hippocampus. *Learning and Memory* **6**: 267-275

Abstracts and Poster Presentations

Gerald Reis[*†], Long Ma[*], Luis F. Parada, and Erin M. Schuman. 1999. Normal hippocampal synaptic transmission and long-term potentiation in mice with conditional deletions of the NT-3 gene. Soc. Neurosci. Abs., Vol. 25: 404.7

Gerald F. Reis[†], Michael B. Lee, Karen D. Parfitt. 1997. Adenylate cyclase-mediated forms of synaptic potentiation in hippocampal area CA1 are attenuated in aged Fischer 344 rats. Soc. Neurosci. Abs., Vol. 23

Gerald F. Reis[†] and Karen D. Parfitt. 1996. Isoproterenol enhances synaptic transmission in hippocampal area CA1 of young but not aged Fischer 344 rats.

Ninth Annual Pomona Summer Science Poster Conference, Pomona College, CA

Michael B. Lee, Gerald F. Reis, and Karen D. Parfitt†. 1996. Isoproterenol and forskolin enhance evoked population spikes in hippocampal area CA1 of young but not aged Fischer 344 rats. International Conference on Catecholamines, Asilomar, CA

* These authors contributed equally.
† Poster presenter

ABSTRACT OF THE DISSERTATION

Mechanisms Of Motor Activity Regulation In Axonal Transport

by

Gerald Feliz Reis

Doctor of Philosophy in Neurosciences

University of California, San Diego, 2008

Professor Lawrence Goldstein, Chair

This work explores two unresolved issues in neurobiology. First, we studied the fundamental question of how microtubule motors regulate their activity to achieve bi-directional transport in axons. Because good *in vivo* model systems and quantitative approaches were lacking, we developed an *in vivo* neuronal system and software to study the behavior of fluorescent vesicles. Our approach consisted of quantitative analysis of YFP-tagged amyloid precursor protein (APPYFP) axonal transport in segmental nerves of *Drosophila melanogaster* using heterozygous animals and a standardized imaging system. This allowed us to assess the contribution of individual motor subunits and accessory proteins to coordinated axonal transport. Our approach yielded a novel model for how motor proteins work together to achieve bi-directional transport.

Second, we studied genetic manipulations hypothesized to rescue axonal transport defects induced by overexpression of APP. This research is potentially relevant to Alzheimer's disease (AD) as well as its treatment. We found that APP overexpression disrupts axonal transport, and these deficits can be partially rescued by two separate genetic manipulations. These observations suggest that certain genetic approaches may help reverse axonal transport defects induced by APP overexpression, and this may have implications for the development of novel therapeutic approaches to treat neurodegeneration.

Chapter I -

MOLECULAR MOTORS

AND THEIR RELATIONSHIP TO AMYLOID PRECURSOR PROTEIN

Axonal transport of vesicles and organelles relies on kinesin and dynein motors

Neuronal survival and function requires the active transport of vesicles and organelles. Previous research has identified two superfamilies of proteins—the kinesins and dyneins—as the molecular motors that generate long distance transport in cells by utilizing ATP-dependent movements along microtubules (Goldstein and Philp 1999; Goldstein and Yang 2000; Goldstein 2003). Previous work by the Goldstein lab as well as many other groups have provided us with valuable knowledge on how kinesin and dynein selectively attach to their cargoes, how their motor activity is regulated, and what causes selective targeting of cargoes to different locations in the cell. Emerging from this work were hints that kinesin and dynein motor proteins may play a critical role in neurodegenerative pathways, which is not surprising given their fundamental role in neuronal biology (Goldstein 2003; Cavalli, Kujala et al. 2005; Stokin, Lillo et al. 2005).

Kinesin-1 is a member of the kinesin superfamily of motor proteins. Its function in axonal transport is to power movement of vesicles and organelles in the anterograde direction—transport away from the cell body of neurons toward synaptic terminals. This protein is a heterotetramer made up of two kinesin heavy chains (KHC) and two kinesin light chains (KLC) (Rahman, Friedman et al. 1998). The heavy chains are thought to contain the microtubule-binding and motor domains of kinesin-1 while both the light and heavy chains are important for cargo binding. However, the light chain is primarily important in cargo recognition, specificity, and binding. KLC has a region of six relatively well conserved tetratricopeptide (TRP) repeats that can associate either directly with cargo receptor proteins or indirectly via

scaffolding proteins such as the jun kinase interacting proteins (JIP) (Goldstein and Philp 1999; Bowman, Kamal et al. 2000; Goldstein and Yang 2000). The importance of these proteins is apparent from studies showing that loss of either KHC or KLC lead to axonal transport defects characterized by swellings with massive accumulation of vesicles and organelles in Drosophila segmental nerve (Hurd and Saxton 1996; Gindhart, Desai et al. 1998).

Cytoplasmic dynein is a member of the dynein superfamily and drives axonal transport in the retrograde direction—transport from synaptic terminals to the cell body. This motor is a large complex made up of twelve proteins, which include 2 heavy chains (DHC), 4 intermediate chains (DIC), and 6 light chains (DLC) (Pfister, Shah et al. 2006). Like kinesin, the heavy chain in dynein is thought to have the microtubule-binding and motor domains, but in dynein the cargo binding and regulatory domains are localized to the intermediate and light chains. Another important difference between cytoplasmic dynein and kinesin-1 is that cytoplasmic dynein's function requires dynactin, another multi-protein complex made up of 11 subunits (King and Schroer 2000; Schroer 2004). The function of dynactin is still poorly understood, but it has been implicated in mediating dynein binding to vesicles (Chevalier-Larsen and Holzbaur 2006), enhancement of dynein's processivity (King and Schroer 2000), and more recently coordination between kinesin-1 and cytoplasmic dynein (Gross, Welte et al. 2002).

Dissecting molecular mechanisms of axonal transport by APPYFP movement analysis

Though much knowledge on molecular motors has been gained over the years, it is still largely unknown how kinesin-1 and cytoplasmic dynein regulate their activities to allow for net movement. In addition, most of the available data pertinent to motor protein interactions come from *in vitro* reconstitution approaches, which may differ significantly from *in vivo* biological systems. Thus, an *in vivo* neuronal system is clearly lacking in which to test existing as well as novel models. To achieve this goal, we developed an *in vivo*-imaging assay to look at the movement of yellow fluorescent protein-tagged amyloid precursor protein (APPYFP) vesicles in Drosophila larval axons. APP vesicles comprise an interesting type of vesicle because they have both scientific and medical relevance. From a scientific standpoint, these vesicles are transported over long distances by kinesin-1, exhibit both anterograde and retrograde movements, and can be tagged with fluorescent markers for visualization using standard molecular biology and microscopic techniques. Of course, the study of APP vesicles is also of great medical relevance since the proteolytic processing of APP appears to play a key role in the development of Alzheimer's disease (AD).

Relationship between APP and kinesin-1

Two findings by the Goldstein laboratory linked APP to the motor machinery. First, it was observed that APP and presenilin travel in axons with kinesin-1 (Kamal, Stokin et al. 2000; Kamal, Almenar-Queralt et al. 2001). Second, biochemical studies revealed that APP may interact with KLC (Kamal, Stokin et al. 2000). The nature of this association led to the hypothesis that APP acts as a receptor for kinesin-1, thereby

recruiting this motor to the axonal transport of APP-containing vesicles. If true, this model makes a series of *in vivo* predictions where normal axonal transport would be disrupted by either loss or overexpression of APP function. Indeed, these predictions were confirmed by experiments in both *Drosophila* and mouse models. Loss of the *Drosophila* APP homolog APPL or overexpression of APPL constructs containing kinesin-1 interacting domains led to axonal transport defects (Torroja, Chu et al. 1999; Gunawardena and Goldstein 2001). As in *Drosophila*, mutations leading to loss of APP function led to axonal transport defects in mice (Kamal, Almenar-Queralt et al. 2001)

Another prediction made by the APP-KLC interaction is that reduction in the dosage of kinesin-1 would potentiate the effects of APP overexpression. Again, this prediction held true in both Drosophila (Gunawardena and Goldstein 2001) and mouse experiments (Stokin, Lillo et al. 2005). Thus, experimental evidence supports the hypothesis that APP interacts with kinesin-1 and titrates it away from the soluble pool required for normal axonal transport. Of course, not only may APP titration of kinesin-1 adversely affect the health of a neuron by interfering with the axonal transport of essential vesicle populations but it may also contribute to the cell's demise through the formation of axonal swellings and blockages. Taken together, these observations illustrate the relationship between axonal transport, APP, and pathways that may lead to neurodegeneration.

The above findings raise a second intriguing question. If manipulations to kinesin-1 can worsen the phenotypes induced by APP overexpression, can these phenotypes be rescued? One study suggested that this could be accomplished. In

Drosophila, reductions in dynein gene dosage decreased the number of swellings observed in APP overexpression models (Gunawardena and Goldstein 2001). However, the situation may be more complicated since *in vivo* analysis of APPYFP movement in a dynein light chain reduction background showed the presence of axonal swellings (unpublished observations made by graduate student Richard Brush). Resolving this controversy is important because these experiments may hold great potential for our search of therapies to treat or slow down the progression of neurodegenerative diseases such as AD.

Questions addressed by thesis work

The present work focuses on two primary issues. In chapter II, I investigate how opposing motor proteins regulate their activity to achieve bi-directional axonal transport. In chapter III, I explore strategies for rescuing axonal transport defects induced by APP overexpression.

References

Bowman, A. B., A. Kamal, et al. (2000). "Kinesin-dependent axonal transport is mediated by the sunday driver (SYD) protein." Cell **103**(4): 583-94.

Cavalli, V., P. Kujala, et al. (2005). "Sunday Driver links axonal transport to damage signaling." J Cell Biol **168**(5): 775-87.

Chevalier-Larsen, E. and E. L. Holzbaur (2006). "Axonal transport and neurodegenerative disease." Biochim Biophys Acta **1762**(11-12): 1094-108.

Gindhart, J. G., Jr., C. J. Desai, et al. (1998). "Kinesin light chains are essential for axonal transport in Drosophila." J Cell Biol **141**(2): 443-54.

Goldstein, L. S. (2003). "Do disorders of movement cause movement disorders and dementia?" Neuron **40**(2): 415-25.

Goldstein, L. S. and A. V. Philp (1999). "The road less traveled: emerging principles of kinesin motor utilization." Annu Rev Cell Dev Biol **15**: 141-83.

Goldstein, L. S. and Z. Yang (2000). "Microtubule-based transport systems in neurons: the roles of kinesins and dyneins." Annu Rev Neurosci **23**: 39-71.

Gross, S. P., M. A. Welte, et al. (2002). "Coordination of opposite-polarity microtubule motors." J Cell Biol **156**(4): 715-24.

Gunawardena, S. and L. S. Goldstein (2001). "Disruption of axonal transport and neuronal viability by amyloid precursor protein mutations in Drosophila." Neuron **32**(3): 389-401.

Hurd, D. D. and W. M. Saxton (1996). "Kinesin mutations cause motor neuron disease phenotypes by disrupting fast axonal transport in Drosophila." Genetics **144**(3): 1075-85.

Kamal, A., A. Almenar-Queralt, et al. (2001). "Kinesin-mediated axonal transport of a membrane compartment containing beta-secretase and presenilin-1 requires APP." Nature **414**(6864): 643-8.

Kamal, A., G. B. Stokin, et al. (2000). "Axonal transport of amyloid precursor protein is mediated by direct binding to the kinesin light chain subunit of kinesin-I." Neuron **28**(2): 449-59.

King, S. J. and T. A. Schroer (2000). "Dynactin increases the processivity of the cytoplasmic dynein motor." Nat Cell Biol **2**(1): 20-4.

Pfister, K. K., P. R. Shah, et al. (2006). "Genetic analysis of the cytoplasmic dynein subunit families." PLoS Genet **2**(1): e1.

Rahman, A., D. S. Friedman, et al. (1998). "Two kinesin light chain genes in mice. Identification and characterization of the encoded proteins." J Biol Chem **273**(25): 15395-403.

Schroer, T. A. (2004). "Dynactin." Annu Rev Cell Dev Biol **20**: 759-79.

Stokin, G. B., C. Lillo, et al. (2005). "Axonopathy and transport deficits early in the pathogenesis of Alzheimer's disease." Science **307**(5713): 1282-8.

Torroja, L., H. Chu, et al. (1999). "Neuronal overexpression of APPL, the Drosophila homologue of the amyloid precursor protein (APP), disrupts axonal transport." Curr Biol **9**(9): 489-92.

Chapter II -

MECHANISMS OF MOTOR ACTIVITY REGULATION REVEALED BY QUANTITATIVE ANALYSIS OF APPYFP MOVEMENT

Abstract

Axonal transport is essential for neuronal survival and function. Long-distance transport uses kinesins and dyneins to power movement of vesicles and organelles. Though much is known about these proteins, how they regulate their activity to achieve bi-directional transport remains largely unresolved. We developed an *in vivo* neuronal system to test novel as well as conventional hypotheses in hopes of better understanding this essential cellular process. Our approach consisted of quantitative analysis of YFP-tagged amyloid precursor protein (APPYFP) axonal transport in segmental nerves of *Drosophila melanogaster*. Use of heterozygous animals, a standardized imaging system, and quantitative software allowed us to access the contribution of kinesin-1 and cytoplasmic dynein motor subunits to coordinated transport. In general, we found that kinesin-1 and dynactin reductions led to bi-directional impairment in transport. Surprisingly, we also found evidence suggesting that kinesin-1 may act as a poorly processive motor *in vivo*. Cytoplasmic dynein reductions had mixed effects on movement, with dynein heavy chain (DHC) reductions leading to increases in anterograde movement and dynein intermediate chain (DIC) reductions leading to impairment. From these data we proposed a testable model for how anterograde and retrograde movement may be controlled via a competition mechanism involving kinesin light chain (KLC), DIC, and the $p150^{Glued}$ subunit of dynactin. This work reveals a novel mechanism for axonal transport, which we have termed "inhibitory-competition model."

Introduction

One intriguing problem in the field of axonal transport is how opposite polarity motors regulate their activity to achieve bi-directional movement of vesicles and organelles within axons. Until recently, our understanding of how kinesin, dynein, and dynactin are organized on the surface of vesicles and function together to yield bi-directional transport was limited to the following. For anterograde movement, kinesin has been thought to comprise (1) the sole mediator of anterograde movement within axons (Goldstein and Philp 1999); (2) kinesin-1 is a highly processive motor whose function does not require a co-factor (Block 1995); (3) kinesin-1 activity has no regulatory function on retrograde vesicle movement (Steven Gross unpublished observations, Drosophila meeting, 2007). For dynein, it is thought that cytoplasmic dynein (1) is the sole motor responsible for retrograde axonal transport (Levy and Holzbaur 2006); (2) is a poorly processive motor which requires dynactin to function optimally (King and Schroer 2000). Regarding dynactin, this protein complex is thought to function (1) as the primary enhancer for dynein's processivity (Schroer 2004); (2) as a vesicular attachment factor for cytoplasmic dynein via interactions between arp 1— filamentous base of dynactin—and the spectrin cytoskeleton (Schroer 2004). Together, these reports have led to the "standard model" for axonal transport found in current textbooks and encyclopedias.

Shortcomings of the standard model have been revealed by several recent publications. First, it does not explain switching between opposite motor activities, a behavior which has been observed for many vesicles. Second, it does not take into account recently reported biochemical interactions between DIC and KLC (Ligon,

Tokito et al. 2004). Third, it does not explain why dynactin mutations seem to affect both kinesin-1 and dynein function (Gross, Welte et al. 2002). Fourth, it portrays dynactin as a required dynein attachment factor, but recent work shows that this is not the case for a major population of vesicles in Drosophila (Haghnia, Cavalli et al. 2007). Fifth, it argues that dynactin binding to microtubules is required for optimal cytoplasmic dynein function. However, deletion of the microtubule-binding domain of dynactin showed no impairment in retrograde behavior in S2 cells (Kim, Ling et al. 2007). These are just a few of the observations that call for new experiments and the development of novel testable models.

Most of the work done to date on motor protein function and activity regulation used *in vitro* and culture systems devoid of polarized neuronal cells. While these systems have served an important purpose in advancing our knowledge on several fronts, an *in vivo* polarized neuronal system is clearly lacking in which to test formerly proposed as well as new models. In addition, it is evident that vesicles carry many regulatory proteins (Kamal, Almenar-Queralt et al. 2001), which may have direct or indirect influence on the activity of motor proteins. Thus, we developed an *in vivo* polarized neuronal system in Drosophila to study motor protein regulation. We chose to focus on the amyloid precursor protein (APP) vesicle as our model system because of abundant information available for this protein as well as its likely contribution to neurodegenerative disease pathways. Through analysis of YFP-tagged APP (APPYFP) movement in animals heterozygous for key motor and regulatory proteins, we began dissecting the relative contribution of each component to the functional motor complex mediating bi-directional vesicle movement.

Our rational for the experiments described below follows from a series of observations made for kinesin-1, dynein, and dynactin that do dot fit previously proposed paradigms. One intriguing observation is that kinesin-1 reduction seems to interfere with dynein function. This was first suggested by experiments in squid axoplasm where anti-kinesin antibodies were used to inhibit kinesin-1 function (Brady, Pfister et al. 1990). However, these studies were confounded by the possibility of antibodies indirectly inhibiting retrograde function through steric hindrance. More recently, immunohistochemistry of Drosophila segmental nerves showed that KHC reductions led to the appearance of axonal swellings (Martin, Iyadurai et al. 1999), which were hypothesized to result from defects in bi-directional transport. However, absence of data on vesicle dynamics made this study less credible. In addition, similar experiments by Goldstein and colleagues did not report similar findings for kinesin heterozygous animals (Gunawardena and Goldstein 2001). The controversy is further fueled by recent observations that kinesin-1 reductions do not impair retrograde movement in the lipid droplet system (unpublished observations by Steven Gross and Michael Welte, Drosophila Conference, 2008). Thus, it remains unclear whether kinesin-1 reduction impairs retrograde movement.

As with kinesin-1, studies of cytoplasmic dynein have also yielded controversial findings. *In vitro*, cytoplasmic dynein emerged as an inhibitor of anterograde movement (Vale, Malik et al. 1992). However, in the lipid droplet system it emerged as an activator (Gross, Welte et al. 2002). We have attempted to resolve this discrepancy by looking at how reductions in specific subunits of cytoplasmic dynein affect anterograde movement. If interactions between KLC and DIC are

inhibitory to kinesin-1, then DIC reduction might activate anterograde movement and DIC increase might inhibit it.

No thorough study on this topic would be complete without analysis of dynactin. As described in the context of the standard model, information on dynactin is also plagued by controversial reports. However, two recent studies reported that dynactin plays a crucial role in the coordination of bi-directional movement (Gross, Welte et al. 2002; Haghnia, Cavalli et al. 2007). Intriguingly, dynactin has been proposed to serve as a switcher between anterograde and retrograde movement in *Xenopus* melanophores (Deacon, Serpinskaya et al. 2003). However, the kinesin motor in this system is kinesin-2, which behaves very differently from kinesin-1. In particular, dynactin can bind directly to a subunit of kinesin-2 termed kinesin associated protein (KAP). In contrast, kinesin-1 has no known binding domain for dynactin.

Because dynactin can bind directly to DIC (Schroer 2004), it may activate kinesin-1 indirectly via interactions between DIC and the p150^{Glued} subunit of dynactin. For instance, if DIC inhibits kinesin-1 via DIC-KLC interactions, then dynactin binding to DIC might relieve this inhibition and lead to kinesin activation. In doing so, the role of the dynein-dynactin interaction might be to enhance kinesin-1 activity indirectly. This might setup a mechanism underlined by competition between KLC and p150^{Glued} for DIC binding—a "competition model" for motor activity regulation. This model makes several specific predictions, which we have tested experimentally as described below.

Methods

Imaging protocol

The collection of data was done in L3 animals, making special effort to select animals during the first 24 hours of the L3 stage. Selected larvae freely crawled on food or on the side of the vial. Animals were dissected and imaged on a $3cm^2$ sylgard platform using Ca^{2+}-free medium consisting of NaCl (128 mM), EGTA (1 mM), $MgCl_2$ (4 mM), KCl (2 mM), HEPES (5 mM), and sucrose (36 mM). Dissection took approximately 5 minutes after which animals were inverted onto a cover slip and imaged using a Nikon Eclipse TE2000-U inverted microscope and 100X oil objective (Nikon, 1.40NA, 0.126 microns/pixel). The tape holding the cover slip to the microscope insert plate also serves as support for the sylgard platform. This setup prevents compression of the brain by the cover slip, thereby preventing cytoplasmic contents from being forced into axons. This is especially important when imaging the first axonal segment.

Figure 2-1A shows a schematic diagram of the L3 larva. Our selected driver, SG26.1 Gal4, drives the expression of APPYFP in a small subset of ventral ganglion neurons. The resulting phenotypic expression makes it possible to recognize two prominent cell bodies near the posterior end of the larval brain. These cell bodies give rise to axons that enter two of longest medial nerves in L3. The targets for these two nerves lie in the far posterior end of the animal, approximately 3 mm from the brain. Only one of these two axons gets imaged in any given larva, and the general state of transport in both axons looks similar to the eye. Using this approach we can obtain single axon resolution movies of APPYFP movement (Figure 2-1B).

Four segments along the axon were preferentially imaged to probe for spatial differences. These segments are referred to as "regions" and are defined by the camera frame size displayed on the computer screen. Each frame is 90 microns in length and corresponds to a 90-micron-long axonal segment. The segments imaged are 1, 10, 20, and 30, with segment 1 being continuous with the brain (Figure 2-1A). Segments 10, 20, and 30 are 900, 1800, and 2700 microns from the brain respectively. Region 30 is near the neuromuscular junction. Very proximal or distal regions are difficult to image, presumably because they are near thick tissue such that focusing along the entire 90-micron segment is difficult. For this reason, imaging is done at the nearest usable region from regions 1 and 30. In genotypes where swellings are observed, additional streams are taken of the regions flanking the swelling.

Data collection was done using the Metamorph collection software system running on a PC computer, with stream acquisition at 0.1 Hz—150 frames were collected with 100 ms exposure per frame and no inter-frame interval. The camera used for data collection was the Cool Snap HQ by Roper Scientific. Each region studied was imaged for one minute, which was done by collecting four 15-second streams. Each experiment was prefaced by collection of a still image of the cell body giving rise to the axon being imaged. At the end of the experiment, this cell body was again imaged to probe for changes in signal level as well as tissue integrity. The form of YFP used to tag APP695 in these animals is reportedly pH sensitive according to recent observations made by the Tsien lab, UCSD. Thus, pH changes in the course of the experiment may lead to bleaching of the YFP. Though this was not a significant issue during the 1-minute regional imaging, signal decay in the cell body was indeed

observed in the majority of experiments conducted. We attribute this change in fluorescence to pH fluctuation that likely occurred during the course of the experiment. In spite of this, we did not find that decreases in cell body fluorescence correlated with the degree of movement or signal-noise ratio within the axon. When tissue compromise was observed in the brain regions at the end of an experiment, the experiment was excluded from analysis. Samples were imaged until ten animals were available for analysis. Movement parameters were quantified using the particle tracker software developed in collaboration with the Danuser Lab—The Scripps Research Institute, La Jolla, CA.

The only exception to this imaging protocol was our imaging of EB1GFP. This was done by using time lapse, collecting for 10 minutes at every 3 seconds with an exposure time of 1 second. Four animals were imaged for this condition. Since the first animal was used to setup imaging conditions, we only analyzed 3 animals. This experiment yielded 60 minutes of data for analysis when combining data for regions 10 and 20. Analysis was done using a manual approach where kymograph trajectories were visually inspected and classified as either anterograde or retrograde. No reversing trajectories were observed. Dr. Kristina Schimmelpfeng Henthorn, Ph.D., independently confirmed these results with her analysis of the same data set.

Data Analysis Protocol

We analyzed our streams using a PC computer running MatLab and the "Particle Tracker" software. Basically, the analysis was done in three major steps: Detection, Tracking, and Data Output.

During detection, each movie was automatically copied into a folder containing the necessary sub-folder structure used through the course of the analysis. Then, background for each stream was defined, and the ratios between background and signal were saved for each experiment. In the subsequent step, pixels in each frame were analyzed, and "signal" pixels were defined based on signal-noise ratios.

Tracking is the second major step in the analysis. This step is divided into pre- and post-tracking. At the start of pre-tracking, a kymograph—plot of distance (x-axis) vs. time (y-axis) was generated for each stream. After selection of a region of interest (ROI), a line automatically traced the axon by seeking maxima within the ROI. After kymograph generation, partial tracks were generated. In post-tracking, the gap closer bridges partial tracks into full tracks. Then, computer-generated trajectories can be individually screened for accuracy. Whenever a computer-generated track was not accurate, it was manually generated by carefully clicking on kymograph trajectories with a mouse. The success rate for streams containing only stationary tracks was fairly high, with >80% of trajectories being correctly generated. However, this success rate dropped dramatically to about 10% for streams where movement dominated the picture.

Interpolation is the last step in this part of the analysis. This step accesses whether control points entered by manual kymograph clicking are mapped to experimental points determined during the detection step. In general trajectories requiring >30% interpolation were discarded as weak tracks.

Finally, a quality control step accesses the performance of the interpolation. Each selected track was visually inspected, and the rational for discarded trajectories

was carefully considered. Whenever an unambiguous trajectory was discarded, the human manual trajectory was accepted without conditions imposed by interpolation.

Data Output

After quality control, trajectories from multiple streams were pooled in preparation for statistical and graphical analysis. For comparison of means, a two-tailed Student's t-test was used. Statistical significance for distributions was accessed using the Kolmogorov-Smirnov and Rank Sum tests. Values of $p<0.05$ were taken as statistically significant. Graphing was done using EXCEL.

Definition of Cargo Motion Descriptors

1. Population metrics

(1) [Definition 1: cargo trajectory center]—We define the ***center*** of the trajectory of a cargo to be the mean of its position coordinates over time. That is, if the cargo trajectory is represented using the cargo position coordinate series $(x_1, y_1), (x_2, y_2), ..., (x_N, y_N)$, its center (x_c, y_c) is calculated as:

$$x_c = \frac{1}{N}\sum_{i=1}^{N} x_i, \quad y_c = \frac{1}{N}\sum_{i=1}^{N} y_i, \tag{1}$$

where N is the total number of frames and (x_i, y_i) is the cargo position in frame i. This definition is motivated by the fact that in our imaging experiments we always orient samples such that cargoes move approximately along the horizontal direction of the image plane. In this way, the y coordinates of cargoes usually vary within a small range.

(2) [Definition 2: stationary cargo]—A cargo is called ***stationary*** if maximum deviation distance from its trajectory center is no larger than a threshold value d_{max}. That is, its trajectory satisfies

$$\sqrt{(x_i - x_c)^2 + (y_i - y_c)^2} \le d_{max} \quad for \;\; i = 1..N \tag{2}$$

In our analysis, we set d_{max} to be 700nm (i.e. 5.5 pixels for our setup). This value was determined in the following way: First, trajectories in kymographs are visually inspected. Stationary trajectories were determined and selected empirically. Second, the maximum deviation of all selected stationary trajectories from their centers was calculated and used as d_{max}, which defines the upper limit of allowed position deviation. For most of the stationary trajectories, their average deviation from their centers is less than this upper limit, at approximately 300-400 nm (i.e. 2.5~3 pixels for our setup).

(3) [Definition 3: cargo trajectory reversal]—A cargo is said to undergo a ***reversal*** at a given location (x_k, y_k) $1 < k < N$ if it satisfies two conditions. First, two points $(x_m, y_m), (x_n, y_n)$, one at an earlier time in the trajectory and one at a later time, can be found at a sufficiently large distance away from this given position. That is,

$$\sqrt{(x_m - x_k)^2 + (y_m - y_k)^2} \ge c_{min} \qquad 1 \le m < k$$

$$\sqrt{(x_n - x_k)^2 + (y_n - y_k)^2} \ge c_{min} \qquad k < n \le N \tag{3}$$

Here $c_{min} = 500$ nm (i.e. 4.5 pixels for our setup). This value was determined based on a conservative estimation of the range of random motion of stationary cargoes (see

discussion of definition 2) and was empirically adjusted to provide reversal detection results consistent with subjective visual detections. Second, vectors connecting (x_k, y_k) and $(x_m, y_m), (x_n, y_n)$ point to opposite directions, that is

$$\langle (x_m - x_k, y_m - y_k), (x_n - x_k, y_n - y_k) \rangle < 0, \quad (4)$$

where $\langle \bullet \rangle$ denotes the vector dot product. This definition is motivated by the fact that cargoes undergo small and random position variations along their trajectories. The minimum distance used allows us to exclude these small random changes in cargo motion.

(4) [Definition 4: cargo trajectory pause]—A cargo is said to undergo a ***pause*** at a given location (x_k, y_k) $1 < k < N$ if its instantaneous velocity at this location is less than a given threshold V_{min}. The instantaneous velocity of the cargo at this point is calculated using a sliding window method

$$V_{inst} = \frac{1}{T \cdot (2W+1)} \sum_{i=k-W}^{k+W} \sqrt{(x_i - x_{i-1})^2 + (y_i - y_{i-1})^2} \quad (5)$$

Here T is the imaging sampling period and W is chosen to be 3 frames (the full window width is 7 frames).

(5) [Definition 5: anterograde cargo]—A cargo is called ***anterograde*** if it is not stationary, has no reversal, and moves towards the synapse (i.e. towards the right in our movies and kymographs). Trajectory pauses are allowed.

(6) [Defintion 6: retrograde cargo]—A cargo is called ***retrograde*** if it is not stationary, has no reversal, and moves towards the neuronal cell body (i.e. towards the left in our movies and kymographs). Trajectory pauses are allowed.

(7) [Defintion 7: reversing cargo]—A cargo is called ***reversing*** if it undergoes at least one reversal. Trajectory pauses are allowed.

1.2 Cargo population metrics

For each movie, animal, or genotype, cargoes are classified as being either stationary, anterograde, retrograde, or reversing. The software reports the number of stationary N_{stat}, anterograde N_{ante}, retrograde N_{retro}, and reversing N_{rev} cargoes.

[Definition 8: Fraction of stationary cargo in the total cargo population]

$$P_{stat}^{A} = \frac{N_{stat}}{N_{stat} + N_{ante} + N_{retro} + N_{rev}} \tag{6}$$

[Definition 9: Fraction of anterograde cargo in the total cargo population]

$$P_{ante}^{A} = \frac{N_{ante}}{N_{stat} + N_{ante} + N_{retro} + N_{rev}} \tag{7}$$

[Definition 10: Fraction of retrograde cargo in the total cargo population]

$$P_{retro}^{A} = \frac{N_{retro}}{N_{stat} + N_{ante} + N_{retro} + N_{rev}} \tag{8}$$

[Definition 11: Fraction of reversing cargo in the total cargo population]

$$P_{rev}^{A} = \frac{N_{rev}}{N_{stat} + N_{ante} + N_{retro} + N_{rev}} \tag{9}$$

[Definition 12: Fraction of anterograde cargo in the non-stationary cargo population]

$$P_{ante}^{NS} = \frac{N_{ante}}{N_{ante} + N_{retro} + N_{rev}} \tag{10}$$

[Definition 13: Fraction of retrograde cargo in the non-stationary cargo population]

$$P_{retro}^{NS} = \frac{N_{retro}}{N_{ante} + N_{retro} + N_{rev}} \tag{11}$$

[Definition 14: Fraction of reversing cargo in the non-stationary cargo population]

$$P_{rev}^{NS} = \frac{N_{rev}}{N_{ante} + N_{retro} + N_{rev}} \tag{12}$$

2. Cargo velocity metrics

2.0 Separation of individual trajectories into segments:

If one or multiple reversals or pauses are detected in a cargo trajectory, it is separated into segments at reversal points and pause points so that within each segment the cargo moves toward one direction without pauses and reversals. A trajectory with no reversals and no pauses is considered as a single segment.

[Definition 17: Segmental velocity] The segmental velocity of a cargo is defined as the total distance traveled by the cargo within a segment divided by the lifetime of the segment. For trajectories with no reversals and pauses, this velocity is the same as the average instantaneous velocity. For trajectories with reversals and/or pauses, the velocity is reported for each individual segment. Specifically, for a trajectory segment starting at frame *P* and ending in frame *Q*, it is calculated as

$$V_{seg} = \frac{1}{T(Q-P)} \sum_{i=P+1}^{Q} \sqrt{(x_i - x_{i-1})^2 + (y_i - y_{i-1})^2} \tag{15}$$

This velocity gives consideration to pauses, reversals or random position variations within the trajectory segment. Depending on the direction of the cargo movement within each segment, this velocity is reported for each segment as anterograde or retrograde segmental velocity.

3. Cargo pause metrics

[Definition 20: Pause frequency]

This number is reported for each full cargo trajectory and is the number of pauses within that trajectory. If there are reversals within a trajectory, it is first separated into segments at the reversal points. Pauses, if any, are counted within each trajectory and summed up for anterograde and retrograde, respectively. To express it as a function of time, this number was normalized with respect to movie length—15 seconds.

[Definition 21: Pause duration]

This number is reported for each full cargo trajectory and is the total duration of pauses within that trajectory. If there are reversals within a trajectory, it is first separated into segments at the reversal points. Pause durations are summed for anterograde and retrograde trajectories, respectively.

4. Cargo reversal metrics

[Definition 22: Switch frequency] This number is reported for each full cargo trajectory and is the number of reversals within that trajectory. This metric does not differentiate between anterograde and retrograde directions.

5. Cargo Run Length Metrics

[Definition 25: All-included run length] Under this definition, a run length that is not complete due the limited field-of-view and movie length is still counted in the calculation. This run length can be compared between different genotypes as long as the image conditions remain the same. This run length is reported for each segment and for both direction.

Flux analysis

Flux was determined by setting 10 equidistant monitoring points along the 90-micron axonal segment and computing the number of anterograde or retrograde cargoes that crossed them. This analysis was done for each animal, so all 4 streams collected per given region were used to generate a flux/animal measurement. The data was then pooled for the 10 animals, and the standard deviation and standard error were calculated.

Cluster analysis

The M-cluster statistical package from the "R project from statistical computing" (http://www.r-project.org/) was used to perform in-depth analysis of segmental velocities. The best fitting for control as well as the majority of genotypes yielded 3 clusters, with cluster 1 being slowest and cluster 3 being fastest. The software returned average velocity, standard deviation (SD), and weight for each population. Because each population followed a normal distribution, we used a two-tailed Student's *t* test to access significance between the means. To analyze how weights changed with respect to gene reductions, we took the mean and SD for control and enforced it on other genotypes. This yielded the proportion of the population—

weight—moving at control values. We took 10% above or below the mean to be significant increases or decreases in population weight.

Genetics

Drosophila stocks were maintained at room temperature or at 25°C except when crosses were setup for imaging. L3 larvae obtained for movement analysis were taken from crosses incubated at 29°C. The control group for this study consisted of movement analysis for UAS-APPYFP. The line used in this study was UAS-APPYFP (X)—APPYFP transgene inserted in the X chromosome. Only female L3 larvae were used for imaging of this as well as all other genotypes. In brief, L3 larvae expressing UAS-APPYFP arose from crosses between male UAS-APPYFP flies and SG26.1 Gal4 virgin females. Thus, male animals provided an internal control for the cross since they did not express UAS-APPYFP. To examine the effect of motor gene reductions on vesicle movement, we first generated an UAS-APPYFP; pin^{88K}/ T(2:3) CyO TM6B stable stock. The chromosome carrying T(2:3) CyO, TM6B is referred to as B3 and carries the dominant markers Hu, Tb, and Cyo. This stable stock was created by a multi-step cross scheme where 1) UAS-APPYFP virgins were crossed to pin^{88K}/ B3 males; 2) selected UAS-APPYFP/X; B3/+ virgins were crossed to pin^{88K}/ B3 males; 3) selected UAS-APPYFP /X; pin^{88K}/ B3 were crossed to selected UAS-APPYFP /Y; pin^{88K}/ B3; 4) selected UAS-APPYFP; pin^{88K}/ B3 virgins were crossed to selected UAS-APPYFP /Y; pin^{88K}/ B3.

For kinesin-1 reduction studies, three alleles were used: khc^{8}/CyO, khc^{20}/CyO, and klc^{8ex94}/TM6B. The *khc* alleles are null point mutants, whose translated fragments are thought to be degraded due to instability. The *klc* allele is a deletion allele

spanning the entire gene in chromosome 3. For each of these alleles, virgin UAS-APPYFP; *pin*^{88K}/ B3 flies were crossed to *kinesin*/balancer males. Selected males UAS-APPYFP /Y; *kinesin*/B3 were then crossed to virgin SG26.1 Gal4 animals. Female non-tubby L3 larvae were then selected for imaging.

For cytoplasmic dynein reduction studies, five alleles were used: *p4163*/TM6B, *dhc64c*$^{4-19}$/TM6B, *dic*^{1}/FM7GFP, *dic*^{3}/FM7GFP, and *robl*^{k}/CyO. Like *khc*, the *dhc* alleles *p4163* and *dhc64c*$^{4-19}$ are reportedly protein nulls. In addition, *dic*^{1} and *dic*^{3} are also protein nulls of *dic*. The *dlc* allele *robl*^{k} is a deletion allele spanning the whole *robl* gene in chromosome 2. For crosses involving *dhc* or *dlc*, we proceeded as with kinesin-1. Virgin UAS-APPYFP; *pin*^{88K}/B3 flies were crossed to *dynein*/balancer males. Selected males UAS-APPYFP /Y; *dynein*/B3 were then crossed to virgin SG26.1 Gal4 animals. Female non-tubby L3 larvae were then selected for imaging. For *dic* crosses, schemes were a little more complex since *dic* is located on the X chromosome as is UAS-APPYFP. For these crosses, we proceeded as follows: 1) we crossed UAS-APPYFP; *pin*^{88K}/ B3 virgins to SG26.1 Gal4; 2) selected UAS-APPYFP /Y; SG26.1 Gal4/B3 were then crossed to *dic*/balancer; 3) from non-tubby animals, used a GFP microscope to select female L3 larvae negative for GFP—these female animals are UAS-APPYFP /*dic*; SG26.1 Gal4/+. The *p4163*/TM6B, *dic*^{1}/FM7GFP, and *dic*^{3}/FM7GFP stocks were generously provided to us by Tom Hays—University of Minnesota Dept. of Genetics, Cell Biology, and Development.

For dynactin reduction studies, three alleles were used: *grid*/TM6B, *dmn*^{5499}/CyO, and *gl*^{1}/In(3L)D, *d*^{1} (BL-2394). Both the *grid* and *dmn*^{5499} stocks are

characterized protein nulls, but the gl^{1}/In(3L)D, d^{1} stock is thought to be a dominant negative allele. As for previous crosses, we looked at the effect of dynactin reduction on APPYFP movement by crossing UAS-APPYFP; pin^{88K}/B3 virgins to *dynactin*/balancer. Selected males UAS-APPYFP /Y; *dynactin*/B3 were then crossed to virgin SG26.1 Gal4 animals. Female non-tubby L3 larvae were then selected for imaging.

We conduced two overexpression experiments with kinesin-1 or cytoplasmic dynein. For kinesin-1, we used GEN-KLC/CyO; TM3/TM6B and *sp*/CyO; GEN-KHC stocks. The extra copy of the motor gene in these stocks is under the control of endogenous regulatory domains present in the wild type condition (Saxton, Hicks et al. 1991; Gindhart, Desai et al. 1998). To achieve overexpression of both kinesin-1 subunits, we combined these two backgrounds as follows: 1) crossed GEN-KLC/CyO; TM3/TM6B virgins to *sp*/CyO; GEN-KHC males; 2) crossed selected males and females GEN-KLC/CyO; GEN-KHC/TM6B; 3) selected GEN-KLC; GEN-KHC virgins and crossed to UAS-APPYFP /Y; SG26.1 Gal4/B3. This last mating cross generated the desired L3 animals for imaging— UAS-APPYFP /X; GEN-KLC/+; GEN-KHC/SG26.1. For the cytoplasmic dynein overexpression experiment, we obtained a GEN-DIC stock from Tom Hays (Boylan, Serr et al. 2000). Like GEN-KLC and -KHC, GEN-DIC is also under control of endogenous regulatory domains. We looked at the effects of GEN-DIC on APPYFP movement through the following scheme: 1) crossed UAS-APPYFP; pin^{88K}/B3 virgins to dic^{1}/Y; GEN-DIC males; 2) selected UAS-APPYFP /Y; GEN-DIC/B3 males and crossed to SG26.1 virgins; 3) selected UAS-APPYFP /X; GEN-DIC/+; SG26.1/+ L3 larvae for imaging.

One very important experiment testing our competition model required double reduction of *grid* and *dic*. To achieve this, we undertook an elaborate approach consisting of several crosses using both *dic* alleles obtained from Tom Hays: 1) crossed UAS-APPYFP; pin^{88K}/B3 virgins to *grid*/TM6B males; 2) selected UAS-APPYFP /Y; *grid*/B3 and crossed to UAS-APPYFP; pin^{88K}/B3 virgins; 3) selected UAS-APPYFP; *grid*/B3 virgins and crossed to UAS-APPYFP; pin^{88K}/B3 virgins. This allowed us to generate an UAS-APPYFP; *grid*/B3 stable stock. Then, we created a dic^{3}/FM7GFP; (*Bl*; SG26.1)/B3 stock as follows: 1) crossed SG26.1 virgins to CyO/*Bl*; TM2/TM6B males; 2) selected CyO/+; SG26.1/TM6B males and crossed them CyO/*Bl*; TM2/TM6B; 3) selected CyO/*Bl*; SG26.1/TM6B males and females to establish a stable stock of CyO/*Bl*; SG26.1 with TM6B floating; 4) crossed CyO/*Bl*; SG26.1/TM6B males to pin^{88K}/B3 virgins to generate (*Bl*; SG26.1)/B3; 5) crossed *dic*/FM7GFP females to (*Bl*; SG26.1)/B3 males; 6) selected *dic*/X; *Bl*/+; SG26.1/+ virgins and FM7GFP/Y; B3/+ flies from cross#5 and crossed them to one another; 7) selected for FM7, *Bl*, and B3, which should mark two phenotypically indistinguishable genotypes—i) *dic*/FM7GFP; (*Bl*; SG26.1)/B3 and ii) FM7GFP/X; (*Bl*; SG26.1)/B3; 8) these two genotypes can be differentiated by crossing them to FM7GFP/Y; B3/+ males—generated in cross#5; 9) select for stocks containing only bar-eyed males—stocks not containing the bar marker can only be generated from the cross between FM7GFP/X; (*Bl*; SG26.1)/B3 females and FM7GFP/Y; B3/+ males and are *dic* +; 10) the last cross then was to mate *dic*/FM7GFP; (*Bl*; SG26.1)/B3 virgins to APPYFP/Y; *grid*/B3 males; 11) from the non-tubby animal group, we used a GFP microscope to

select female L3 larvae negative for GFP—these female animals are UAS-APPYFP /*dic*; *Bl*/+; SG26.1Gal4/*grid*.

Western blot analysis

Protein analysis on genetic reductions and overexpressions was done using Western blot analysis and quantification using the Odyssey system. In brief, ten young female adult flies—<24 hours old—were selected from stable stocks and ground in 100 μL 2X LDS sample buffer (Invitrogen) with 2% β-mercaptoethanol. Samples were heated for 10 minutes at 98°C and centrifuged for 5 minutes at 14,000 rpm. The supernatant was then removed, and protein concentration was measured using the Bio-Rad DC protein assay. Samples were loaded on pre-cast 4-12% Bis-Tris gels (Invitrogen), and See-Plus 2 (Invitrogen) was used as the molecular weight marker. Gels ran in MOPS buffer (Invitrogen) at 100V until dye reached the bottom of the gel. Transfer to nitrocellulose membranes was done at 4°C using a wet system and buffer consisting of 25 mM Tris-base, 190 mM Glycine, and 20% methanol. Ponceau S solution (Sigma) was used to assess the success of transfer. KHC and KLC primary antibodies were used at 1:1,000 dilution; KHC was from Cytoskeleton, and KLC was custom made in the Goldstein lab. As a loading control, we probed for syntaxin—used at 1:250 dilution and obtained from the Hybridoma bank. Primary antibody dilutions were prepared in 5% BSA with TBST and left incubating with membranes overnight at 4°C. Kinesin primary antibodies were stable as dilutions in 5% BSA for several months. Thus, we added 0.002% sodium azide to the solutions and re-used them multiple times. The secondary antibody was used at 1:5,000 and

was left incubating with membranes for 2 hours at room temperature. Membranes were scanned either wet or dry, but drying yielded much stronger signals.

Quantification was done using tools provided by the Odyssey software, setting background to be above and below the region of interest. Intensities were corrected by dividing KHC or KLC intensities by those in the syntaxin loading control. Increases above control were calculated using EXCEL, and averages between 10 and 20 microgram loadings were plotted as normalized ratios to control.

Statistics

Statistical significance was accessed using both parametric and non-parametric tests. Normality was determined using the Anderson Darling and Lilliefors statistical tests. We accepted that samples in a population were not normally distributed when $P < 0.05$. A two-tailed Student's t test was used for comparison between normally distributed populations—as in the case of individual clusters in the cluster analysis for segmental velocities. For non-normal distributions, we used the Wilcoxon rank-sum test—run length, pause frequency, pause duration, and switch frequency did not follow a normal distribution. For the cumulative distribution function (CDF) analysis of segmental velocities, we used the Kolmogorov-Smirnov test. P values < 0.05 were considered significant for all tests used.

Results

SG26.1 Gal4 characterization

As previously observed in the lab, SG26.1 Gal4 induced expression of UAS-APPYFP in a few CNS cell bodies of L3 larvae. This pattern of expression is consistent with anterograde movement being directed away from the cell body and towards the periphery. To test this hypothesis, we looked at the movement of end-binding protein tagged with GFP (EB1GFP). Since EB1 localizes primarily to the distal tips of microtubules (Morrison 2007), it marks the plus ends of filaments. We found that EB1GFP moved primarily to the periphery, consistent with what we expected (Figure 2-2). Out of the 165 particles tracked for analysis, 160 particles moved anterogradely. In addition, we observed no change in directionality for any given particle. This suggests that we can unambiguously differentiate anterograde and retrograde movements in our system since microtubules within an axon are polarized with plus ends oriented away from the cell body.

APPYFP movement and parameters

APPYFP vesicles move bi-directionally within axons, similar to what has been reported for other vesicles and organelles. This makes APPYFP an appropriate vesicle type for studying motor protein activity regulation and coordination in axonal transport. We found that expression of the APPYFP transgene by SG26.1 Gal4 resulted in no apparent disruption to axonal transport. For example, axonal swellings were not observed and larval locomotor behavior was indistinguishable for that of wild type animals.

Given that APP is reportedly a kinesin-1 cargo (Kamal, Stokin et al. 2000), we expected that APPYFP vesicles would have around 0.8 μm run length (RL) and 0.8 μm/sec segmental velocity (SV) as reported for the kinesin-1 motor *in vitro* (Vale, Malik et al. 1992). Indeed, we observed that APPYFP anterograde (A) average SV was around 0.8 μm/sec in both regions 10 and 20 [region 10 ASV = 0.86 ± 0.02 μm/sec (mean ± SEM); region 20 ASV = 0.87 ± 0.02 μm/sec; Table 2-1]. However, we were surprised to find that a fast-moving population of vesicles reached velocities as high as 3 μm/sec. In addition, APPYFP vesicles moved on average > 7 μm, which is also many times higher than reported *in vitro* [region 10 ARL = 7.63 ± 0.26 μm; region 20 = ARL = 7.44 ± 0.28 μm; Table 2-1]. Remarkably, some cargoes moved distances > 40 μm. Thus, it seems like kinesin-1 may behave differently *in vivo* than *in vitro*.

As for anterograde cargoes, mean retrograde segmental velocity (RSV) was also in the neighborhood of those reported for cytoplasmic dynein *in vitro* [region 10 RSV = 0.87 ± 0.02 μm/sec; region 20 RSV = 0.98 ± 0.02 μm/sec; Tables 2-1 and 2-2]. However, like kinesin-1 some retrograde vesicles moved as fast as 3 μm/sec, which was not predicted by the *in vitro* data. As for retrograde run length (RRL), means were also significantly longer *in vivo*, and some vesicles moved for > 40 μm [region 10 RRL = 7.08 ± 0.25 μm; region 20 RRL = 8.462 ± 0.27 μm; Table 2-1].

Because we hypothesized that transport within axons may not be homogeneous across the length of the fiber, we collected and analyzed our data according to defined axonal locations (see Methods). When we compared ARL and ASV parameters

between regions 10 and 20, we found no significant inter-regional difference [P = N.S.]. However, for RSV and RRL, we found that these parameters were significantly different with region 20 showing a significant increase in both RSV and RRL [$P < 0.001$]. Thus, whereas kinesin-1 behavior seems to be location independent, this is not the case for cytoplasmic dynein. The higher RSV and RRL suggest the possibility that more cytoplasmic dynein is active in posterior regions of the axon.

Role of kinesin-1 in APPYFP movement

In Drosophila, single genes encode the KHC and KLC subunits of kinesin-1, and complete removal of either of these genes results in lethality. A single copy reduction of one of these genes, however, permits survival of animals to adulthood. Thus, we studied heterozygous null animals to look at the role of kinesin-1 reduction on APPYFP vesicle movement. We observed that *khc*/+ and *klc*/+ L3 larvae crawled normally and did not display phenotypic markers of axonal transport defects such as tail flipping (Martin, Iyadurai et al. 1999). To test that 50% reduction in KHC or KLC gene dosage led to protein reduction of motor subunits, we performed Western blot analysis on APPYFP adult flies heterozygous for kinesin-1. As expected, we found that these animals contained about 50% less protein as compared to wild type (Figure 2-3). Thus, 50% reduction in kinesin-1 gene dosage translates into 50% protein reduction. Interestingly, KHC gene reduction resulted in decreases to both KHC and KLC protein levels whereas KLC reduction led to KLC decrease alone. This suggests that KLC gene expression is sensitive to changes in KHC gene expression but not vice-versa.

We next looked at how kinesin-1 motor reduction affects the movement of APPYFP. Qualitative inspection of movies and kymographs showed very obvious effects of kinesin-1 reduction on bi-directional movement of APPYFP. There was less overall movement and increased presence of axonal swellings filled with APPYFP vesicles. In most cases, these swellings did not seem to block moving cargoes as APPYFP vesicles could be seen moving in and out of the swellings. In a few cases, however, large swellings were observed. These span as much as 30-40 microns and most likely constituted blockages since very few stationary APPYFP vesicles could be observed in downstream regions. These large swellings were usually present distal to region 10.

In agreement with the observations described above, our quantitative analysis of cargo populations in kinesin-1 heterozygous animals showed an increase in the percentage of stationary cargoes with a concomitant decrease in anterograde, retrograde, and reversing populations (Figure 2-4A; Table 2-3 left) [$P < 0.001$ for all conditions]. Not surprisingly, there was also a significant decrease in flux for both anterograde and retrograde populations (Table 2-3 right) [$P < 0.001$ for all conditions]. A similar trend was observed for region 20 (Table 2-4). These observations suggest that kinesin-1 reduction adversely affects bi-directional movement.

A limitation of our current analysis method is that we cannot quantify the absolute number of vesicles present in an axonal swelling. Thus, the decrease in total cargo number observed in *kinesin-1*/+ animals might be due to our inability to accurately count the number of vesicles comprising axonal swellings (control = 1890; khc^{8}/+ = 1270; khc^{20}/+ = 1263; klc^{8ex94}/+ = 1581). In truth, increases in the stationary

cargo population percentage seem to be a good indication of depressed axonal transport. However, understanding how motor reductions affect vesicle movement might be better accomplished by looking at the ratio between moving particles. One potentially revealing measurement is the ratio between anterograde and retrograde (A/R ratio) moving particles. This ratio can be accurately obtained because it seems that each moving trajectory represents the behavior of a single particle. Furthermore, changes in the probability of directional movement might be revealed in changes to this ratio. Thus, we looked at the A/R ratio for kinesin-1 reductions. In region 10, we found that this ratio did not change significantly for khc^{8}/+ or klc^{8ex94}/+, but there was a significant decrease for khc^{20}/+ (Figure 2-4A, right panel; Table 2-3). In region 20, there was a similar finding though the other KHC allele, khc^{8}, showed a significant decrease there (Table 2-4). Thus, reductions in KHC can lead to a decrease in anterograde APPYFP movement, consistent with the idea that kinesin-1 powers anterograde movement of APPYFP vesicles.

Effects of kinesin-1 reduction on APPYFP anterograde movement

A large body of *in vitro* work suggests that kinesin-1 is a highly processive motor (Block, Goldstein et al. 1990; Vale, Funatsu et al. 1996). These observations led us to predict that reductions in kinesin-1 motor number would have no significant impact on anterograde velocity. In addition, we expected run length to be reduced and pause frequency and duration to increase. As expected, all three kinesin alleles studied showed a significant decrease in mean ARL as compared to control in region 10 (Figure 2-4B, left panel; Table 2-1). There was also a significant increase in mean anterograde pause frequency for klc^{8ex94}/+ animals (Figure 2-4C, left panel; Table 2-1),

and anterograde pause duration was significantly increased for all three alleles (Figure 2-4C, right panel; Table 2-1). A similar trend was shown for region 20, with a significant decrease in ARL being observed for all kinesin-1 reductions (Table 2-2). APF also increased for khc^{8}/+, and both *khc* reduction alleles showed significant increases in APD (Table 2-2).

We next looked at the effects of kinesin-1 reductions on anterograde velocity. We were surprised to find that mean ASV in region 10 was significantly reduced for all three alleles studied (Figure 2-4B, right panel; Table 2-1). Significant decreases were also observed for region 20. To obtain more information on how the ASV changed with kinesin-1 reductions, we examined the cumulative distribution frequency (CDF) for the ASV values. We found that kinesin-1 reductions led to a leftward shift in ASV curves (Figure 2-5), suggesting that a higher proportion of vesicles moved with significantly slower velocities when kinesin-1 amounts were reduced [$P < 0.001$ for all alleles studied].

To gain more insight into how ASV changed with kinesin-1 reductions, we performed a cluster analysis on region 10 data (see Methods). For controls, the best fit of the data returned three clusters, with clusters 1, 2, and 3 comprising 26.15%, 39.40%, and 34.45% of the total population and having velocity means of 0.37, 0.66, and 1.46 respectively. As predicted from the cumulative frequency distribution, kinesin reductions generally resulted in a significant shift towards slower velocity means (Table 2-5, left). Even though the khc^{8}/+ ASV mean increased for cluster 1 and 2, the weight of cluster 1 about doubled for khc^{8}/+ (control = 26.15%; khc^{8}/+ = 54.69%). Thus, analysis of just mean velocities can be misleading. To correct for

this, we conducted a new cluster analysis where we enforced the control mean ± SD values on the kinesin-1 reduction data (Table 2-5, right). As expected, this new method clearly showed the enhancement in cluster 1 for all kinesin-1 reduction alleles as well as a decrease in cluster 3 for the *khc*/+ alleles. Interestingly, cluster 3 increased from 34.06% in control to 37.78% in klc^{8ex94}/+ (about 11% increase), but this increase was relatively small compared to the 50% increase in klc^{8ex94}/+ cluster 1 (control = 26.04%; klc^{8ex94}/+ = 39.18%). Thus, the decrease in anterograde velocity that accompanied kinesin-1 reductions is likely to be a real phenomenon.

Our velocity data suggest the intriguing possibility that kinesin-1 *in vivo* does not behave like a highly processive motor as predicted from the *in vitro* data. If so, one would expect that run length and velocity would be correlated. To test this possibility, we performed a correlation analysis between ARL and velocity. Indeed, analysis of the APPYFP control data showed a strong correlation between RL and velocity. In addition, reductions in kinesin-1 did not affect this correlation but rather reduced fast-moving and long-moving populations (Figure 2-6). This analysis supports the idea that kinesin-1 behaves as a poorly processive motor *in vivo*.

A simple explanation for the surprising effect of kinesin reduction on anterograde velocity is that a poorly processive anterograde motor competes with kinesin-1 for APP transport. There are several reasons why this is unlikely to play a role here. First, there are no reports to date showing that a motor other than kinesin-1 can transport APP. Second, experiments using APP C-terminus deletions showed APP accumulation in the cell body and failure to enter the axon (Gunawardena and Goldstein 2001). This agrees with the hypothesis that the C-terminus domain of APP

interacts with the KLC subunit of kinesin-1 and is required for APP transport. Third, if a non-processive motor competes with kinesin-1 for transport of APP, then removal of kinesin-1 would be expected to enhance the interaction between APP and the poorly processive motor. The end result would be that kinesin-1 reductions would lead to faster anterograde velocities, which is opposite to what we observed. In spite of these arguments, we set out to test the hypothesis that a poorly processive motor competes with kinesin-1 for APP transport.

Kinesin-3—UNC104 in *Drosophila*—is a poorly processive motor required for axonal transport of synaptic vesicle proteins (Yonekawa, Harada et al. 1998). Alongside kinesin-1, kinesin-3 constitutes the other major kinesin motor thus far found to be involved in anterograde axonal transport. Thus, kinesin-3 comprises the most likely candidate to compete with kinesin-1 for APPYFP transport.

If UNC104 is responsible for fast movement of APPYFP cargoes, we predicted that reduction in this motor would cause a significant decrease in fast-moving populations. In region 10, we found that UNC104 reduction led to a small but significant decrease in mean ASV (Table 2-1; control = 0.86 ± 0.015; *unc104*/+ = 0.70 ± 0.014 [P <0.001]). To gain more insight into this behavior, we performed cluster analysis on these data. We found that the ASV mean for all 3 clusters decreased significantly in *unc104*/+ region 10 (Table 2-5, left). However, cluster weight analysis showed no significant change in *unc104/*+ cluster 3—the fastest moving population cluster (Table 2-5, right; cluster 3: control = 34.06%; *unc104*/+ = 34.35%). In addition, our analysis of region 20 further confirmed that kinesin-3 is not responsible for the fast anterograde movement observed for APPYFP vesicles. In this more distal

region, UNC104 reduction led to a small but significant increase in mean ASV (control = 0.866 ± 0.017; *unc104*/+ = 0.900 ± 0.020 [P <0.01]). Furthermore, cluster analysis of region 20 ASV data revealed a significant increase in mean ASV for all 3 clusters (cluster 1: control = 0.37 ± 0.11; *unc104*/+ = 0.42 ± 0.17 (mean ± SD) [P < 0.001; cluster 2: control = 0.70 ± 0.20; *unc104*/+ = 0.76 ± 0.25 [P < 0.001]; cluster 3: control = 1.44 ± 0.52; *unc104*/+ = 1.60 ± 0.37 [P < 0.001]). Consistent with this, weight cluster analysis revealed a shift from slow moving to fast moving populations (cluster 1: control = 31.16%; *unc104*/+ = 22.47% [39% decrease]; cluster 2: control = 32.36%; *unc104*/+ = 37.96% [17% increase]; cluster 3: control = 36.48%; *unc104*/+ = 39.57% [8% increase]). Taken together these data suggest that kinesin-3 is not likely a direct contributor to movement for APPYFP cargoes.

Effects of kinesin-1 reduction on APPYFP retrograde movement

Kinesin-1 has been proposed to play a role in movement powered by cytoplasmic dynein (Brady, Pfister et al. 1990; Martin, Iyadurai et al. 1999). However, potential antibody steric effects confounded the results in the first study, and the second study did not assay movement of cargoes. Thus, we tested the hypothesis that kinesin-1 is required for optimal cytoplasmic dynein function. If this is the case, decreases in kinesin-1 should result in impairment of retrograde movement parameters. In agreement with this idea, we found that all three kinesin alleles showed a dramatic decrease in mean retrograde run length (RRL) in both regions 10 and 20 (Figure 2-7A left; Table 2-1, region 10; Table 2-2, region 20). In addition, mean retrograde pause frequency (RPF) and mean retrograde pause duration (RPD) increased significantly for *khc*/+ in both regions (Figure 2-7B; Tables 2-1 and 2-2).

For *klc*^{8ex94}/+, RPF and RPD increased significantly only in region 20 (Tables 2-1 and 2-2).

Kinesin-1 reduction also had a dramatic impact on retrograde velocity. We observed a highly significant decrease in mean retrograde segmental velocity (RSV) in both regions 10 and 20 (Figure 2-7A right; Tables 2-1 and 2-2). As with anterogradely moving cargoes, there was a dramatic leftward shift in the RSV CDF curve for APPYFP kinesin heterozygotes (Figure 2-7C). Moreover, the cluster analysis showed a dramatic decrease in RSV mean for all clusters, and there was a dramatic increase in the weight of slow moving populations (Table 2-5 left). Taken together, these data suggest that kinesin-1 is required for optimal dynein function and raises the intriguing possibility that kinesin-1 acts as a processivity factor for cytoplasmic dynein.

Effects of kinesin-1 reduction on synaptotagmin movement

The bi-directional effects of kinesin-1 reduction on APPYP movement led us to ask if this was a specific effect on the APPYFP vesicle pathway or a global toxicity effect on axonal transport. To test this idea we looked at the movement of synaptotagmin-GFP (SYTGFP) on two kinesin-1 heterozygous backgrounds. SYTGFP is a kinesin-3 cargo thought not to depend on kinesin-1 for its movement (Yonekawa, Harada et al. 1998). We found that reductions in kinesin-1 did not impair the movement of SYTGFP. Indeed, kinesin-1 reduction even led to activation rather than inhibition of SYTGFP movement in some cases.

For anterogradely SYTGFP moving cargoes, there was no change in ARL, APF, or APD for *khc*^{8}/+ in either region 10 or 20 (Table 2-6). As for ASV, KHC

reduction led to a significant decrease in region 10 but no change in region 20. Similarly, KLC reduction had no effect on APF or APD in either region 10 or 20. Interestingly, we observed significant increases in ARL and ASV for klc^{8ex94}/+. In region 10, both of these parameters were significantly increased, but only ASV was significantly up in region 20.

For retrograde movement of SYTGFP cargoes, we found that kinesin-1 reduction led to significant increases in both RRL and RSV in region 10 (Table 2-6, top right). In addition, these increases were accompanied by significant decreases in both RPF and RPD. For region 20, KHC reduction led to significant increases in RSV and decreases in RPF without change in RRL or RPD. As for klc^{8ex94}/+, only RPF and RPD changed significantly in region 20—decreased (Table 2-6, bottom right). Thus, our analysis of SYTGFP bi-direction movement on two kinesin-1 reduction backgrounds shows that kinesin-1 does not adversely affect the movement of synaptotagmin. This suggests that the effects of kinesin-1 reduction on APPYFP movement are specific to the APPYFP vesicle pathway.

Effects of cytoplasmic dynein reduction on APPYFP vesicle movement

To study the role of cytoplasmic dynein on bi-directional APPYFP movement, we looked at how reductions in cytoplasmic dynein affected the movement of APPYFP cargoes. As compared to kinesin-1, cytoplasmic dynein reductions differed phenotypically in two important ways. First, none of the five cytoplasmic dynein reduction alleles studied caused axonal swellings or blockages. Second, the effects of dynein reductions were much more complex. Whereas reduction of kinesin-1 light or heavy chains had approximately the same effect on APPYFP movement, we

were surprised to find that the effects of dynein reductions were subunit dependent. In general, DHC and DLC reductions behaved the same and were opposite to those of DIC. For example, DHC and DLC reductions led to a significant increase in the anterograde population in region 10 at the expense of decreases in stationary and reversing populations (Figure 2-8A; Table 2-3, left)—except for *dhc64c*$^{4\text{-}19}$/+, which showed no change in stationary cargo percentage. In addition, there was a significant increase in A/R ratio for *p4163*/+ and *robl*^{k}/+. Decreases in DIC, however, showed an increase in stationary cargo percentage and a decrease in moving population percentages (Figure 2-8A; Table 2-3 left; *dic*^{1}/+ showed a significant decrease in retrograde and reversing percentages; *dic*^{3}/+ showed a significant decrease in anterograde and reversing). Furthermore, there was a significant decrease in A/R ratio for *dic*^{3}/+. For the most part, region 20 showed a similar trend with significant increases in anterograde percentage and A/R ratio for *dhc64c*$^{4\text{-}19}$/+ and *robl*^{k}/+ and increases in stationary percentage for both *dic*/+ alleles. No significant changes in A/R were observed for *dic*^{1}/+ and *dic*^{3}/+ in region 20.

Consistent with the findings described above, we observed that DHC and DLC reductions led to significant increases in anterograde flux (Table 2-3, region 10; Table 2-4, region 20). This was seen for *p4163*/+ in region 10 and for *dhc64c*$^{4\text{-}19}$/+ and *robl*^{k}/+ in region 20. As for DIC, both reduction alleles led to a significant decrease in anterograde flux for both regions 10 and 20. Given that motor number determines retrograde run length and velocity for a poorly processive motor, we were not surprised to find that reductions in cytoplasmic dynein led to decreases in retrograde flux. This was observed for all 5 alleles in region 10 and 3/5 in region 20.

Taken together, these data suggest that cytoplasmic dynein can affect movement in a subunit-dependent fashion.

Effects of cytoplasmic dynein reductions on APPYFP retrograde movement

If the *in vivo* behavior of dynein is like that of *in vitro*, one would expect that reductions in cytoplasmic dynein would lead to decreases in retrograde velocity and run length and increases in pause frequency and duration. Indeed, our analysis of retrograde velocity and run length showed a significant decrease in both RSV and RRL, which is consistent with the idea that dynein behaves as a poorly processive motor (Figure 2-8B, Table 2-1, region 10; Table 2-2, region 20). Surprisingly, not all cytoplasmic dynein reduction genotypes showed the same effect for pause frequency and duration. Pause frequency is inversely proportional to run length, so increases in pause frequency should accompany decreases in run length. For dic^{3}/+, this is precisely what we observed—a decrease in run length and increase in pause frequency (RRL, Figure 2-8B, left; RPF, Figure 2-8C, left). However, we observed decreases in both RRL and RPF for *p4163*/+ and $robl^{k}$/+. In regards to pause duration, dic^{3}/+ and $robl^{k}$/+ showed significant increases in RPD, but *p4163*/+ showed a significant decrease. Though the pause frequency and duration data are somewhat perplexing, the trends are also true for region 20 data (Table 2-2). Thus, these data generally support the idea that cytoplasmic dynein *in vivo* acts as a poorly processive motor. In addition, the pause frequency analysis also highlights that DHC and DLC behave opposite to DIC.

Effects of cytoplasmic dynein reductions on APPYFP anterograde movement

In vitro experiments using a microtubule gliding assay have shown that only the strong state of cytoplasmic dynein binding to microtubules provides considerable drag to kinesin-1 (Vale, Malik et al. 1992). We tested this hypothesis using our DHC reduction alleles. If true, we expected that decreases in DHC would lead to decreases in cytoplasmic dynein motor number, subsequent reduction in dynein binding to microtubules, decreased drag force on kinesin-1, and ultimately faster anterograde velocities. Consistent with this hypothesis, we found that DHC reductions resulted in increases in mean ASV in both regions 10 and 20 (Figure 2-9A, right; Table 2-1, region 10; Table 2-2 region 20). In addition, cluster analysis on ASV data revealed a significant increase in mean ASV for 3/3 clusters in *dhc64c*$^{4\text{-}19}$/+ and 2/3 for *p4163/+* (Table 2-5, left). There was also an enhancement in the relative weight of ASV cluster 3 for *p4163/+* (Table 2-5, right; [control = 34.06%; *p4163/+* = 47.86%; percent increase above control = 41%]). These data suggest that DHC can in fact inhibit kinesin-1 powered movement *in vivo*.

Because we observed subunit-dependent effects for cytoplasmic dynein reductions in our analysis of retrograde movement, we looked to see if this was also true for anterograde movement. As discussed above, DHC reduction led to a significant increase in ASV. In addition, it led to increases in ARL in both regions 10 and 20 (Figure 2-9A, left; Table 2-1, region 10; Table 2-2, region 20). DLC reduction had little effect on anterograde movement, but observed effects were similar to those for DHC (Table 2-1, note significant increase in ARL; Figure 2-9A, left). However, ASV and ARL analysis revealed that DIC reductions had opposite effects compared to

DHC. DIC reductions showed a highly significant impairment in ASV and ARL in both regions 10 and 20 (Figure 2-9A and Table 2-1, region 10; Table 2-2, region 20). These changes were accompanied by increases in APF and APD in region 10 (Figure 2-9B; Table 2-1; dic^{3}/+ also showed a significant increase in APF and APD in region 20). In addition, cluster analysis of the *dic*/+ ASV data showed a significant decrease in mean ASV for all 3 clusters, and weight analysis revealed a dramatic shift from fast to slow moving clusters (Table 2-5). Thus, DHC and DIC reductions have opposite effects on anterograde movement, with DHC emerging as a potential inhibitor and DIC an activator of kinesin-1 motion.

Effects of dynactin reductions on APPYFP anterograde movement

Reductions in dynactin have been reported to affect bi-directional movement (Gross, Welte et al. 2002; Haghnia, Cavalli et al. 2007). We tested this hypothesis by looking at how reduction in single components of the dynactin complex affected APPYFP movement. We began by looking at how dynactin reductions affected cargo populations. This analysis revealed that all dynactin reductions caused a significant decrease in retrograde and reversing populations in region 10. Surprisingly, we observed no change in stationary and anterograde percentages for *grid*/+ or gl^{1}/+ (Figure 2-10A, left; Table 2-3, left), but flux analysis revealed a significant decrease in bi-directional flux (Table 2-3, right. Intriguingly, dmn^{5499}/+ showed a significant decrease in all populations except for anterograde, which was significantly increased. In addition, flux and A/R ratio increased significantly in dmn^{5499}/+ (Figure 2-10A, right; Table 2-3). However, these changes were only observed in region 10 as dmn^{5499}/+ showed no effect on cargo percentages, A/R ratio, and anterograde flux in

region 20 (Table 2-4). The only observed change for *dmn*^{5499}/+ in region 20 was retrograde flux, which decreased significantly. There was also a change in behavior for *grid*/+ and *gl*^{1}/+ in region 20, with significant enhancement in stationary cargo percentage for both conditions and decrease in all other moving populations for *gl*^{1}/+ (Table 2-4, left). Changes in flux followed those observed in region 10, with significant decreases to bi-directional flux in both *grid*/+ and *gl*^{1}/+ (Table 2-4, right). Thus, the effects of dynactin on APPYFP transport seem to be subunit dependent like what we observed for cytoplasmic dynein.

Effects of dynactin reductions on APPYFP retrograde movement

Dynactin has been proposed to serve as a processivity factor for cytoplasmic dynein (King and Schroer 2000; Schroer 2004). We tested this hypothesis by looking at how reductions in dynactin affect retrograde movement. In region 10, we observed a significant decrease in both RRL and RSV for all conditions studied (Figure 2-10B; Table 2-1). RPF and RPD changed significantly only in *dmn*^{5499}/+, with pause frequency decreasing and pause duration increasing significantly. In general, a similar effect was observed in region 20, with *grid*/+ and *gl*^{1}/+ showing a significant decrease in RRL and RSV (Table 2-2). In addition, RPF and RPD increased significantly in these groups. For *dmn*^{5499}/+, the only significant change was decrease in RSV. Taken together, these data support the hypothesis that dynactin is a processivity factor for cytoplasmic dynein.

Effects of dynactin reductions on APPYFP anterograde movement

Although *grid*/+ and *gl*^{1}/+ animals did not show significant changes in the percentage of anterograde cargoes in region 10, the observed decrease in anterograde

flux is suggestive of movement impairment. Thus, we looked at how anterograde transport parameters were affected with dynactin reductions. We found that in region 10 ASV was significantly reduced in all groups (Figure 2-11A, right; Table 2-1), and ARL was significantly reduced in *grid*/+ animals (Figure 2-11A, left; Table 2-1). In addition, there was a significant increase in APF and APD for all conditions studied (Figure 2-11B; Table 2-1). A similar scenario was observed for *grid*/+ in region 20, with decreases in GRID leading to significant decreases in ASV and ARL (Table 2-2). No significant changes in APF and APD accompanied these changes. Surprisingly, ARL increased for dmn^{5499}/+ in region 20 again showing that different subunits of dynactin can have different effects on anterograde movement. Overall, these data are consistent with the idea of dynactin as a key regulator of anterograde movement.

Effects of kinesin-1 overexpression on APPYFP movement

As described above, kinesin-1 decreases impaired bi-directional transport of APPYFP. Though we expected to see a decrease in ARL, APF, and APD with kinesin-1 reductions, the profound effects on RRL, RPF, and RPD were surprising. One intriguing possibility is that kinesin-1 acts as an activator and processivity factor for cytoplasmic dynein. If so, increases in kinesin-1 would be expected to activate bi-directional transport due to increased motor number on APPYFP vesicles. If such increased occurred, both ARL and RRL would be expected to increase due to further enhancement of cytoplasmic dynein processivity by kinesin-1. We set out to test this hypothesis by measuring APPYFP movement in a kinesin-1 background where both KLC and KHC subunits were overexpressed. Since both KHC and KLC transgenes were under control of endogenous promoter and regulatory domains (see Methods),

we expected that overexpression of kinesin-1 would be roughly double that found in wild type animals. As expected, Western blot analysis of kinesin-1 genomic lines showed that increasing kinesin-1 gene expression resulted in increases in kinesin-1 protein levels (Figure 2-12). As for the kinesin-1 reduction Western, KLC expression was affected by changes in KHC expression but not vice versa.

We next looked at how overexpression in both KLC and KHC affected APPYFP transport. Cargo population analysis in region 10 showed a significant increase in anterograde and decrease in reversing percentages (Figure 2-13A; Table 2-3, left). However, this increase in anterograde percentage did not significantly change the A/R ratio. Neither did it seem to lead toward improved movement because there was a bi-directional decrease in flux (Table 2-3, right). Similarly, analysis of region 20 revealed a significant increase in stationary and decrease in anterograde cargo percentages (Table 2-4, left). This significantly affected the A/R ratio, causing it to decrease significantly. As with region 10, there was also a significant decrease in bi-direction flux (Table 2-4, right).

To determine if kinesin-1 overexpression causes enhancement in anterograde behavior, we analyzed anterograde APPYFP movement. We observed that kinesin-1 increases led to significant decreases in both mean ASV and ARL, and this was true for both regions 10 and 20 (Figure 2-13B; Table 2-1, region 10; Table 2-2, region 20). Furthermore, there was a significant increase in APF and APD in region 10 (Figure 2-13C). Consistent with these findings, anterograde cluster analysis showed a dramatic shift in weight, with enhancement in clusters 1 and 2 and decrease in cluster 3 (Table 2-5, right). Thus, increases in kinesin-1 did not activate anterograde movement.

We next looked to see if kinesin-1 overexpression activates retrograde movement. Our analysis of retrograde transport parameters showed a significant decrease in both mean RSV and RRL in both regions 10 and 20 (Figure 2-14A; Table 2-1, region 10; Table 2-2, region 20). Though there was no change in RPF and RPD in region 10 (Figure 2-14B), region 20 data showed a significant increase in RPF and RPD. These data clearly show that kinesin-1 overexpression does not activate retrograde movement.

Effects of DIC overexpression on APPYFP movement

As discussed above, we observed that DHC and DIC reductions had opposite effects on anterograde movement, with *dhc/+* improving and *dic/+* impairing transport. These experiments show that dynein can be both activating and inhibitory to kinesin-1. To test the hypothesis that DIC plays an activating role to kinesin-1, we overexpressed DIC (GENDIC) and looked at how this manipulation affected anterograde movement. Cargo population analysis for GENDIC region 10 showed a significant decrease in stationary and reversing cargo percentages with concomitant increase in anterograde percentage (Figure 2-13A; Table 2-3). In agreement with these findings, anterograde flux increased significantly for GENDIC in region 10 (Table 2-3, right). Interestingly, no observed changes in cargo population and flux were found in region 20 (Table 2-4).

We next looked to see if DIC overexpression had any effect on anterograde transport. Indeed, we observed a significant increase in both ASV and ARL for region 10 (Figure 2-13, Table 2-1). Cluster analysis of ASV also showed a significant increase in mean values for all 3 clusters (Table 2-5, left). Intriguingly, our cluster

weight analysis showed a 41% decrease in ASV cluster 2 weight but a bi-modal enhancement in both clusters 1 and 3 [cluster 1 increase = 30%; cluster 3 increase = 13%]. Though these results may appear perplexing at first, they are consistent with our previous findings that DHC and DIC have different effects on anterograde movement. Thus, the observed enhancement in cluster 1 might be due to enhanced DHC drag on kinesin-1 and the increase in cluster 3 the effect of DIC activation on kinesin-1.

If DIC overexpression translates into increases to motor number, one might expect to see improvements to retrograde RL and SV in GENDIC. Indeed, we found a significant increase in both RRL and RSV for GENDIC in region 10 (Figure 2-14A; Table 2-1). In addition, the increase in RRL was accompanied by significant decreases in RPF (Figure 2-14B, left; Table 2-1). Surprisingly, RPD increased significantly (Figure 2-14B, right).

Though evidence from the above data clearly supports a model for DIC activation of kinesin-1, this was not supported by analysis of region 20 data. In this posterior region, GENDIC led to significant bi-directional decreases in ASV and ARL and a significant increase in RPF and RPD (Table 2-2). These findings support the idea of regional differences in axonal transport.

Testing of a KLC-DIC-p150^{Glued} switching model

Previous biochemical evidence suggests that kinesin-1 and cytoplasmic dynein can interact directly via KLC-DIC (Ligon, Tokito et al. 2004). In addition, DIC has been shown to interact directly with p150^{Glued} (Schroer 2004). We asked if these interactions might lie at the heart of a switching mechanism between anterograde and

retrograde motion. We hypothesized that dynactin acts as a regulator of bi-directional transport by competing with kinesin-1 for binding to cytoplasmic dynein. Under this "competition model," the KLC-DIC interaction is presumed to inhibit kinesin-1. When switching occurs, $p150^{Glued}$ engages DIC thereby removing inhibition on kinesin-1.

We tested this model by studying a double reduction background where both GRID and DIC were reduced (i.e., *dic*^{3}/+; *grid*/+). If the competition model were correct, the prediction would be that in the double mutant there should be rescuing of anterograde movement as compared to *grid*/+ (i.e., the KLC-DIC interaction is increased in *grid*/+). Our analysis of cargo populations in region 10 revealed a significant decrease in stationary and increase in anterograde percentages for *dic*^{3}/+; *grid*/+ (Table 2-3; statistical comparison between *grid*/+ and *dic*^{3}/+; *grid*/+ is at the bottom). In addition, anterograde flux was significantly increased in *dic*^{3}/+; *grid*/+ (Table 2-3, right). We next inspected anterograde motion parameters and found a significant increase in both ASV and ARL with concomitant decrease in APF and APD (Table 2-1). Interestingly, activation of anterograde movement was only observed in the proximal region. In region 20, there was no significant change to either ASV or ARL (Table 2-2).

Surprisingly, double reductions in DIC and GRID also showed activation of retrograde movement. This is perplexing given that the single allelic reductions showed a dramatic worsening in RRL and RSV (Table 2-1). In particular, we observed that RRL increased significantly for *grid*/+; *dic*^{3}/+ in both regions 10 and 20 (Table 2-1, region 10; Table 2-2, region 20). For region 10, increased RRL was the

only observed change. However, RSV increased significantly in region 20, and there were significant decreases in both RPF and RPD (Table 2-2). Thus, the *grid*/+; *dic*^{3}/+ data in region 10 supported the proposed competition model, but not all experimental results could be easily reconciled.

Discussion

We set out to study how kinesin-1 and cytoplasmic dynein regulate their activity to achieve bi-directional movement. Using a novel *in vivo* polarized neuronal system, we tested conventional as well as novel hypotheses for how these motors function and interact. Thousands of trajectories were generated for APPYFP vesicles, which we analyzed and compared to several models describing axonal transport. Five possible models were scrutinized using this vast data set: 1) the standard model; 2) the tug-of-war model; 3) the ternary complex model; 4) the competition-inhibitory model; and 5) the competition-activating model. For all these models, kinesin-1, cytoplasmic dynein, and dynactin are thought to co-exist on the surface of vesicles. However, each model makes unique predictions based on interactions between motors and how the activity of a motor impacts the function of the other (Table 2-7).

As described above, the standard model for axonal transport found in textbooks and encyclopedias states that kinesin-1 (1) moves unidirectionally within axons and powers anterograde movement; (2) is a highly processive motor whose function does not require a co-factor; (3) does not regulate retrograde activity. For cytoplasmic dynein, the motor is thought to (1) move unidirectionally within axons and power retrograde movement; (2) behave as a poorly processive motor; (3) require dynactin for attachment to vesicles and processive movement. However, neither our data nor a host of recent reports support the standard model. For instance, we observed that reductions in kinesin-1 dramatically impaired APPYFP retrograde movement. In addition, cytoplasmic dynein reduction interfered with anterograde

movement. Furthermore, dynactin reduction impaired bi-directional movement. These observations do not fit the predictions made by the standard model (Table 2-7).

Another possible mechanism for motor regulation in axonal transport is the tug-of-war model. In this model, both motors are predicted to be active simultaneously, and differences in motor number or activity determine net movement (Gross 2004). As a result, decreases in one polarity motor are predicted to improve the movement of opposite polarity motors. In general, our data was not consistent with this model (Table 2-7). For instance, decreases in kinesin-1 did not improve retrograde movement. Remarkably, decreases in DHC had an activating effect on anterograde movement, which we interpret as evidence for dynein-mediated drag on kinesin-1 (Vale, Malik et al. 1992). The fact that other studies did not report similar findings for DHC (Gross, Welte et al. 2002) may have to do with the extent of dynein reduction or the vesicle type studied. Indeed, we have found that reductions in DHC and DIC have opposite effects on anterograde transport, with DIC reductions impairing it. This suggests that heterogeneity may exist in cytoplasmic dynein complexes such that partial complexes lacking only DHC may exist. If so, milder reductions in DHC may not significantly affect DIC levels. Of course, some amount of regulation and inter-dependence must exist where removal of one subunit begins to adversely affect that of the other. This would explain why complete removal of DLC is reportedly lethal (Gunawardena and Goldstein 2001). Thus, the results reported by Gross and colleagues may differ from ours because we only reduced DHC by 50% whereas they almost completely removed DHC by using a trans-heterozygous approach.

In the lipid droplet system, Gross and colleagues have found much evidence in favor of a coordination mechanism between kinesin and dynein motors. Interestingly, their work also showed a balance between the stalling force in anterograde and retrograde directions (Gross 2004). As implied by its name, the stalling force is the laser trap force required to stall a single vesicle and may correlate to the number of active motors. Because the stalling force for a single kinesin-1 and cytoplasmic dynein motor was found to be identical—1.1 pN, this suggests that active kinesin and dynein motors may exist as identical ratios on the surface of vesicles. Thus, we wondered if a "ternary complex" consisting of kinesin-1, cytoplasmic dynein, and dynactin might exist as a motor complex unit that is minimally required for functional transport. If so, evidence in support of a ternary complex model would follow specific predictions. First, reduction in any component of the complex would be expected to have detrimental implications for bi-directional transport. Similarly, overexpression of a single component might activate bi-directional transport if one assumes that no component is particularly limiting. If components were limiting no improvement would be expected. Switching under this model would be expected to rely on antagonist force generated by the opposite polarity motor, curbing any such role for dynactin.

Several examples can be found in our data set to support the ternary complex model (Table 2-7). For example, reductions in kinesin-1 and dynactin led to bi-directional transport impairment. In addition, DIC overexpression led to bi-directional activation in region 10. However, many other pieces of data do not support this model. For instance, DHC reduction increased ARL and ASV, and overexpression of

kinesin-1 resulted in bi-directional impairment. In addition, switch frequency decreased significantly for the majority of conditions we studied, which is not predicted by the ternary complex model. This is especially true for conditions such as kinesin-1 reductions where swelling number increased dramatically.

As we surveyed the literature looking for key interactions between motors and key accessory proteins that could comprise the core of a regulatory mechanism, we found only two potential targets. Biochemical evidence supports a direct interaction between (1) KLC and DIC and (2) DIC and the $p150^{Glued}$ subunit of dynactin (Ligon, Tokito et al. 2004; Schroer 2004). This is intriguing because it suggests the possibility of a switch mechanism with dynactin as the regulator between anterograde and retrograde movement. From our single reduction experiments, we noted that DIC reductions led to impairment in anterograde movement. This suggests that the KLC-DIC interaction is activating to kinesin-1. However, DHC reduction yielded improvement of anterograde behavior, which suggests that dynein can also be inhibitory to kinesin-1. Whichever the role of cytoplasmic dynein to anterograde movement, we realized that the DIC-$p150^{Glued}$ interaction could be competitive to KLC-DIC. This constitutes the core of a switch mechanism in the proposed "competition model," which we hypothesized could take two forms: the competition-inhibitory model and the competition-activating model. The only difference between these would lie in the role of the KLC-DIC interaction to anterograde movement. If the KLC-DIC interaction emerges as inhibitory, then reductions in DIC would be predicted to improve anterograde movement. If activating, the opposite would be true.

In general, our data agrees most with the competition-inhibitory model (Table 2-7). First, we observed that reductions in DHC led to increases in ARL. Second, reductions in dynactin generally led to impairment in anterograde behavior. This was especially true in *grid*/+, which comprised our best-characterized reduction. In Drosophila, complete removal of GRID—the arp1 mammalian homologue—appears to destabilize the entire dynactin complex (Haghnia, Cavalli et al. 2007). Third, overexpression of DIC showed a substantial increase in the weight of cluster 1—the slowest moving cluster (Table 2-5). Fourth, our GRID and DIC double reduction showed a significant increase in both ARL and ASV in region 10.

In spite of the above evidence, there are cases in which the data appears to contradict the competition-inhibitory model. Some of these discrepancies can be accounted for by considering the predictions made by our hypothesis that cytoplasmic dynein can form partial complexes. Under this notion, DHC and DIC can each form a partial complex with DLC. Reductions in DHC or DIC would be expected to enrich a partial complex pool lacking only the subunit being reduced. For example, DIC reductions would be expected to change the composition of dynein complexes on the surface of vesicles such that 50% of them would be comprised of DHC-DLC only. Though a stable protein complex, DHC-DLC may not necessary function optimally. The lack of DIC on these complexes removes their ability to communicate directly with KLC and $p150^{Glued}$, interactions that may be important for precise regulation of motor activity. DIC-DLC partial complexes, on the other hand, would be expected to bind normally to KLC and $p150^{Glued}$. Therefore, their impact on complex regulation and switching may not be significantly impaired.

Our analysis of DIC reductions revealed bi-directional impairment of RL and SV, which on the surface is not consistent with an inhibitor role for KLC-DIC on anterograde movement. However, this is in agreement with the partial complex hypothesis proposed above. Under this view, DIC reduction would be expected to impair retrograde movement due to loss of the DIC- $p150^{Glued}$ interaction that is important for processive movement of retrograde cargoes. As for anterograde, impairment could be expected if DHC-DLC complexes behave aberrantly and provide increased drag to kinesin-1. Thus, the first major apparent contradiction in the data can be resolved in light of the partial complex hypothesis.

The second major apparent inconsistency in the data comes from analysis of DIC overexpression. We observed a significant bi-directional enhancement of movement in region 10. The increase in retrograde behavior is consistent with increase in cytoplasmic dynein motor number. The increase in ARL and ASV, however, does not appear to support the inhibitory-competition model. Interestingly, careful inspection of the data revealed that it could also be explained in light of the partial complex hypothesis. Cluster analysis of ASV data showed a bi-modal enhancement in the weight of clusters 1 and 3. This finding is highly suggestive of increases in DHC-DIC-DLC as well as DIC-DLC cytoplasmic dynein complexes. Increases in the full complex would be expected to present increased drag on kinesin-1; increases in DIC-DLC would be expected to present less drag on kinesin-1. Seen from this angle, the DIC overexpression data is consistent with the inhibitory-competition model.

At first we were surprised by the lack of consistency between regions 10 and 20 in the DIC overexpression data. While in region 10 there was bi-directional enhancement in transport, region 20 did not show a similar effect. One possible explanation for this lies in protein diffusive behavior that likely plays a role here. Unlike fast axonal transport—which is in the order of 1 μm/sec, diffusion is many times slower. It is known that the rate of diffusional transport decreases with the square of the distance and can be roughly estimated by the equation $t = L^2/D_c$, where t = time, L = length of the process, and D_c = diffusion coefficient (Popov and Poo 1992). For a neurite axoplasm, the diffusion coefficient for a 60 kD protein has been estimated to be around 68 μm^2/sec (Popov and Poo 1992). Since region 20 is located approximately 2,000 μm from the cell body, DIC would take approximately 16 hours to reach this region! Thus, it is reasonable to assume that in DIC overexpression most of the effect would be localized to more anterior regions. If so, we would expect to see an even more dramatic effect for DIC overexpression by analyzing the data that we collected from regions 1.

In conclusion, the present study describes a novel mechanism for motor activity regulation and coordination in axonal transport. This testable model termed "inhibitory-competition model" was born out of data analysis for thousands of cargo trajectories. We believe that this study comprises the most complete such study to date. In the process, we developed a powerful analytical tool for accurately and effectively extracting transport parameters from single cargo trajectories. We hope that this tool will eventually benefit many laboratories working on similar problems. In addition, we hope to make our data set available to the public so in-depth analysis

using diverse perspectives may be applied to the same data set. Thus, we believe that the present study lays a strong foundation for follow-up studies on the topic of axonal transport.

Though most of our data supports the inhibitory-competition model, we realize that several issues remain unresolved. For one, it would be interesting to further investigate factors underlying the observed regional variability reported above. A second interesting set of experiments could focus on better understanding protein changes induced by single motor or motor accessory subunits. We have reported here that KLC seems to be sensitive to changes in KHC gene dosage but not vice-versa. Many other interesting interactions may be noted by similar protein analysis experiments. Their implications to transport could then be mapped back to movement parameters in our data. It should be noted that a major hurdle for Western blot studies at the moment is the availability of good antibodies. For this study we were fortunate to have good commercially available anti-KHC and anti-syntaxin antibodies. In addition, we used a good anti-KLC antibody recently generated by Dr. Jason Duncan, a postdoctoral fellow in the Goldstein lab. However, we tested many other antibodies for dynein subunits, but none gave good results. We hope that advances in the field will make better reagents available for these important experiments. Third, single vesicle analysis should allow extraction of information, which might help settle issues we were not able to resolve so far. For instance, immunofluorescence on single vesicles might help us determine how motor number changes with gene reduction. This would help us rule out the possibility that kinesin-1 reductions lead to cytoplasmic dynein reduction on the surface of vesicles. We have already begun to

develop an IF technique to test this possibility, and preliminary experiments have been encouraging. In addition, fluorescent labeling of motor protein subunits should help us confirm correlations between motor number, velocity and run length. This might be particularly interesting for kinesin-1, which seems to change behavior so dramatically *in vivo*. Fourth, biochemistry on vesicle floats might help determine if the hypothesis of partial complexes for cytoplasmic dynein has any solid basis. Together these additional studies would add important building blocks towards a more complete understanding of axonal transport mechanisms. This information will undoubtedly help us better understand basic biological pathways, which can better equip us to effectively remedy neurodegenerative diseases caused by failures in axonal transport.

Chapter 2 will be submitted for publication: Reis GR, Yang G, Szpankowski L, Danuser G, Goldstein LSB. "Mechanisms of motor activity regulation in axonal transport." The dissertation author was the primary author and investigator of this paper.

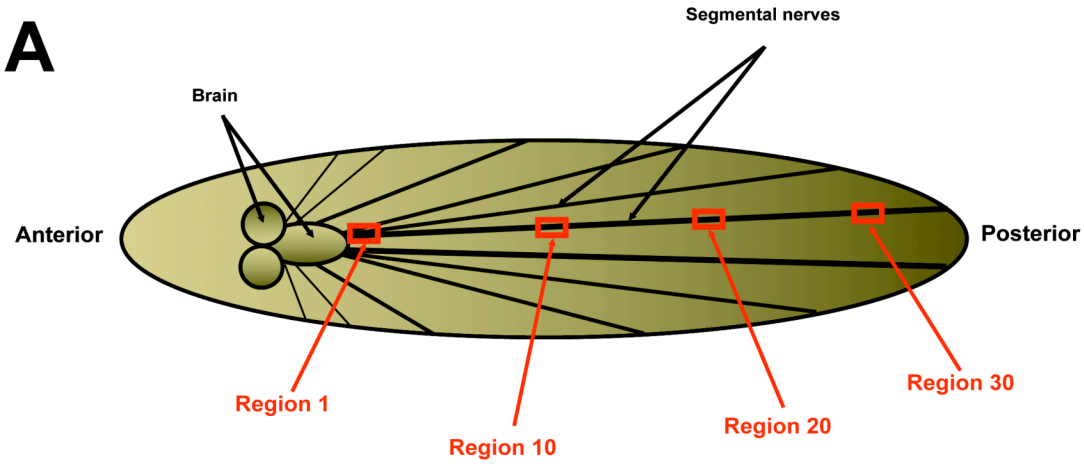

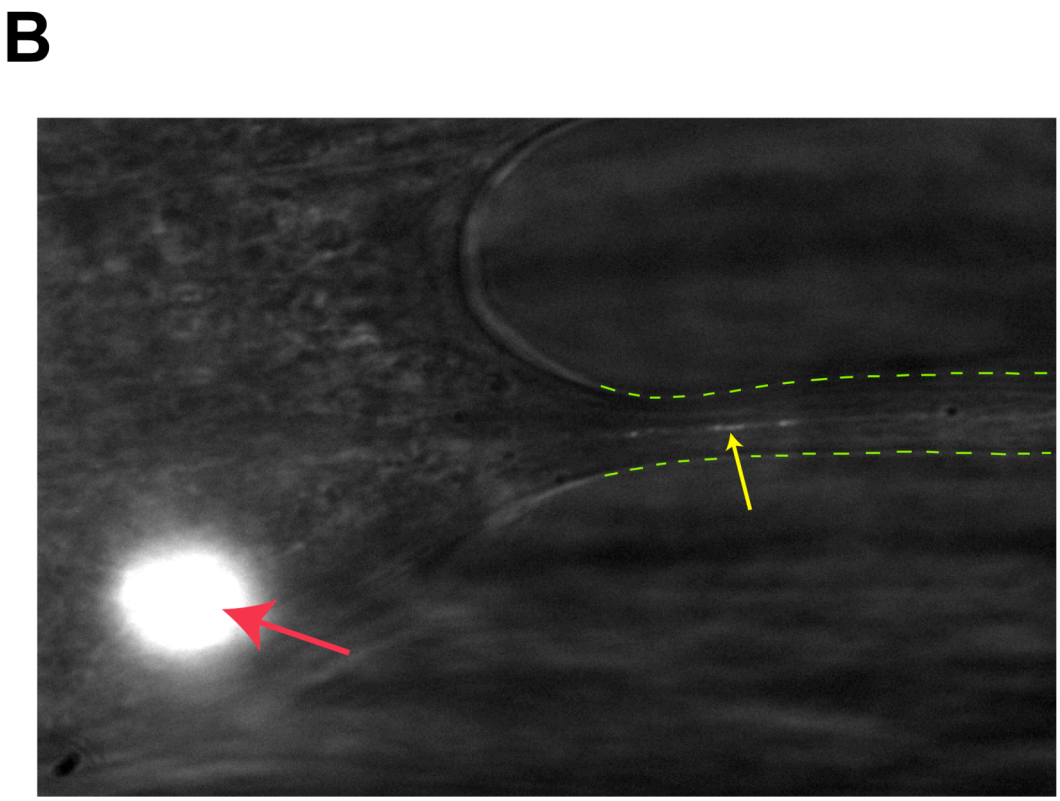

Figure 2-1. Imaging method and SG26.1 Gal4 UAS-APPYFP expression pattern. A) Schematic diagram of L3 Drosophila larvae showing important anatomical structures and regions imaged for each experiment. Each region is 900 microns apart, and region 1 is the first axonal regions from the cell body. B) Image taken from an L3 larvae at 100X showing a neuronal cell body (red arrow) and axon (yellow arrow) expressing APPYFP driven by SG26.1 Gal4. The fluorescent image is overlaid onto the DIC image, and the green dotted lines outline the nerve boundaries for region 1.

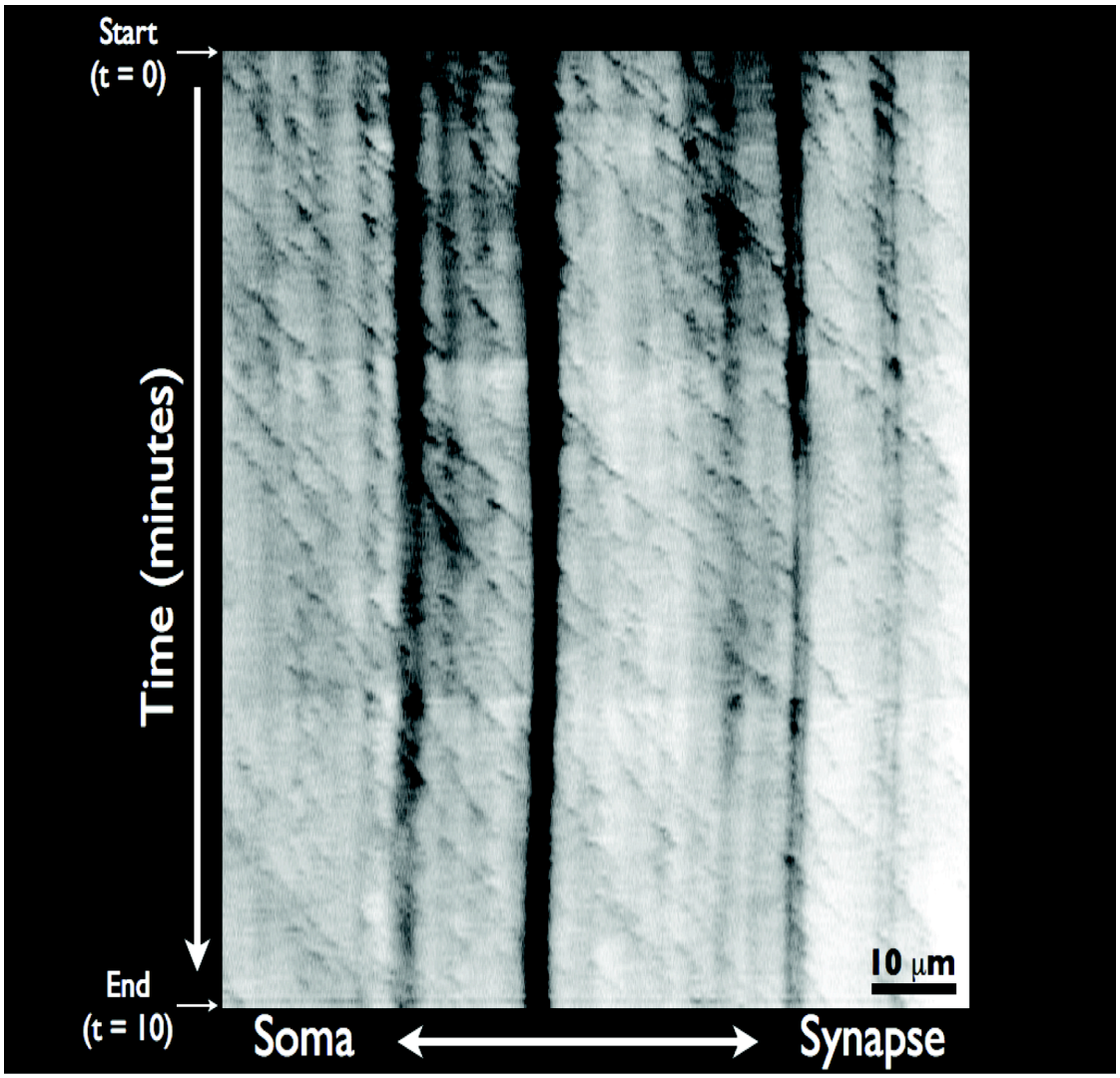

Figure 2-2. Movement of UAS-EB1GFP driven by SG26.1 Gal4 is primarily directed towards the synapse. Shown is a kymograph obtained by 10-minute time lapse imaging of UAS-EB1GFP (see Methods). The plus ends of microtubules are oriented towards the periphery of neurons ("synapse"); minus ends are oriented towards the cell body ("soma"). This kymograph suggests that anterograde movement can be unambiguously differentiated from retrograde in our system.

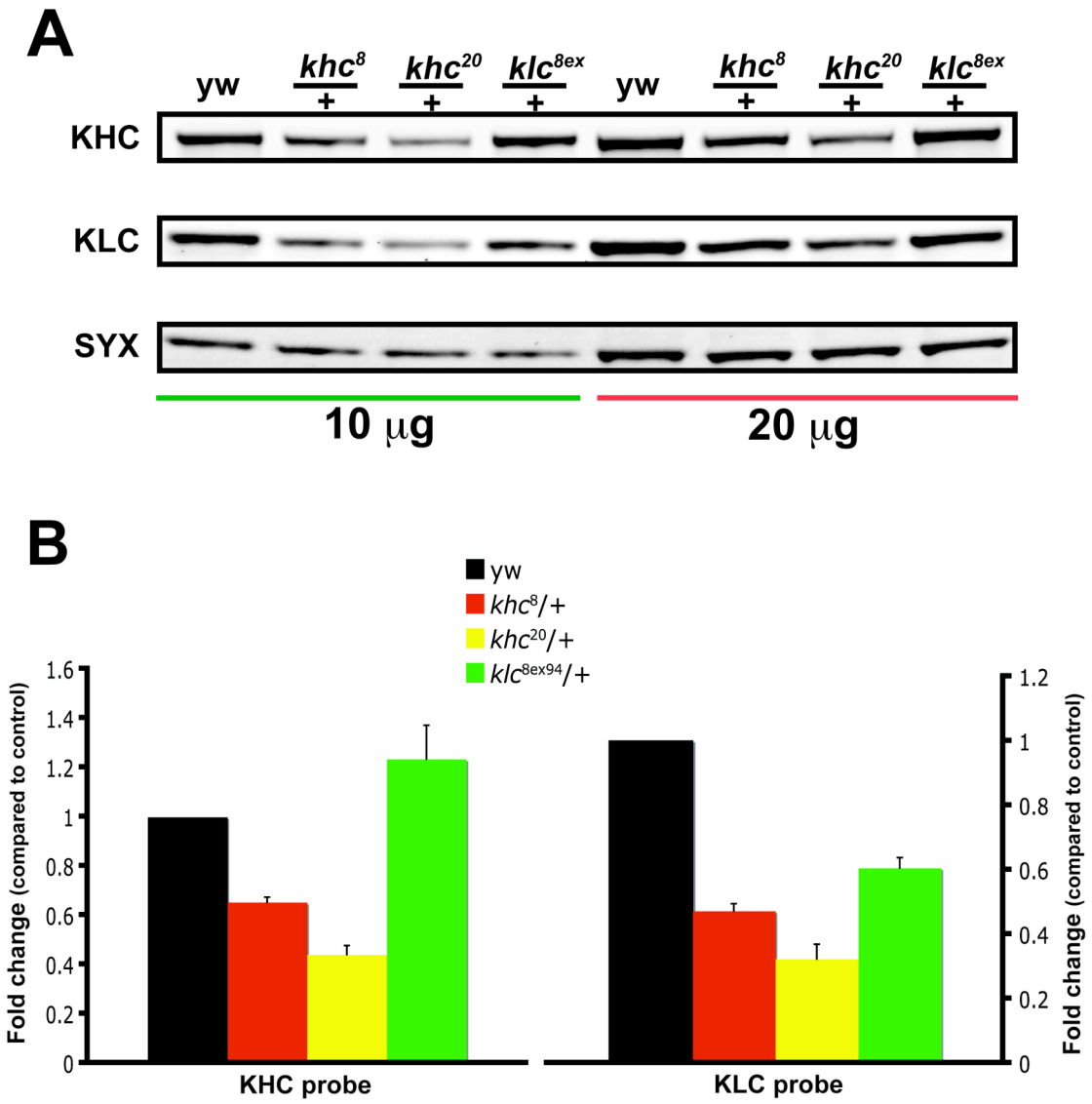

Figure 2-3. Kinesin-1 gene reduction leads to kinesin-1 protein reduction. A) Shown are 10 and 20 mg loadings of yellow white (yw) [control], khc8/+ and khc20/+ heterozygous point nulls, and the klc8ex94/+ heterozygous deletion null. Syntaxin was used as a loading control. B) Quantification of Western blot analysis. Left graph shows quantification for KHC probing. There was a 45% decrease in KHC protein for khc8/+ (0.65 ± 0.02) and 56% for khc20/+ (0.44 ± 0.04) [mean ± SEM]. KHC protein increased slightly when klc was reduced (klc8ex94/+ = 1.24 ± 0.14). The right graph shows quantification for the KLC probe. Both KHC and KLC protein decreased with klc reduction (khc8/+ = 0.47 ± 0.02; khc20/+ = 0.32 ± 0.05; klc8ex94/+ = 0.61 ± 0.03) [mean ± SEM].

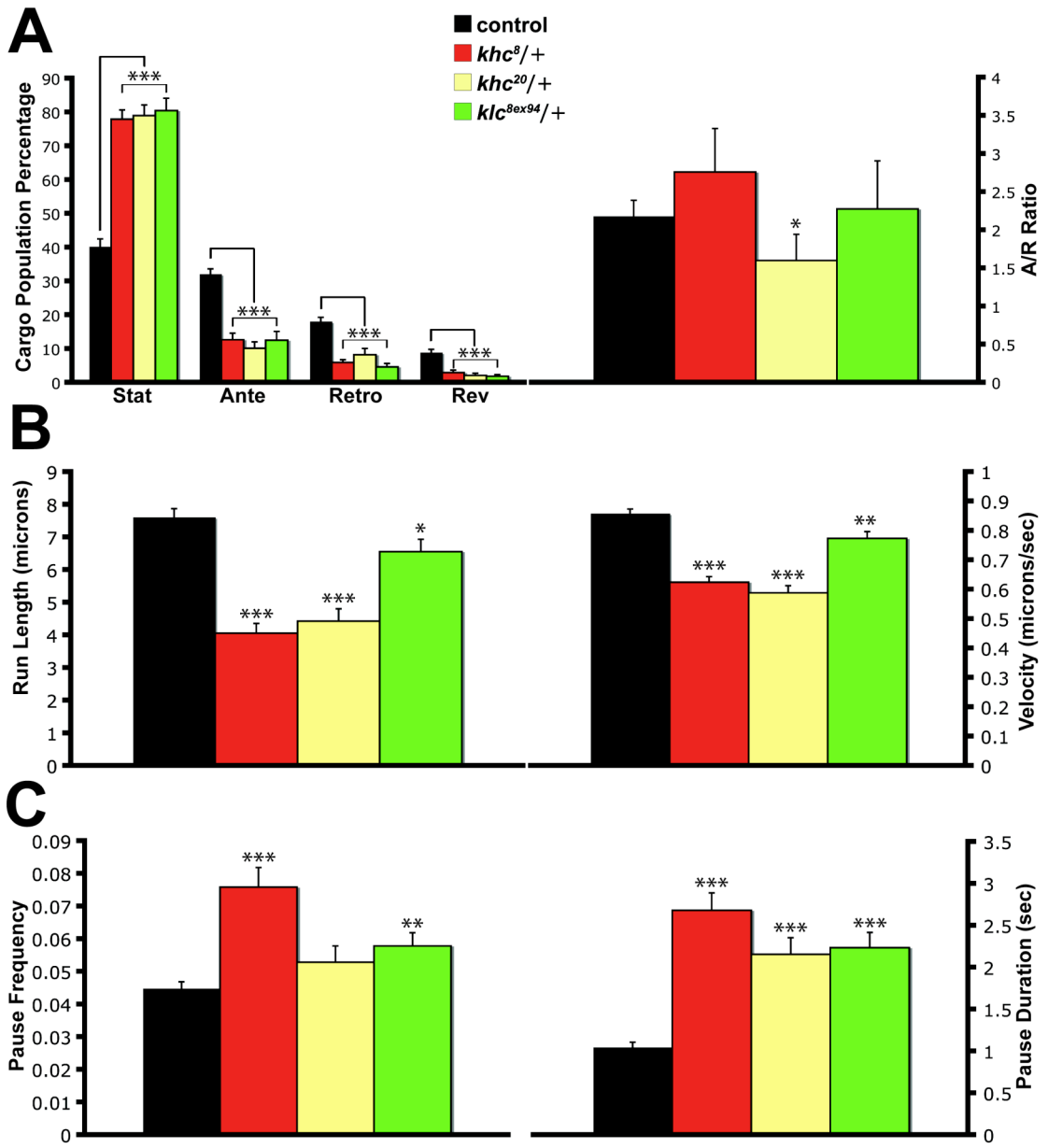

Figure 2-4. Effects of kinesin-1 gene reduction on APPYFP movement. A) Left: Cargo population analysis shows a significant increase in stationary cargo percentage and decrease in all moving populations. Abbreviations: stat, stationary; antero, anterograde; retro, retrograde; rev, reversing. Right: A/R ratio showing a significant decrease for khc20/+ . Refer to Table 2-3 for population percentage and A/R mean values. B) Left: ARL decreases significantly for kinesin-1 hets; Right: ASV decreases significantly in kinesin-1 hets. C) Left: APF increases significantly for khc8/+ and klc8ex94/+; Right: APD increases significantly in kinesin-1 hets. Statistical significance: * = $P < 0.05$; ** = $P < 0.01$; *** = $P < 0.001$. Refer to Table 2-1 for ARL, ASV, APF, and APD mean values. See Methods for a detailed definition for each parameter.

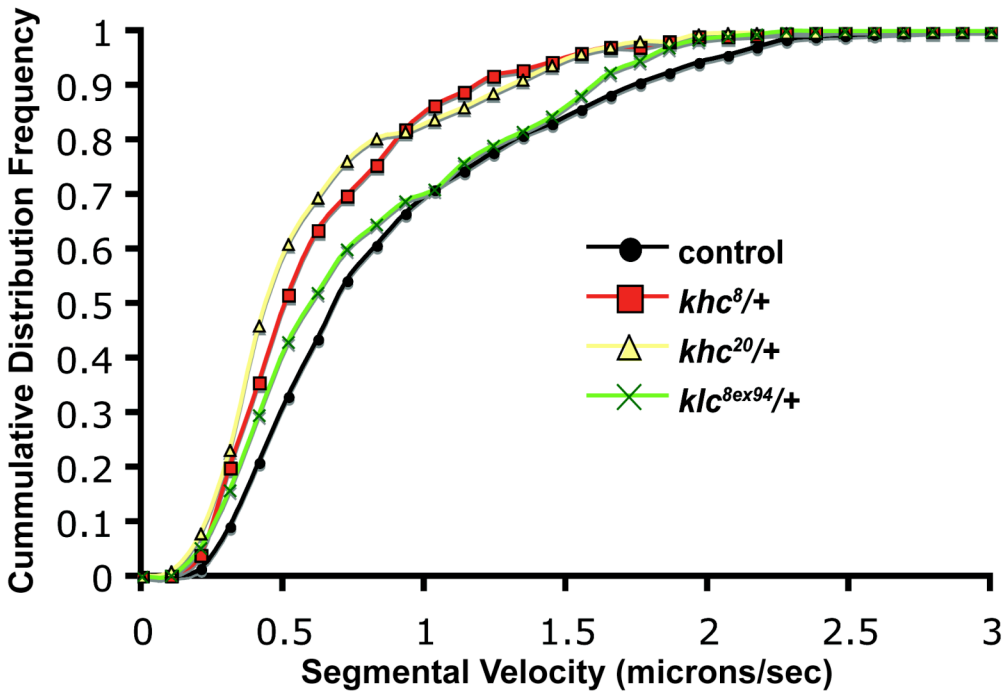

Figure 2-5. Effects of kinesin-1 gene reduction on anterograde segmental velocity. Cumulative frequency distribution plot showing a leftward shift in ASV with kinesin-1 reductions. Curves are for region 10 data. The leftward shift is significant [Kolmogorov-Smirnov test: $P < 0.001$ for the khc/+ alleles; $P < 0.01$ for the klc/+ allele].

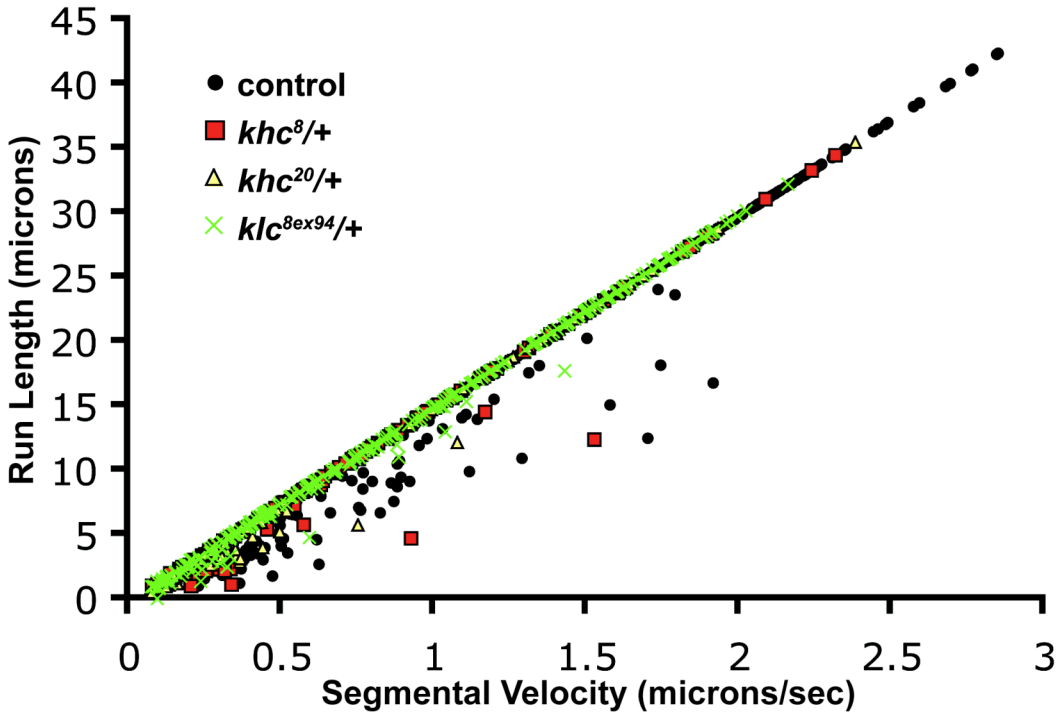

Figure 2-6. Anterograde segmental velocity vs. anterograde run length correlation analysis. Shown here are the overlaid scatter plots for control and kinesin-1 reduction genotypes using region 10 data. Remarkably, kinesin-1 reductions do not change the slope of the correlation, but they decrease fast moving and long moving populations.

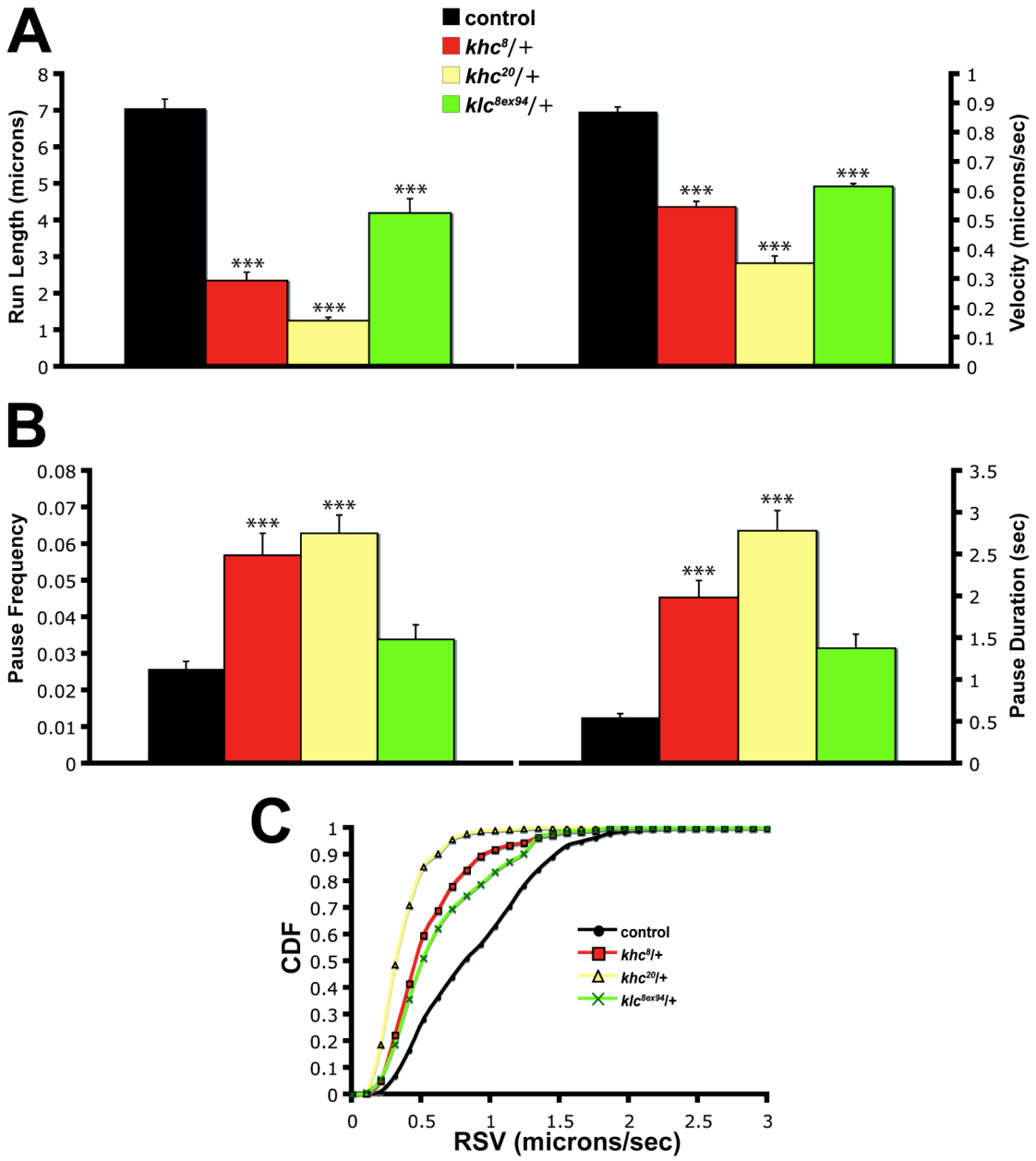

Figure 2-7. Effects of kinesin-1 gene reduction on retrograde movement of APPYFP vesicles. A) Left: RRL decreases significantly in kinesin-1 heterozygotes (hets); Right: RSV decreases significantly in kinesin-1 hets. B) Left: RPF increases significantly for khc8/+ and khc20/+; Right: RPD increases significantly for khc8/+ and khc20/+. Statistical significance: *** = $P < 0.001$. Refer to Table 2-1 for RRL, RSV, RPF, and RPD mean values. See Methods for a detailed definition of each parameter. C) Cumulative frequency distribution (CDF) plot showing a leftward shift in RSV with kinesin-1 reductions. Curves are for region 10 data. The leftward shift is significant [Kolmogorov-Smirnov test: $P < 0.001$ for all alleles].

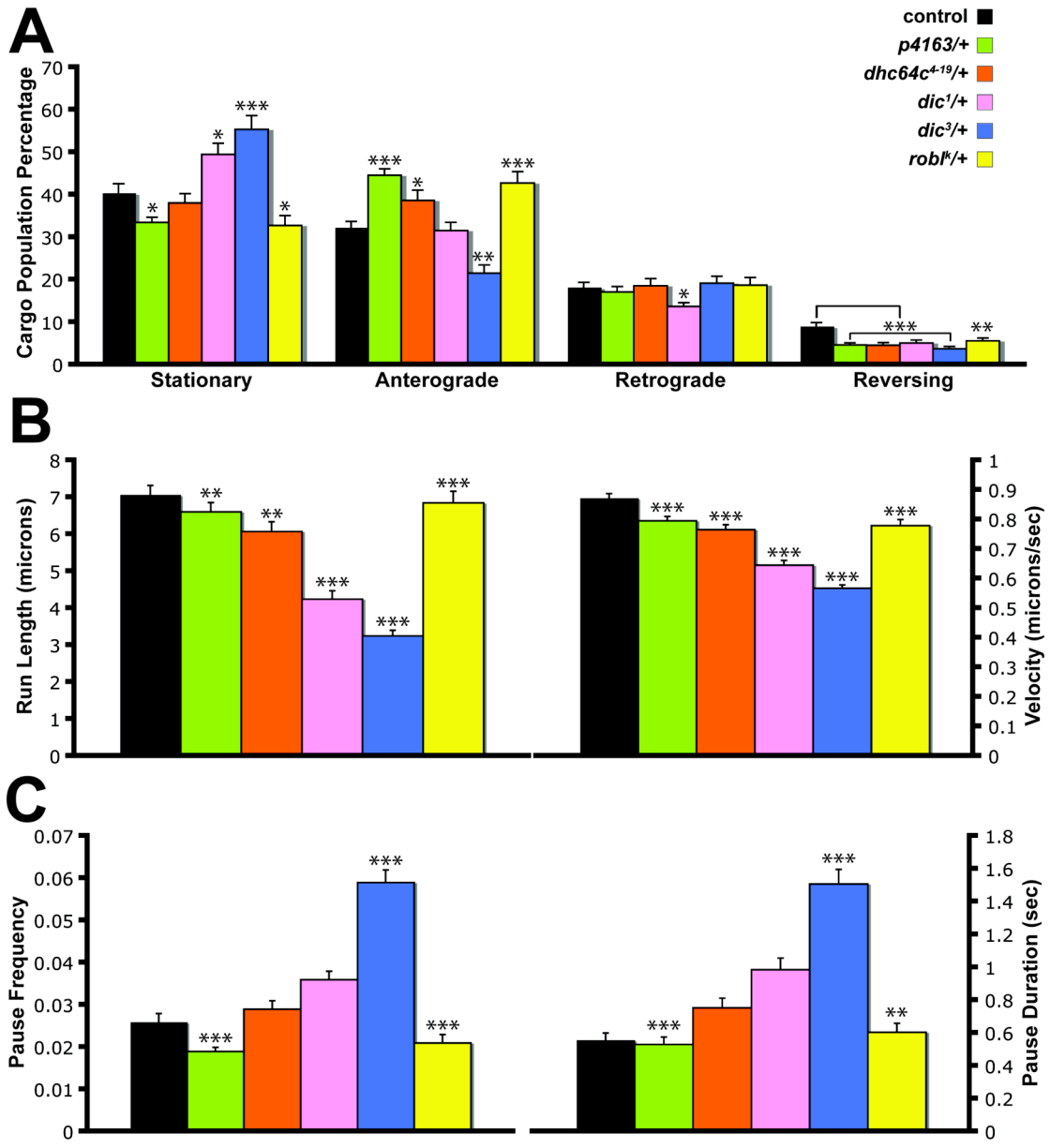

Figure 2-8. Effects of cytoplasmic dynein gene reductions on retrograde APPYFP movement for region 10. A) Cargo population analysis showing the mixed effects of cytoplasmic dynein reductions on population percentages. DHC and DLC reductions generally increase anterograde and decrease stationary percentages significantly; DIC reductions generally increase stationary percentage significantly at the expense of moving cargo percentages. B) RRL (Left) and RSV (Right) decrease significantly in all cytoplasmic dynein hets. C) RPF (Left) and RPD (Right) increase significantly for p4163/+, dic3/+ and roblk/+. Statistical significance: * = $P < 0.05$; ** = $P < 0.01$; *** = $P < 0.001$. Refer to Table 2-1 for RRL, RSV, RPF, and RPD mean values. See Methods for a detailed definition for each parameter.

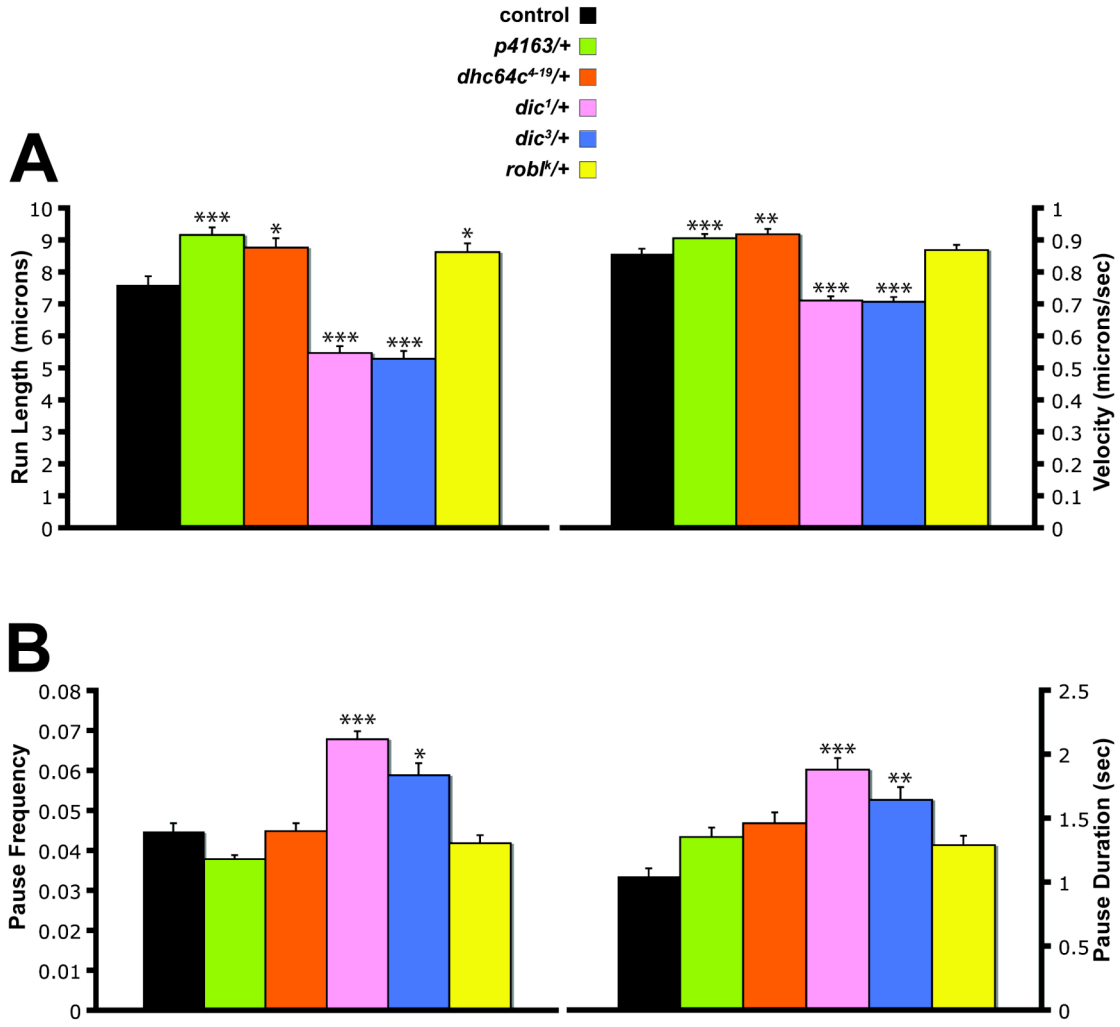

Figure 2-9. Effects of cytoplasmic dynein gene reductions on anterograde APPYFP movement for region 10. A) ARL (Left) and ASV (Right) can increase or decrease depending on the cytoplasmic dynein subunit being reduced: DHC reductions lead to increases in ARL and ASV; DIC reductions lead to decreases in ARL and ASV. B) APF (Left) and APD (Right) increase significantly for dic1/+ and dic3/+ alleles. Other dynein alleles have no effect on APF and APD. Statistical significance: * = $P < 0.05$; ** = $P < 0.01$; *** = $P < 0.001$. Refer to Table 2-1 for ARL, ASV, APF, and APD mean values. See Methods for a detailed definition of each parameter.

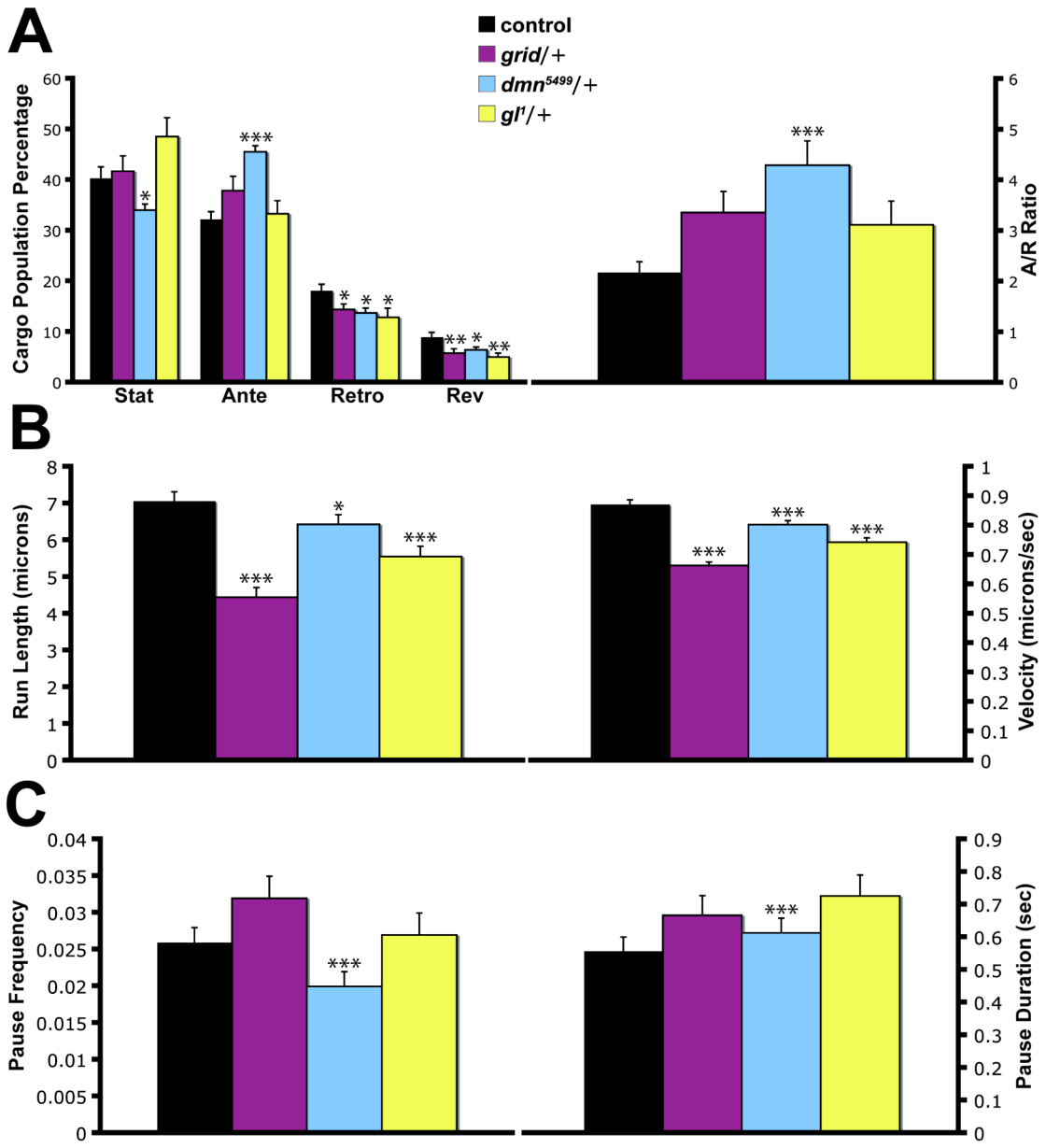

Figure 2-10. Effects of dynactin reductions on retrograde APPYFP movement. A) Left: Cargo population analysis showed a significant decrease in retrograde and reversing percentages for all conditions. For dmn5499/+, there was also a significant decrease in stationary and increase in anterograde percentages. Abbreviations: stat, stationary; antero, anterograde; retro, retrograde; rev, reversing. Right: A/R ratio showing a significant increase for dmn5499/+. Refer to Table 2-3 for population percentage and A/R mean values. B) RRL (Left) and RSV (Right) decreased significantly with dynactin reductions. C) RPF (Left) decreased and RPD (Right) increased significantly only for dmn5499/+. Statistical significance: * = $P < 0.05$; ** = $P < 0.01$; *** = $P < 0.001$. Refer to Table 2-1 for RRL, RSV, RPF, and RPD mean values. See Methods for a detailed definition of each parameter.

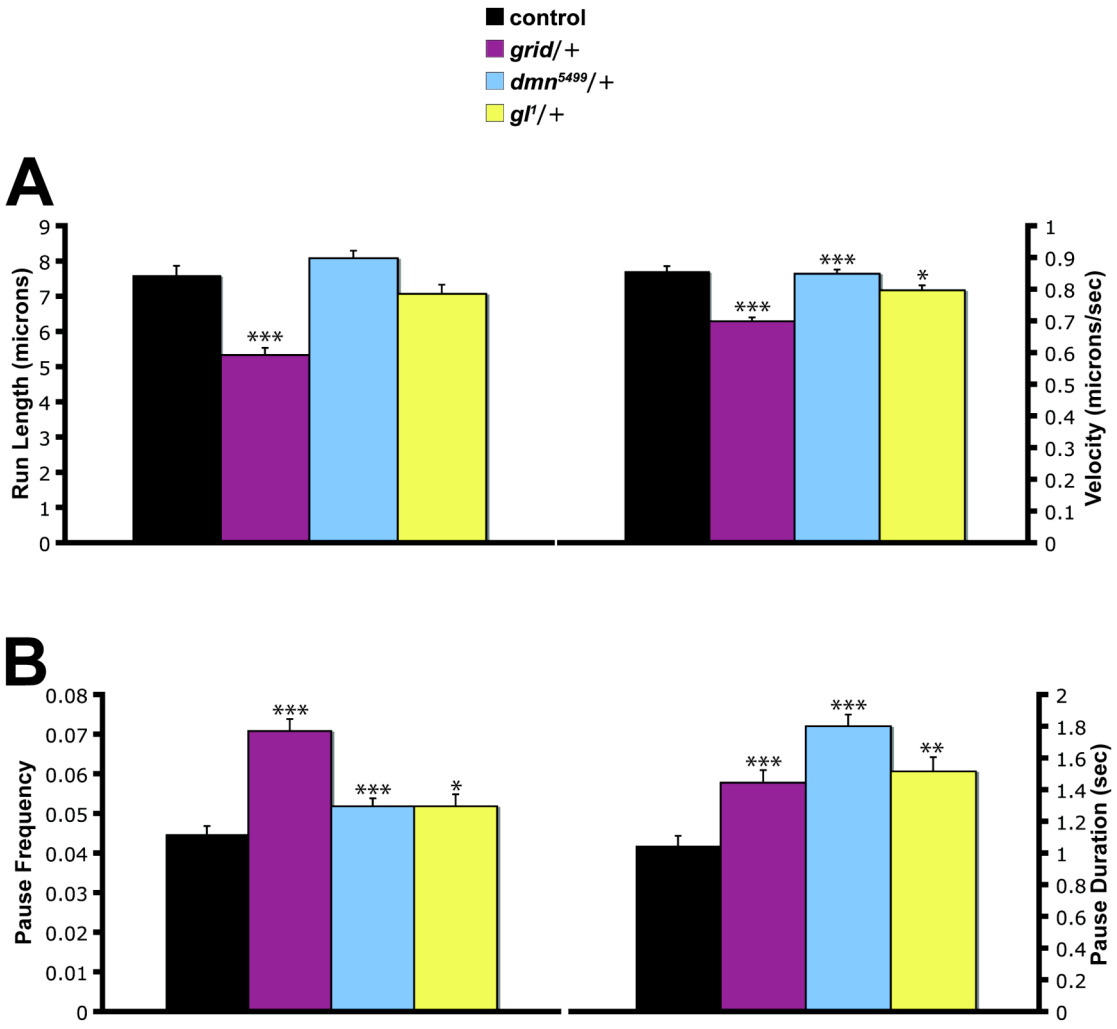

Figure 2-11. Effects of dynactin reductions on anterograde APPYFP movement for region 10. A) (Left): ARL decreased significantly in grid/+; (Right) ASV decreased significantly for all conditions studied. B) APF (Left) and APD (Right) increased significantly for all conditions studied. Statistical significance: * = $P < 0.05$; ** = $P < 0.01$; *** = $P < 0.001$. Refer to Table 2-1 for ARL, ASV, APF, and APD mean values. See Methods for a detailed definition of each parameter.

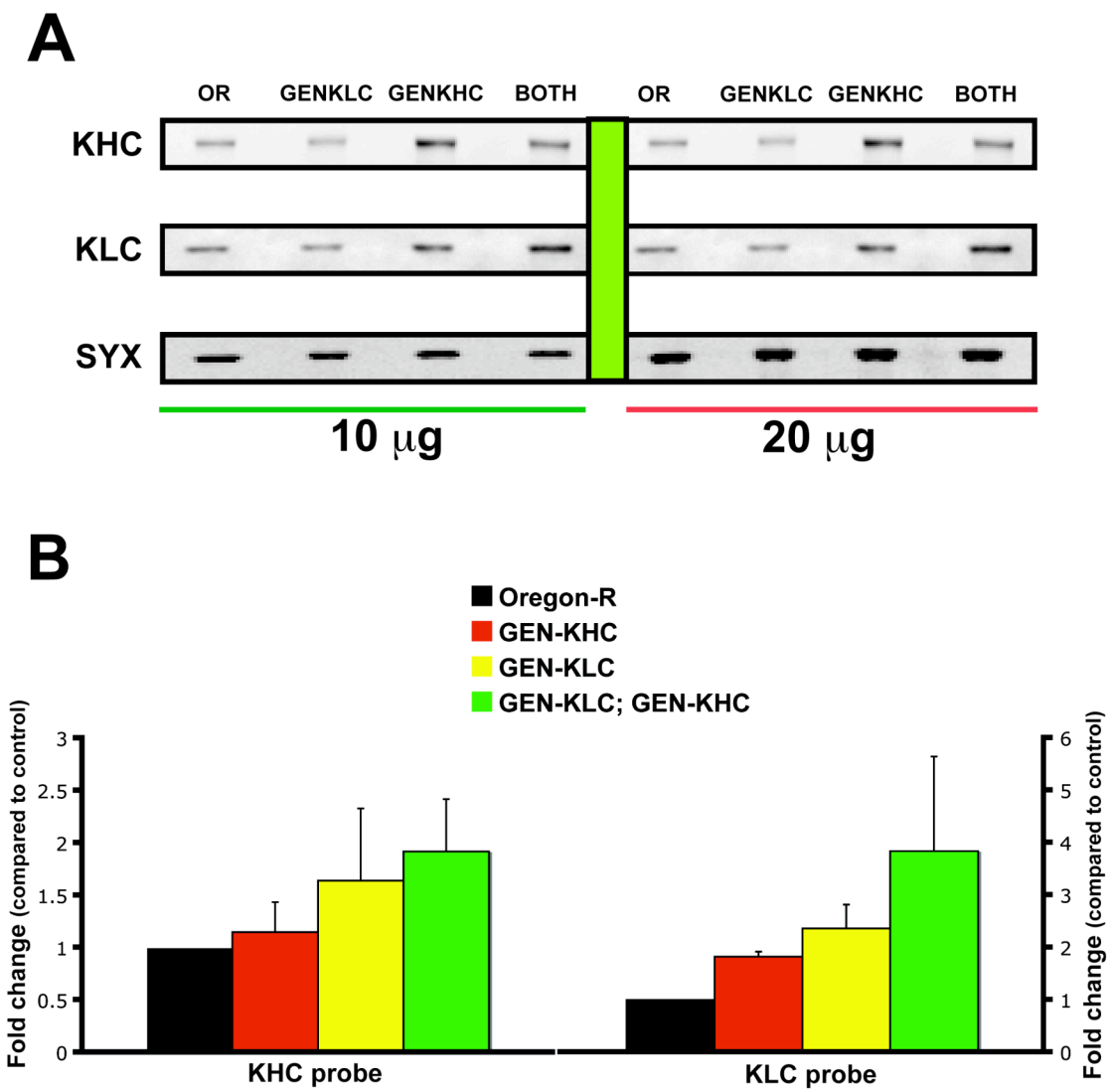

Figure 2-12. The overexpression of kinesin-1 gene leads to kinesin-1 protein overexpression. A) Shown are 10 and 20 mg loadings of Oregon-R (OR) [control], GEN-KLC, GEN-KHC, and GEN-KLC + GEN-KHC (BOTH). Syntaxin was used as a loading control. B) Quantification of Western blot analysis. Left) Quantification of KHC probe: GEN-KLC = (1.15 ± 0.29), GEN-KHC = (1.64 ± 0.69), and BOTH = (1.92 ± 0.50) [mean ± SEM]. Right) Quantification of KLC probe: GEN-KLC = (1.82 ± 0.10), GEN-KHC = (2.37 ± 0.45), and BOTH = (3.84 ± 1.81) [mean ± SEM]. KLC expression seems to be affected by KHC expression but not vice-versa.

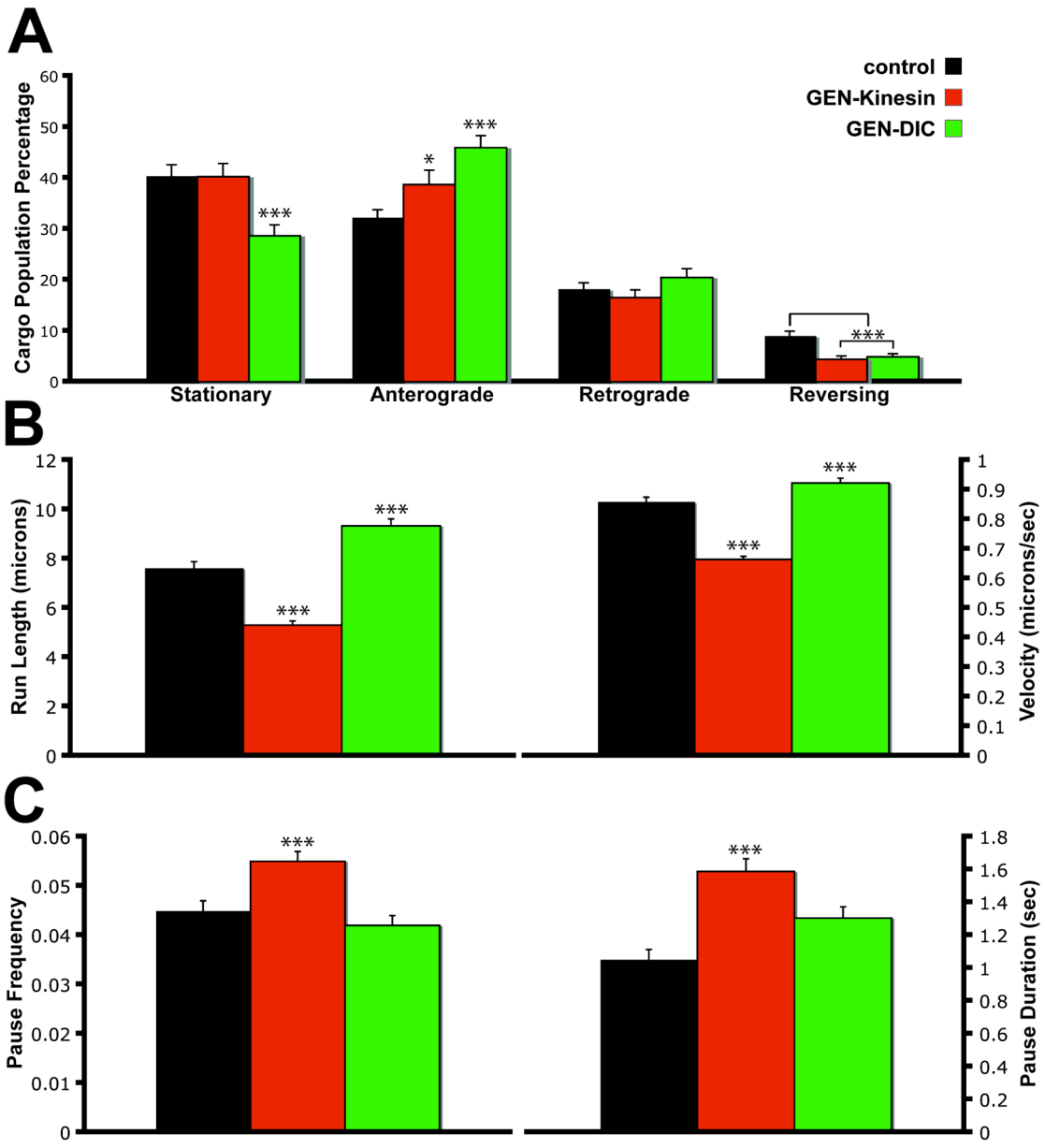

Figure 2-13. Effects of kinesin-1 and DIC overexpression on anterograde APPYFP movement for region 10. A) Cargo population analysis showing a significant decrease in stationary percentage for GEN-Kinesin and GEN-DIC. All conditions showed a significant increase in anterograde percentage and decrease in reversing. Refer to Table 2-3 for population percentage values. B) ARL (Left) and ASV (Right) decreased significantly for GEN-Kinesin but increased for GEN-DIC. C) APF (Left) and APD (Right) increased significantly for GEN-Kinesin. Statistical significance: * = $P < 0.05$; ** = $P < 0.01$; *** = $P < 0.001$. Refer to Table 2-1 for ARL, ASV, APF, and APD mean values. See Methods for a detailed definition of each parameter.

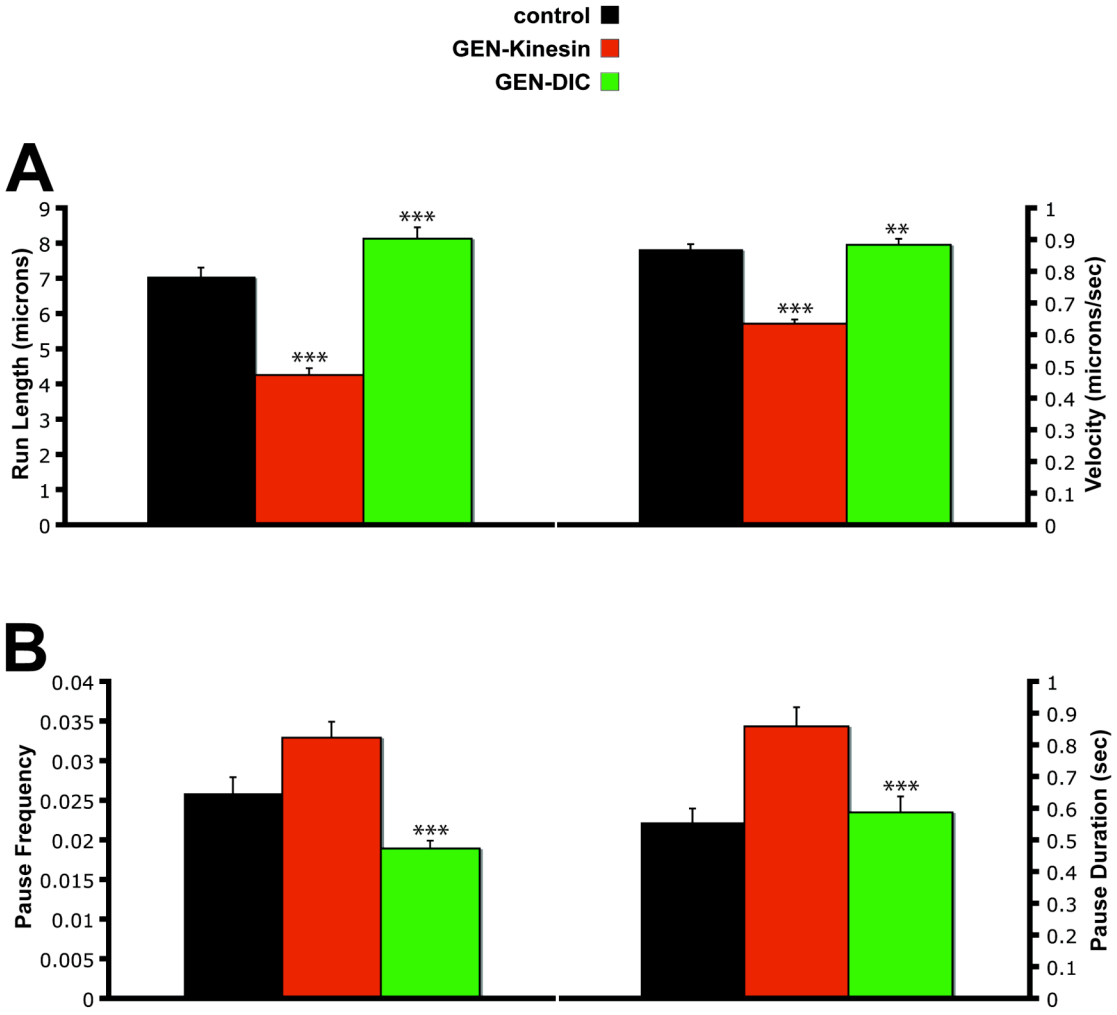

Figure 2-14. Effects of kinesin-1 and DIC overexpression on retrograde APPYFP movement in region 10. A) ARL (Left) and ASV (Right) increased significantly in GEN-DIC and decreased significantly in GEN-Kinesin and dic3/+; grid/+. B) APF (Left) decreased significantly in GEN-DIC and APD (Right) increased significantly in GEN-DIC. Statistical significance: * = $P < 0.05$; ** = $P < 0.01$; *** = $P < 0.001$. Refer to Table 2-1 for RRL, RSV, RPF, and RPD mean values. See Methods for a detailed definition of each parameter.

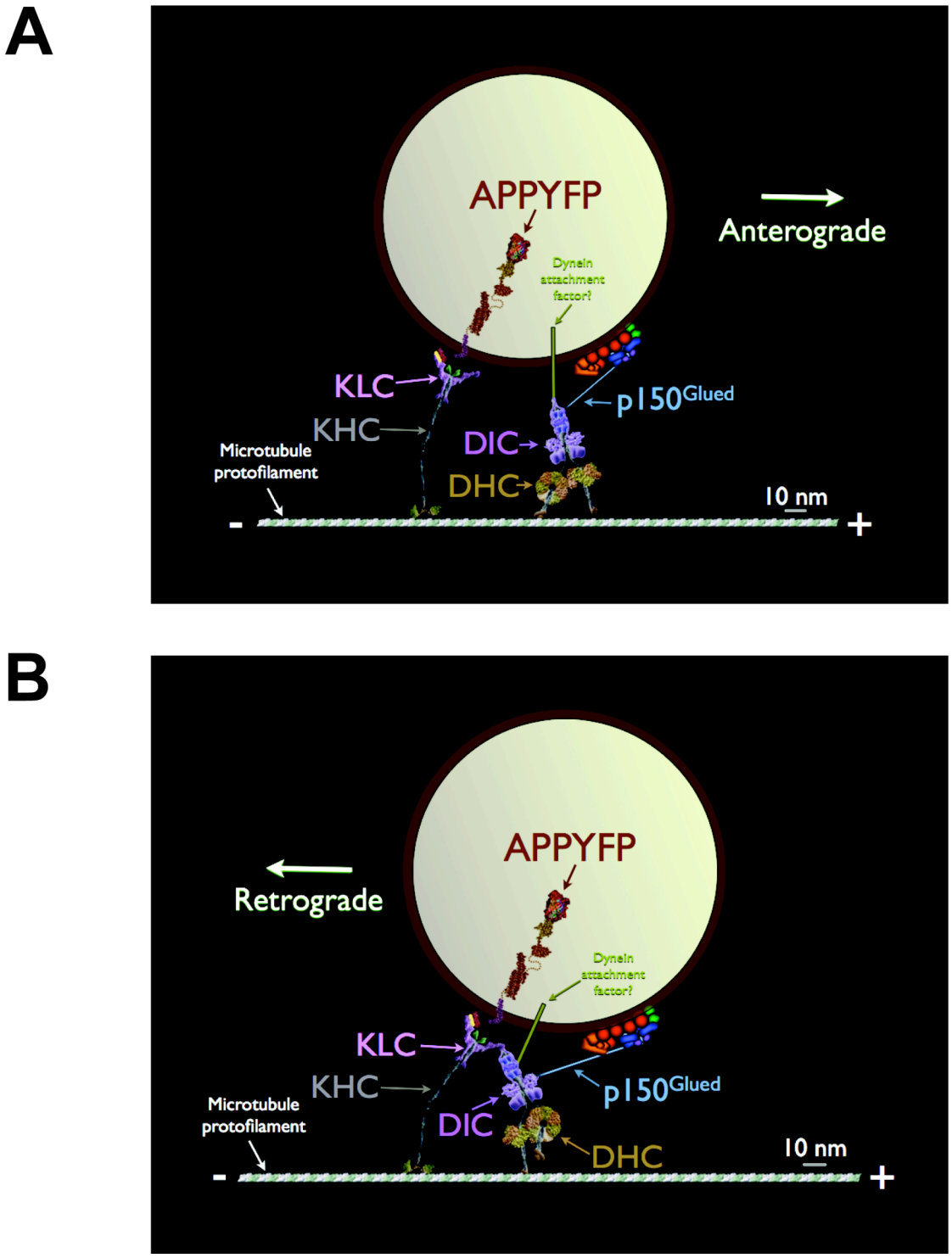

Figure 2-15. Schematic diagram for the inhibitory competition model. (A) DIC-p150^{Glued} interaction inhibits retrograde movement and activates anterograde. (B) DIC-KLC interaction inhibits anterograde movement and promotes retrograde. See the Discussion section for a detailed explanation of this model.

Table 2-1. Summary of transport parameters for APPYFP vesicle movement in axonal region 10. Statistical significance on mean segmental velocities was accessed using the Kolmogorov-Smirnov test. For all other parameters, the Wilcoxon rank-sum test was used. Cells colored red denote significant increases above the APPYFP control mean, with 1 arrow signifying $p<0.05$, 2 arrows $p<0.01$, and 3 arrows $p<0.001$. Cells colored blue represent significant downward changes with the number of arrows representing the level of p value significance as described for red-colored cells. Abbreviations: A, anterograde; R, retrograde; SV, segmental velocity (microns/second); RL, run length (microns); PF, pause frequency (number of pauses/15 seconds); PD, pause duration (seconds); SF, switch frequency (number of switches/trajectory). See Methods for a detailed definition of each parameter.

Table of Transport Parameters and Statistics
APPYFP – REGION 10

Anterograde

Genotype	A_SV (Mean ± SEM)	A_RL (Mean ± SEM)	A_PF (Mean ± SEM)	A_PD (Mean ± SEM)
Control	0.86 ± 0.015	7.628 ± 0.256	0.045 ± 0.002	1.053 ± 0.06
khc^{5}/+	0.626 ± 0.019	4.073 ± 0.299	0.076 ± 0.006	2.686 ± 0.208
khc^{26}/+	0.59 ± 0.024	4.441 ± 0.379	0.053 ± 0.005	2.161 ± 0.198
klc^{Ncd34}/+	0.775 ± 0.023	6.57 ± 0.378	0.058 ± 0.004	2.241 ± 0.182
p4163/+	0.908 ± 0.013	9.181 ± 0.235	0.038 ± 0.002	1.358 ± 0.074
dhc64c$^{6-19}$/+	0.92 ± 0.017	8.784 ± 0.296	0.045 ± 0.002	1.466 ± 0.085
dic^{1}/+	0.713 ± 0.013	5.486 ± 0.214	0.068 ± 0.003	1.885 ± 0.089
dic^{3}/+	0.709 ± 0.015	5.31 ± 0.241	0.059 ± 0.003	1.649 ± 0.099
robl^{R}/+	0.871 ± 0.016	8.643 ± 0.271	0.042 ± 0.002	1.294 ± 0.073
grid/+	0.701 ± 0.012	5.352 ± 0.206	0.071 ± 0.003	1.449 ± 0.078
dmn^{5499}/+	0.851 ± 0.013	8.102 ± 0.211	0.052 ± 0.002	1.805 ± 0.073
gl^{1}/+	0.799 ± 0.015	7.089 ± 0.263	0.052 ± 0.003	1.52 ± 0.089
GENKHC; GENKLC	0.665 ± 0.001	5.309 ± 0.171	0.055 ± 0.002	1.589 ± 0.077
GENDIC	0.923 ± 0.016	9.339 ± 0.28	0.042 ± 0.002	1.305 ± 0.069
dic^{3}/+; grid/+	0.713 ± 0.01	6.943 ± 0.188	0.04 ± 0.002	1.319 ± 0.07
unc^{104}/+	0.70 ± 0.014	7.445 ± 0.251	0.034 ± 0.002	1.517 ± 0.088

Compared to Control	A_SV	A_RL	A_PF	A_PD
khc^{5}/+	↓↓↓	↓↓↓	↑↑↑	↑↑↑
khc^{26}/+	↓↓↓	↓↓↓	→	↑↑↑
klc^{Ncd34}/+	↓↓↓	↓	↑↑	↑↑↑
p4163/+	↑↑↑	↑↑↑	→	→
dhc64c$^{6-19}$/+	↑	↑↑	→	→
dic^{1}/+	↓↓↓	↓↓↓	↑↑↑	↑↑↑
dic^{3}/+	↓↓↓	↓↓↓	↑	↑↑
robl^{R}/+	→	↑	→	→
grid/+	↓↓↓	↓↓↓	↑↑↑	↑↑↑
dmn^{5499}/+	↓↓↓	→	↑↑↑	↑↑↑
gl^{1}/+	↓	→	↑	↑↑
GENKHC; GENKLC	↓↓↓	↓↓↓	↑↑↑	↑↑↑
GENDIC	↑↑	↑↑↑	→	→
dic^{3}/+; grid/+	↓↓↓	→	→	→
unc^{104}/+	↓↓↓	↓	↓	→

Compared to grid/+	A_SV	A_RL	A_PF	A_PD
dic^{3}/+; grid/+	↑↑↑	↑↑↑	↓↓↓	↓↓↓

Retrograde

Genotype	R_SV (Mean ± SEM)	R_RL (Mean ± SEM)	R_PF (Mean ± SEM)	R_PD (Mean ± SEM)
Control	0.873 ± 0.015	7.076 ± 0.246	0.026 ± 0.002	0.559 ± 0.042
khc^{5}/+	0.547 ± 0.019	2.360 ± 0.232	0.057 ± 0.005	1.990 ± 0.201
khc^{26}/+	0.355 ± 0.01	1.267 ± 0.088	0.063 ± 0.005	2.787 ± 0.243
klc^{Ncd34}/+	0.617 ± 0.023	4.21 ± 0.392	0.034 ± 0.004	1.383 ± 0.167
p4163/+	0.796 ± 0.015	6.611 ± 0.251	0.019 ± 0.001	0.531 ± 0.045
dhc64c$^{6-19}$/+	0.766 ± 0.017	6.074 ± 0.267	0.029 ± 0.002	0.754 ± 0.059
dic^{1}/+	0.646 ± 0.016	4.249 ± 0.225	0.036 ± 0.002	0.987 ± 0.071
dic^{3}/+	0.568 ± 0.011	3.254 ± 0.149	0.059 ± 0.003	1.509 ± 0.089
robl^{R}/+	0.78 ± 0.02	6.853 ± 0.316	0.021 ± 0.002	0.605 ± 0.055
grid/+	0.665 ± 0.016	4.459 ± 0.258	0.032 ± 0.003	0.668 ± 0.06
dmn^{5499}/+	0.804 ± 0.017	6.438 ± 0.26	0.02 ± 0.001	0.614 ± 0.045
gl^{1}/+	0.744 ± 0.018	5.562 ± 0.279	0.027 ± 0.002	0.727 ± 0.064
GENKHC; GENKLC	0.637 ± 0.013	4.273 ± 0.195	0.033 ± 0.002	0.861 ± 0.06
GENDIC	0.886 ± 0.019	8.15 ± 0.318	0.019 ± 0.001	0.589 ± 0.05
dic^{3}/+; grid/+	0.643 ± 0.013	4.752 ± 0.207	0.023 ± 0.002	0.685 ± 0.052
unc^{104}/+	0.611 ± 0.016	4.790 ± 0.242	0.026 ± 0.002	0.995 ± 0.075

Compared to Control	R_SV	R_RL	R_PF	R_PD
khc^{5}/+	↓↓↓	↓↓↓	↑↑↑	↑↑↑
khc^{26}/+	↓↓↓	↓↓↓	↑↑↑	↑↑↑
klc^{Ncd34}/+	↓↓↓	↓↓↓	→	→
p4163/+	↓↓↓	↓↓	↓↓↓	↓↓↓
dhc64c$^{6-19}$/+	↓↓↓	↓↓	→	→
dic^{1}/+	↓↓↓	↓↓↓	→	→
dic^{3}/+	↓↓↓	↓↓↓	↑↑↑	↑↑↑
robl^{R}/+	↓↓↓	↓↓↓	↓↓↓	↑↑
grid/+	↓↓↓	↓↓↓	→	→
dmn^{5499}/+	↓↓↓	↓	↓↓↓	↑↑
gl^{1}/+	↓↓↓	↓↓↓	→	→
GENKHC; GENKLC	↓↓↓	↓↓↓	→	→
GENDIC	↑↑	↑↑↑	↓↓↓	↑↑↑
dic^{3}/+; grid/+	↓↓↓	↓↓↓	→	→
unc^{104}/+	↓↓↓	↓↓↓	→	→

Compared to grid/+	R_SV	R_RL	R_PF	R_PD
dic^{3}/+; grid/+	→	↑↑↑	→	→

Statistical Significance
↓↓↓ / ↑↑↑ = p<0.001
↓↓ / ↑↑ = p<0.01
↓ / ↑ = p<0.05
→ = p>0.05

Abbreviations

A = Anterograde
R = Retrograde
SV = Segmental Velocity (microns/second)
RL = Run Length (microns)
PF = Pause Frequency (pause number/time)
PD = Pause Duration (seconds)
SF = Switch Frequency (switch number/trajectory)

Genotype	SF (Mean ± SEM)
Control	0.235 ± 0.019
khc^{5}/+	0.176 ± 0.029
khc^{26}/+	0.115 ± 0.022
klc^{Ncd34}/+	0.133 ± 0.023
p4163/+	0.1 ± 0.012
dhc64c$^{6-19}$/+	0.106 ± 0.013
dic^{1}/+	0.135 ± 0.014
dic^{3}/+	0.131 ± 0.017
robl^{R}/+	0.129 ± 0.014
grid/+	0.153 ± 0.017
dmn^{5499}/+	0.142 ± 0.012
gl^{1}/+	0.147 ± 0.017
GENKHC; GENKLC	0.124 ± 0.014
GENDIC	0.102 ± 0.012
dic^{3}/+; grid/+	0.082 ± 0.01
unc^{104}/+	0.105 ± 0.012

Compared to Control	SF
khc^{5}/+	↓
khc^{26}/+	↓↓
klc^{Ncd34}/+	↓
p4163/+	↓↓↓
dhc64c$^{6-19}$/+	↓↓↓
dic^{1}/+	↓↓↓
dic^{3}/+	↓↓↓
robl^{R}/+	↓↓↓
grid/+	↓↓
dmn^{5499}/+	↓↓↓
gl^{1}/+	↓↓↓
GENKHC; GENKLC	↓↓↓
GENDIC	↓↓↓
dic^{3}/+; grid/+	↓↓↓
unc^{104}/+	↓↓↓

Compared to grid/+	SF
dic^{3}/+; grid/+	↓↓↓

Color scheme
Red = up
Blue = down

Table 2-2. Summary of transport parameters for APPYFP vesicle movement in axonal region 20. Statistical significance on mean segmental velocities was accessed using the Kolmogorov-Smirnov test. For all other parameters, the Wilcoxon rank-sum test was used. Cells colored red denote significant increases above the APPYFP control mean, with 1 arrow signifying $p<0.05$, 2 arrows $p<0.01$, and 3 arrows $p<0.001$. Cells colored blue represent significant downward changes with the number of arrows representing the level of p value significance as described for red-colored cells. Abbreviations: A, anterograde; R, retrograde; SV, segmental velocity (microns/second); RL, run length (microns); PF, pause frequency (number of pauses/15 seconds); PD, pause duration (seconds); SF, switch frequency (number of switches/trajectory). See Methods for a detailed definition of each parameter.

Table of Transport Parameters and Statistics
APPYFP – REGION 20

Anterograde

Genotype	A_SV (Mean ± SEM)	A_RL (Mean ± SEM)	A_PF (Mean ± SEM)	A_PD (Mean ± SEM)
Control	0.866 ± 0.017	7.436 ± 0.284	0.041 ± 0.002	1.082 ± 0.069
$khc^{5}/+$	0.545 ± 0.018	2.538 ± 0.229	0.068 ± 0.006	2.498 ± 0.228
$khc^{26}/+$	0.748 ± 0.037	5.485 ± 0.545	0.04 ± 0.004	1.983 ± 0.214
$klc^{Bex94}/+$	0.605 ± 0.036	3.826 ± 0.536	0.053 ± 0.007	2.043 ± 0.281
p4163/+	0.862 ± 0.016	7.753 ± 0.275	0.038 ± 0.002	1.096 ± 0.073
$dhc64c^{k-19}/+$	1.044 ± 0.002	10.823 ± 0.342	0.034 ± 0.002	1.372 ± 0.087
$dic^{1}/+$	0.756 ± 0.017	5.732 ± 0.275	0.041 ± 0.002	1.102 ± 0.079
$dic^{5}/+$	0.752 ± 0.015	5.555 ± 0.245	0.053 ± 0.003	1.533 ± 0.096
$robl^{k}/+$	0.861 ± 0.016	7.709 ± 0.273	0.052 ± 0.003	1.416 ± 0.085
grid/+	0.739 ± 0.018	5.587 ± 0.302	0.046 ± 0.003	1.389 ± 0.112
$dmn^{5499}/+$	0.809 ± 0.018	8.262 ± 0.308	0.034 ± 0.002	1.641 ± 0.099
$gl^{1}/+$	0.831 ± 0.018	6.837 ± 0.317	0.053 ± 0.003	1.337 ± 0.094
GENKHC; GENKLC	0.692 ± 0.018	4.873 ± 0.289	0.045 ± 0.003	1.377 ± 0.097
GENDIC	0.812 ± 0.016	6.52 ± 0.264	0.052 ± 0.003	1.278 ± 0.075
$dic^{5}/+$; grid/+	0.731 ± 0.012	5.901 ± 0.204	0.06 ± 0.003	1.374 ± 0.076
$unc^{104}/+$	0.900 ± 0.020	8.852 ± 0.359	0.029 ± 0.002	0.937 ± 0.079

Compared to Control	A_SV	A_RL	A_PF	A_PD
$khc^{5}/+$	↓↓↓	↓↓↓	↑↑↑	↑↑↑
$khc^{26}/+$	↓↓	↓	→	↑↑
$klc^{Bex94}/+$	↓↓↓	↓↓↓	→	→
p4163/+	→	→	→	→
$dhc64c^{k-19}/+$	↑↑↑	↑↑↑	→	→
$dic^{1}/+$	↓↓↓	↓↓↓	→	→
$dic^{5}/+$	↓↓↓	↓↓↓	↑	↑
$robl^{k}/+$	→	→	↑↑	↑
grid/+	↓↓↓	↓↓	→	→
$dmn^{5499}/+$	↓	↑↑↑	→	→
$gl^{1}/+$	→	→	↑	↑
GENKHC; GENKLC	↓↓↓	↓↓↓	→	→
GENDIC	↓↓↓	↓↓↓	→	→
$dic^{5}/+$; grid/+	↓↓↓	↓	↑↑↑	↑↑↑
$unc^{104}/+$	↑↑	↑↑↑	↓	↓↓

Compared to grid/+	A_SV	A_RL	A_PF	A_PD
$dic^{5}/+$; grid/+	→	→	↑↑↑	↓↓

Retrograde

Genotype	R_SV (Mean ± SEM)	R_RL (Mean ± SEM)	R_PF (Mean ± SEM)	R_PD (Mean ± SEM)
Control	0.979 ± 0.017	8.462 ± 0.273	0.028 ± 0.002	0.682 ± 0.056
$khc^{5}/+$	0.534 ± 0.019	2.299 ± 0.198	0.081 ± 0.006	2.742 ± 0.226
$khc^{26}/+$	0.638 ± 0.026	4.018 ± 0.319	0.05 ± 0.005	1.994 ± 0.213
$klc^{Bex94}/+$	0.457 ± 0.02	2.398 ± 0.241	0.062 ± 0.007	2.354 ± 0.279
p4163/+	0.799 ± 0.012	6.397 ± 0.206	0.028 ± 0.002	0.599 ± 0.045
$dhc64c^{k-19}/+$	0.949 ± 0.02	8.343 ± 0.321	0.019 ± 0.001	0.637 ± 0.063
$dic^{1}/+$	0.658 ± 0.012	4.603 ± 0.181	0.053 ± 0.003	1.359 ± 0.081
$dic^{5}/+$	0.91 ± 0.015	6.919 ± 0.241	0.035 ± 0.002	0.849 ± 0.064
$robl^{k}/+$	0.856 ± 0.017	7.214 ± 0.289	0.023 ± 0.002	0.578 ± 0.053
grid/+	0.654 ± 0.016	4.615 ± 0.242	0.049 ± 0.003	1.429 ± 0.104
$dmn^{5499}/+$	0.815 ± 0.017	7.334 ± 0.254	0.024 ± 0.001	1.007 ± 0.073
$gl^{1}/+$	0.736 ± 0.019	4.846 ± 0.269	0.046 ± 0.003	1.231 ± 0.096
GENKHC; GENKLC	0.673 ± 0.011	4.656 ± 0.174	0.055 ± 0.003	1.427 ± 0.086
GENDIC	0.76 ± 0.013	5.493 ± 0.205	0.045 ± 0.003	1.016 ± 0.067
$dic^{5}/+$; grid/+	0.699 ± 0.014	4.88 ± 0.222	0.029 ± 0.002	0.7 ± 0.06
$unc^{104}/+$	0.819 ± 0.016	7.304 ± 0.277	0.027 ± 0.002	0.81 ± 0.072

Compared to Control	R_SV	R_RL	R_PF	R_PD
$khc^{5}/+$	↓↓↓	↓↓↓	↑↑↑	↑↑↑
$khc^{26}/+$	↓↓↓	↓↓↓	↑↑↑	↑↑↑
$klc^{Bex94}/+$	↓↓↓	↓↓↓	↑↑↑	↑↑↑
p4163/+	↓↓↓	↓↓↓	→	→
$dhc64c^{k-19}/+$	→	→	↓↓↓	↓↓↓
$dic^{1}/+$	↓↓↓	↓↓↓	↑↑↑	↑↑↑
$dic^{5}/+$	↓↓	↓↓	↑↑	↑↑
$robl^{k}/+$	↓↓↓	↓↓	↓	↓
grid/+	↓↓↓	↓↓↓	↑↑↑	↑↑↑
$dmn^{5499}/+$	↓↓↓	→	→	→
$gl^{1}/+$	↓↓↓	↓↓↓	↑↑↑	↑↑↑
GENKHC; GENKLC	↓↓↓	↓↓↓	↑↑↑	↑↑↑
GENDIC	↓↓↓	↓↓↓	↑↑↑	↑↑↑
$dic^{5}/+$; grid/+	↓↓↓	↓↓↓	→	→
$unc^{104}/+$	↓↓↓	↓↓	→	→

Compared to grid/+	R_SV	R_RL	R_PF	R_PD
$dic^{5}/+$; grid/+	↑↑↑	↑	↓↓↓	↓↓↓

Statistical Significance
↓↓↓ / ↑↑↑ = p<0.001
↓↓ / ↑↑ = p<0.01
↓ / ↑ = p<0.05
→ = p>0.05

Abbreviations	
A = Anterograde	SV = Segmental Velocity (microns/second)
R = Retrograde	RL = Run Length (microns)
	PF = Pause Frequency (pause number/time)
	PD = Pause Duration (seconds)
	SF = Switch Frequency (switch number/trajectory)

Genotype	SF (Mean ± SEM)
Control	0.192 ± 0.019
$khc^{5}/+$	0.269 ± 0.046
$khc^{26}/+$	0.278 ± 0.047
$klc^{Bex94}/+$	0.142 ± 0.04
p4163/+	0.189 ± 0.019
$dhc64c^{k-19}/+$	0.154 ± 0.015
$dic^{1}/+$	0.191 ± 0.02
$dic^{5}/+$	0.161 ± 0.017
$robl^{k}/+$	0.17 ± 0.019
grid/+	0.172 ± 0.022
$dmn^{5499}/+$	0.101 ± 0.011
$gl^{1}/+$	0.201 ± 0.025
GENKHC; GENKLC	0.171 ± 0.02
GENDIC	0.187 ± 0.018
$dic^{5}/+$; grid/+	0.104 ± 0.015
$unc^{104}/+$	0.141 ± 0.018

Compared to Control	SF
$khc^{5}/+$	↑
$khc^{26}/+$	↑
$klc^{Bex94}/+$	→
p4163/+	→
$dhc64c^{k-19}/+$	→
$dic^{1}/+$	→
$dic^{5}/+$	→
$robl^{k}/+$	→
grid/+	→
$dmn^{5499}/+$	↓↓
$gl^{1}/+$	→
GENKHC; GENKLC	→
GENDIC	→
$dic^{5}/+$; grid/+	↓↓↓
$unc^{104}/+$	→

Compared to grid/+	SF
$dic^{5}/+$; grid/+	↓↓

Color scheme
Red = up
Blue = down

Table 2-3. Cargo population and flux analysis for APPYFP vesicle movement in axonal region 10. Statistical significance on means was accessed by using a Wilcoxon rank-sum test. Cells colored red denote significant increases above the APPYFP control mean, with 1 arrow signifying $p<0.05$, 2 arrows $p<0.01$, and 3 arrows $p<0.001$. Cells colored blue represent significant downward changes with the number of arrows representing the level of p value significance as described for red cells. Abbreviations: A, anterograde; R, retrograde. See Methods for detailed information on how these parameters were defined.

Cargo Population and Flux Analysis
APPYFP – REGION 10

Cargo Population Mean Percentage

Genotype	Stationary Percentage (Mean ± SEM)	Anterograde Percentage (Mean ± SEM)	Retrograde Percentage (Mean ± SEM)	Reversing Percentage (Mean ± SEM)	A:R Ratio
Control	40.42 ± 2.22	32.29 ± 1.49	18.23 ± 1.20	9.058 ± 0.88	2.19 ± 0.21
$khc^{5}/+$	78.03 ± 2.75	12.80 ± 1.93	6.10 ± 0.79	3.07 ± 0.74	2.77 ± 0.57
$khc^{26}/+$	79.13 ± 3.12	10.28 ± 1.89	8.35 ± 1.87	2.24 ± 0.62	1.61 ± 0.34
$klc^{bmd04}/+$	80.59 ± 3.67	12.65 ± 2.59	4.76 ± 1.02	2.00 ± 0.49	2.29 ± 0.63
p4163/+	33.52 ± 1.25	44.62 ± 1.51	17.16 ± 1.29	4.70 ± 0.48	3.95 ± 0.54
$dhc64c^{k-15}/+$	38.12 ± 2.18	38.67 ± 2.46	18.59 ± 1.72	4.62 ± 0.59	3.07 ± 0.38
$dic^{1}/+$	49.52 ± 2.65	31.60 ± 1.94	13.73 ± 0.89	5.15 ± 0.70	2.57 ± 0.20
$dic^{3}/+$	55.44 ± 3.19	21.58 ± 2.79	19.22 ± 1.61	3.77 ± 0.53	1.81 ± 0.59
$rob^{k}/+$	32.81 ± 2.31	42.80 ± 2.70	18.75 ± 1.78	5.65 ± 0.66	3.70 ± 0.68
grid/+	41.77 ± 3.02	37.92 ± 2.83	14.46 ± 1.08	5.85 ± 0.84	3.37 ± 0.42
$dmn^{j4399}/+$	34.11 ± 1.15	45.60 ± 1.20	13.80 ± 0.94	6.49 ± 0.55	4.30 ± 0.48
$gl^{1}/+$	48.60 ± 3.72	33.38 ± 2.57	12.94 ± 1.77	5.09 ± 0.74	3.12 ± 0.47
GENKHC; GENKLC	40.28 ± 2.57	38.73 ± 2.83	16.56 ± 1.51	4.43 ± 0.65	5.80 ± 1.54
GENDIC	28.65 ± 2.17	45.99 ± 2.34	20.47 ± 1.76	4.89 ± 0.64	2.98 ± 0.33
$dic^{3}/+$; grid/+	31.37 ± 1.93	46.68 ± 2.59	17.40 ± 1.23	4.56 ± 0.56	4.12 ± 0.67
$unc^{104}/+$	39.18 ± 3.94	38.03 ± 3.95	17.79 ± 1.52	5.00 ± 0.83	4.38 ± 1.22
Compared to Control (rank-sum test)	**Stationary**	**Anterograde**	**Retrograde**	**Reversing**	**Compared to Control (rank-sum test)**
$khc^{5}/+$	↑ ↑ ↑	↓ ↓ ↓	↓ ↓ ↓	↓ ↓ ↓	→
$khc^{26}/+$	↑ ↑ ↑	↓ ↓ ↓	↓ ↓ ↓	↓ ↓ ↓	↓
$klc^{bmd04}/+$	↑ ↑ ↑	↓ ↓ ↓	↓ ↓ ↓	↓ ↓ ↓	→
p4163/+	↓	↑ ↑ ↑	→	↓ ↓ ↓	↑
$dhc64c^{k-15}/+$	→	↑	→	↓ ↓ ↓	→
$dic^{1}/+$	↑	→	↓	↓ ↓ ↓	→
$dic^{3}/+$	↑ ↑ ↑	↓ ↓	→	↓ ↓ ↓	↓ ↓ ↓
$rob^{k}/+$	↓	↑ ↑ ↑	→	↓ ↓	↑
grid/+	→	→	↓	↓ ↓	→
$dmn^{j4399}/+$	↓	↑ ↑ ↑	↓	↓	↑ ↑ ↑
$gl^{1}/+$	→	→	↓	↓ ↓	→
GENKHC; GENKLC	→	↑	→	↓ ↓ ↓	→
GENDIC	↓ ↓ ↓	↑ ↑ ↑	→	↓ ↓ ↓	→
$dic^{3}/+$; grid/+	↓ ↓	↑ ↑ ↑	→	↓ ↓ ↓	↑
$unc^{104}/+$	→	→	→	↓ ↓ ↓	→
Compared to grid/+ (rank-sum test)	**Stationary**	**Anterograde**	**Retrograde**	**Reversing**	**Compared to grid/+ (rank-sum test)**
$dic^{3}/+$; grid/+	↓	↑	→	→	→
Statistical Significance				**Color scheme**	
↓↓↓ / ↑↑↑ = p<0.001				Red = up	
↓↓ / ↑↑ = p<0.01				Blue = down	
↓ / ↑ = p<0.05					
→ = p>0.05					

A/R

Flux Analysis

Genotype	Anterograde (Mean ± SEM)	Retrograde (Mean ± SEM)
Control	11.16 ± 2.02	6.42 ± 1.32
$khc^{5}/+$	1.97 ± 0.57	0.98 ± 0.29
$khc^{26}/+$	1.50 ± 0.46	0.44 ± 0.23
$klc^{bmd04}/+$	3.38 ± 1.21	1.12 ± 0.51
p4163/+	15.41 ± 2.91	4.78 ± 1.02
$dhc64c^{k-15}/+$	11.85 ± 2.54	4.77 ± 1.00
$dic^{1}/+$	8.60 ± 1.74	3.33 ± 0.71
$dic^{3}/+$	6.14 ± 1.61	3.35 ± 0.75
$rob^{k}/+$	12.76 ± 2.36	4.86 ± 1.08
grid/+	7.27 ± 1.68	2.70 ± 0.59
$dmn^{j4399}/+$	17.55 ± 3.18	5.19 ± 1.04
$gl^{1}/+$	8.30 ± 1.77	3.27 ± 0.69
GENKHC; GENKLC	9.23 ± 1.82	3.81 ± 0.99
GENDIC	15.11 ± 2.93	6.31 ± 1.25
$dic^{3}/+$; grid/+	11.15 ± 2.15	3.51 ± 0.86
$unc^{104}/+$	8.61 ± 1.90	3.35 ± 0.83
Compared to Control (rank-sum test)	**Anterograde**	**Retrograde**
$khc^{5}/+$	↓ ↓ ↓	↓ ↓ ↓
$khc^{26}/+$	↓ ↓ ↓	↓ ↓ ↓
$klc^{bmd04}/+$	↓ ↓ ↓	↓ ↓ ↓
p4163/+	↑ ↑	↓
$dhc64c^{k-15}/+$	→	↓
$dic^{1}/+$	↓ ↓	↓ ↓ ↓
$dic^{3}/+$	↓ ↓ ↓	↓ ↓ ↓
$rob^{k}/+$	→	↓
grid/+	↓ ↓ ↓	↓ ↓ ↓
$dmn^{j4399}/+$	↑ ↑ ↑	→
$gl^{1}/+$	↓ ↓	↓ ↓ ↓
GENKHC; GENKLC	↓	↓ ↓ ↓
GENDIC	↑	→
$dic^{3}/+$; grid/+	→	↓ ↓ ↓
$unc^{104}/+$	↓ ↓ ↓	↓ ↓ ↓
Compared to grid/+ (rank-sum test)	**Anterograde**	**Retrograde**
$dic^{3}/+$; grid/+	↑ ↑ ↑	→
Statistical Significance		
↓↓↓ / ↑↑↑ = p<0.001		
↓↓ / ↑↑ = p<0.01		
↓ / ↑ = p<0.05		
→ = p>0.05		

Table 2-4. Cargo population and flux analysis for APPYFP vesicle movement in axonal region 10. Statistical significance on means was accessed by using a Wilcoxon rank-sum test. Cells colored red denote significant increases above the APPYFP control mean, with 1 arrow signifying $p<0.05$, 2 arrows $p<0.01$, and 3 arrows $p<0.001$. Cells colored blue represent significant downward changes with the number of arrows representing the level of p value significance as described for red cells. Abbreviations: A, anterograde; R, retrograde. See Methods for detailed information on how these parameters were defined.

Cargo Population and Flux Analysis
APPYFP – REGION 20

Cargo Population Mean Percentage

Genotype	Stationary Percentage (Mean ± SEM)	Anterograde Percentage (Mean ± SEM)	Retrograde Percentage (Mean ± SEM)	Reversing Percentage (Mean ± SEM)
Control	42.236 ± 1.232	27.848 ± 1.797	23.478 ± 1.589	6.438 ± 0.667
$khc^{5}/+$	83.575 ± 2.574	6.455 ± 1.071	6.986 ± 1.435	2.984 ± 0.677
$khc^{26}/+$	80.943 ± 2.745	6.847 ± 1.387	8.143 ± 1.672	4.067 ± 0.835
$klc^{hmt04}/+$	82.85 ± 3.563	8.524 ± 1.999	7.26 ± 2.506	1.366 ± 0.406
p4163/+	40.414 ± 1.997	30.045 ± 1.976	22.9 ± 1.277	6.641 ± 0.855
$dhc64c^{k-10}/+$	40.745 ± 1.869	35.334 ± 1.952	17.214 ± 1.449	6.708 ± 0.644
$dic^{1}/+$	56.736 ± 2.969	16.186 ± 1.803	21.512 ± 1.959	5.566 ± 0.672
$dic^{3}/+$	46.023 ± 1.962	26.067 ± 1.783	22.045 ± 1.439	5.864 ± 0.791
$rob^{K}/+$	38.226 ± 1.906	37.467 ± 1.466	17.459 ± 1.064	6.848 ± 0.604
grid/+	54.914 ± 2.348	20.38 ± 2.418	20.004 ± 1.447	4.702 ± 0.739
$dmn^{sk99}/+$	40.199 ± 1.621	32.702 ± 1.768	22.129 ± 1.214	4.97 ± 0.603
$gl^{1}/+$	62.095 ± 3.935	20.201 ± 2.662	13.087 ± 1.722	4.617 ± 0.782
GENKHC; GENKLC	50.272 ± 2.198	17.876 ± 1.804	26.734 ± 1.969	5.118 ± 0.675
GENDIC	42.779 ± 2.322	26.658 ± 1.559	24.008 ± 2.44	6.555 ± 0.727
$dic^{3}/+$; grid/+	53.8 ± 3.086	31.028 ± 2.018	12.074 ± 1.314	3.099 ± 0.459
$unc^{104}/+$	28.637 ± 1.633	35.644 ± 2.498	28.483 ± 2.196	7.236 ± 0.842
Compared to Control (rank-sum test)	**Stationary**	**Anterograde**	**Retrograde**	**Reversing**
$khc^{5}/+$	↑ ↑ ↑	↓ ↓ ↓	↓ ↓ ↓	↓ ↓ ↓
$khc^{26}/+$	↑ ↑ ↑	↓ ↓ ↓	↓ ↓ ↓	↓ ↓
$klc^{hmt04}/+$	↑ ↑ ↑	↓ ↓ ↓	↓ ↓ ↓	↓ ↓ ↓
p4163/+	→	→	→	→
$dhc64c^{k-10}/+$	→	↑	↓ ↓	→
$dic^{1}/+$	↑ ↑ ↑	↓ ↓ ↓	→	→
$dic^{3}/+$	↑	→	→	→
$rob^{K}/+$	→	↑ ↑ ↑	↓ ↓	→
grid/+	↑ ↑ ↑	↓	→	→
$dmn^{sk99}/+$	→	→	→	→
$gl^{1}/+$	↑ ↑ ↑	↓	↓ ↓ ↓	↓
GENKHC; GENKLC	↑ ↑	↓ ↓ ↓	→	→
GENDIC	→	→	→	→
$dic^{3}/+$; grid/+	↑ ↑	→	↓ ↓ ↓	↓ ↓ ↓
$unc^{104}/+$	↓ ↓ ↓	→	↑ ↑	→
Compared to grid/+ (rank-sum test)	**Stationary**	**Anterograde**	**Retrograde**	**Reversing**
$dic^{3}/+$; grid/+	→	↑ ↑	↓ ↓ ↓	→

Statistical Significance
↓↓↓ / ↑↑↑ = p<0.001
↓↓ / ↑↑ = p<0.01
↓ / ↑ = p<0.05
→ = p>0.05

Color scheme
Red = up
Blue = down

A/R

A:R Ratio
1.69 ± 0.36
1.09 ± 0.25
1.35 ± 0.33
1.97 ± 0.61
1.59 ± 0.69
3.61 ± 0.80
1.00 ± 0.13
1.71 ± 0.26
2.58 ± 0.22
1.87 ± 0.48
1.79 ± 0.20
2.19 ± 0.38
1.20 ± 0.33
1.58 ± 0.18
3.42 ± 0.65
1.57 ± 0.35
Compared to Control (rank-sum test)
↓
→
→
→
↑ ↑
→
→
↑ ↑ ↑
→
→
→
↓ ↓
→
↑ ↑ ↑
→
Compared to grid/+ (rank-sum test)
↑ ↑ ↑

Flux Analysis

Genotype	Anterograde (Mean ± SEM)	Retrograde (Mean ± SEM)
Control	8.33 ± 1.65	7.46 ± 1.49
$khc^{5}/+$	0.76 ± 0.25	0.74 ± 0.35
$khc^{26}/+$	1.33 ± 0.68	1.10 ± 0.42
$klc^{hmt04}/+$	0.7 ± 0.19	0.51 ± 0.19
p4163/+	9.14 ± 1.79	5.77 ± 1.08
$dhc64c^{k-10}/+$	12.25 ± 2.21	5.55 ± 1.26
$dic^{1}/+$	5.08 ± 1.22	5.07 ± 1.02
$dic^{3}/+$	6.11 ± 1.23	5.98 ± 1.18
$rob^{K}/+$	10.56 ± 1.93	4.71 ± 0.94
grid/+	3.79 ± 0.87	3.21 ± 0.79
$dmn^{sk99}/+$	8.10 ± 1.45	5.22 ± 1.07
$gl^{1}/+$	6.02 ± 1.64	3.26 ± 0.85
GENKHC; GENKLC	3.71 ± 0.85	5.11 ± 0.97
GENDIC	8.47 ± 1.58	6.42 ± 1.35
$dic^{3}/+$; grid/+	8.18 ± 1.58	3.00 ± 0.64
$unc^{104}/+$	6.85 ± 1.56	4.86 ± 1.03
Compared to Control (rank-sum test)	**Anterograde**	**Retrograde**
$khc^{5}/+$	↓ ↓ ↓	↓ ↓ ↓
$khc^{26}/+$	↓ ↓ ↓	↓ ↓ ↓
$klc^{hmt04}/+$	↓ ↓ ↓	↓ ↓ ↓
p4163/+	→	→
$dhc64c^{k-10}/+$	↑ ↑ ↑	↓
$dic^{1}/+$	↓ ↓ ↓	↓ ↓
$dic^{3}/+$	↓	→
$rob^{K}/+$	↑	↓ ↓
grid/+	↓ ↓ ↓	↓ ↓ ↓
$dmn^{sk99}/+$	→	↓
$gl^{1}/+$	↓ ↓ ↓	↓ ↓ ↓
GENKHC; GENKLC	↓ ↓ ↓	↓ ↓
GENDIC	→	→
$dic^{3}/+$; grid/+	→	↓ ↓ ↓
$unc^{104}/+$	↓	↓ ↓
Compared to grid/+ (rank-sum test)	**Anterograde**	**Retrograde**
$dic^{3}/+$; grid/+	↑ ↑ ↑	→

Statistical Significance
↓↓↓ / ↑↑↑ = p<0.001
↓↓ / ↑↑ = p<0.01
↓ / ↑ = p<0.05
→ = p>0.05

Table 2-5. Segmental velocity cluster analysis for APPYFP vesicle movement in axonal region 10. Clusters were obtained using the M-Cluster package of R (see Methods). Statistical significance on mean segmental velocities was accessed using a two-tailed Student's *t* test. Cells colored red denote significant increases above the APPYFP control mean, with 1 arrow signifying $p<0.05$, 2 arrows $p<0.01$, and 3 arrows $p<0.001$. Cells colored blue represent significant downward changes with the number of arrows representing the level of p value significance as described for red-colored cells. Abbreviations: A, anterograde; R, retrograde.

Segmental Velocity Cluster
APPYFP – REGION 10

Anterograde

Genotype	A_Cluster 1 Percentage (Mean ± STD)	A_Cluster 2 Percentage (Mean ± STD)	A_Cluster 3 Percentage (Mean ± STD)
Control	26.15% (0.37 ± 0.11)	39.40% (0.66 ± 0.20)	34.45% (1.46 ± 0.50)
$khc^{5}/+$	54.69% (0.38 ± 0.13)	31.97% (0.75 ± 0.23)	13.34% (1.36 ± 0.44)
$khc^{26}/+$	39.61% (0.30 ± 0.10)	37.31% (0.50 ± 0.15)	23.08% (1.23 ± 0.39)
$klc^{bmd4}/+$	31.77% (0.32 ± 0.11)	30.08% (0.57 ± 0.11)	38.15% (1.32 ± 0.40)
p4163/+	35.83% (0.44 ± 0.16)	27.92% (0.86 ± 0.28)	36.25% (1.41 ± 0.45)
$dhc64c^{6-19}/+$	36.46% (0.42 ± 0.14)	27.36% (0.69 ± 0.22)	36.16% (1.60 ± 0.53)
$dic1^{1}/+$	63.74% (0.42 ± 0.15)	20.05% (0.82 ± 0.26)	16.21% (1.72 ± 0.43)
$dic^{3}/+$	34.00% (0.34 ± 0.11)	38.10% (0.58 ± 0.11)	27.90% (1.34 ± 0.50)
$robl^{9}/+$	27.93% (0.34 ± 0.13)	36.03% (0.66 ± 0.21)	36.04% (1.49 ± 0.55)
grid/+	38.59% (0.40 ± 0.10)	35.07% (0.61 ± 0.17)	26.34% (1.26 ± 0.47)
$dmn^{3459}/+$	16.99% (0.24 ± 0.08)	36.92% (0.57 ± 0.20)	44.09% (1.35 ± 0.49)
$gl^{1}/+$	31.84% (0.36 ± 0.12)	33.07% (0.65 ± 0.19)	35.09% (1.34 ± 0.46)
GENKLC; GENKHC	49.16% (0.42 ± 0.14)	36.37% (0.70 ± 0.22)	14.47% (1.40 ± 0.49)
GENDIC	46.67% (0.43 ± 0.17)	25.61% (0.88 ± 0.29)	27.71% (1.60 ± 0.44)
$dic^{3}/+$; grid/+	41.33% (0.40 ± 0.14)	44.46% (0.80 ± 0.27)	14.21% (1.33 ± 0.43)
$unc^{104}/+$	30.68% (0.28 ± 0.10)	31.76% (0.56 ± 0.17)	37.56% (1.16 ± 0.44)
Compared to Control mean (2-tailed *t* test)	**A_Cluster 1**	**A_Cluster 2**	**A_Cluster 3**
$khc^{5}/+$	↑↑	↑↑↑	→
$khc^{26}/+$	↓↓↓	↓↓↓	↓↓↓
$klc^{bmd4}/+$	↓↓↓	↓↓↓	↓↓↓
p4163/+	↑↑↑	↑↑↑	→
$dhc64c^{6-19}/+$	↑↑↑	↑↑↑	↑↑↑
$dic1^{1}/+$	↑↑↑	↑↑↑	↑↑↑
$dic^{3}/+$	↓↓↓	↓↓↓	↓↓↓
$robl^{9}/+$	↓↓↓	→	→
grid/+	↑↑↑	↓↓↓	↓↓↓
$dmn^{3459}/+$	↓↓↓	↓↓↓	↓↓↓
$gl^{1}/+$	↓	↓↓	↓↓↓
GENKLC; GENKHC	↑↑↑	↑↑↑	→
GENDIC	↑↑↑	↑↑↑	↑↑↑
$dic^{3}/+$; grid/+	↑↑↑	↑↑↑	→
$unc^{104}/+$	↓↓↓	↓↓↓	↓↓↓
Compared to grid/+ mean (2-tailed *t* test)	**A_Cluster 1**	**A_Cluster 2**	**A_Cluster 3**
$dic^{3}/+$; grid/+	→	↑↑↑	↑↑↑
Statistical Significance			
↓↓↓ / ↑↑↑ = p<0.001			
↓↓ / ↑↑ = p<0.01			
↓ / ↑ = p<0.05			
→ = p>0.05			

Retrograde

Genotype	R_Cluster 1 Percentage (Mean ± STD)	R_Cluster 2 Percentage (Mean ± STD)	R_Cluster 3 Percentage (Mean ± STD)
Control	35.60% (0.44 ± 0.14)	57.87% (1.07 ± 0.33)	6.53% (1.50 ± 0.54)
$khc^{5}/+$	60.60% (0.30 ± 0.09)	31.60% (0.56 ± 0.18)	7.80% (1.09 ± 0.39)
$khc^{26}/+$	28.97% (0.20 ± 0.05)	48.60% (0.34 ± 0.09)	22.43% (0.56 ± 0.21)
$klc^{bmd4}/+$	35.35% (0.32 ± 0.10)	30.23% (0.50 ± 0.12)	34.43% (1.03 ± 0.31)
p4163/+	33.39% (0.45 ± 0.16)	33.64% (0.78 ± 0.23)	32.98% (1.17 ± 0.36)
$dhc64c^{6-19}/+$	42.24% (0.38 ± 0.12)	15.68% (0.64 ± 0.08)	4.21% (1.20 ± 0.44)
$dic1^{1}/+$	35.25% (0.31 ± 0.10)	34.52% (0.55 ± 0.18)	30.23% (1.15 ± 0.43)
$dic^{3}/+$	34.14% (0.30 ± 0.09)	40.17% (0.51 ± 0.15)	25.69% (1.00 ± 0.34)
$robl^{9}/+$	9.23% (0.17 ± 0.05)	35.47% (0.41 ± 0.14)	55.30% (1.22 ± 0.45)
grid/+	23.59% (0.32 ± 0.07)	42.97% (0.53 ± 0.13)	33.43% (1.09 ± 0.39)
$dmn^{3459}/+$	20.97% (0.24 ± 0.08)	28.11% (0.59 ± 0.21)	5.09% (1.15 ± 0.39)
$gl^{1}/+$	40.94% (0.39 ± 0.13)	36.41% (0.82 ± 0.25)	22.65% (1.27 ± 0.37)
GENKLC; GENKHC	33.14% (0.33 ± 0.10)	27.37% (0.50 ± 0.13)	39.49% (0.99 ± 0.36)
GENDIC	30.61% (0.33 ± 0.14)	29.82% (0.85 ± 0.31)	39.57% (1.34 ± 0.40)
$dic^{3}/+$; grid/+	45.44% (0.38 ± 0.14)	40.78% (0.77 ± 0.25)	13.78% (1.13 ± 0.37)
$unc^{104}/+$	31.28% (0.27 ± 0.09)	32.22% (0.70 ± 0.25)	36.49% (1.35 ± 0.50)
Compared to Control mean (2-tailed *t* test)	**R_Cluster 1**	**R_Cluster 2**	**R_Cluster 3**
$khc^{5}/+$	↓↓↓	↓↓↓	↓↓↓
$khc^{26}/+$	↓↓↓	↓↓↓	↓↓↓
$klc^{bmd4}/+$	↓↓↓	↓↓↓	↓↓↓
p4163/+	→	↓↓↓	↓↓↓
$dhc64c^{6-19}/+$	↓↓↓	↓↓↓	↓↓↓
$dic1^{1}/+$	↓↓↓	↓↓↓	↓↓↓
$dic^{3}/+$	↓↓↓	↓↓↓	↓↓↓
$robl^{9}/+$	↓↓↓	↓↓↓	↓↓↓
grid/+	↓↓↓	↓↓↓	↓↓↓
$dmn^{3459}/+$	↓↓↓	↓↓↓	↓↓↓
$gl^{1}/+$	↓↓↓	↓↓↓	↓↓↓
GENKLC; GENKHC	↓↓↓	↓↓↓	↓↓↓
GENDIC	↓↓↓	↓↓↓	↓↓↓
$dic^{3}/+$; grid/+	↓↓↓	↓↓↓	↓↓↓
$unc^{104}/+$	↓↓↓	↓↓↓	↓↓↓
Compared to grid/+ mean (2-tailed *t* test)	**R_Cluster 1**	**R_Cluster 2**	**R_Cluster 3**
$dic^{3}/+$; grid/+	→	↑↑↑	↑↑↑
Statistical Significance			
↓↓↓ / ↑↑↑ = p<0.001			
↓↓ / ↑↑ = p<0.01			
↓ / ↑ = p<0.05			
→ = p>0.05			

Control-Enforced Mean and SD

Genotype	Anterograde Cluster 1 Percentage	Anterograde Cluster 2 Percentage	Anterograde Cluster 3 Percentage
Control	26.04%	39.90%	34.06%
$khc^{5}/+$	48.09%	29.65%	22.26%
$khc^{26}/+$	63.14%	10.43%	26.43%
$klc^{bmd4}/+$	39.18%	23.04%	37.78%
p4163/+	19.53%	32.61%	47.86%
$dhc64c^{6-19}/+$	29.70%	34.31%	35.99%
$dic1^{1}/+$	46.26%	34.20%	19.55%
$dic^{3}/+$	44.17%	32.10%	23.72%
$robl^{9}/+$	31.64%	31.64%	36.72%
grid/+	37.19%	43.64%	19.17%
$dmn^{3459}/+$	34.89%	21.83%	43.28%
$gl^{1}/+$	31.95%	33.56%	34.50%
GENKLC; GENKHC	36.34%	49.13%	14.53%
GENDIC	33.07%	28.31%	38.61%
$dic^{3}/+$; grid/+	28.27%	40.56%	31.17%
$unc^{104}/+$	44.03%	21.60%	34.35%
Compared to Control (10% ± mean control)	**A_Cluster 1**	**A_Cluster 2**	**A_Cluster 3**
$khc^{5}/+$	↑	↓	↓
$khc^{26}/+$	↑	↓	↓
$klc^{bmd4}/+$	↑	↓	↑
p4163/+	↓	↓	↑
$dhc64c^{6-19}/+$	↑	↓	→
$dic1^{1}/+$	↑	↓	↓
$dic^{3}/+$	↑	↓	↓
$robl^{9}/+$	↑	↓	→
grid/+	↑	→	↓
$dmn^{3459}/+$	↑	↓	↑
$gl^{1}/+$	↑	↓	→
GENKLC; GENKHC	↑	↑	↓
GENDIC	↑	↓	↑
$dic^{3}/+$; grid/+	→	→	→
$unc^{104}/+$	↑	↓	→
Compared to grid/+ (10% ± mean control)	**A_Cluster 1**	**A_Cluster 2**	**A_Cluster 3**
$dic^{3}/+$; grid/+	↓	→	↑
Statistical Significance			
Arbitrary, taking 10% ± control mean as cutoff			

Table 2-6. Summary of transport parameters for synaptotagmin-GFP (SYTGFP) vesicle movement in axonal regions 10 and 20. Statistical significance on mean segmental velocities was accessed using the Kolmogorov-Smirnov test. For all other parameters, the Wilcoxon rank-sum test was used. Cells colored red denote significant increases above the SYTGFP control mean; cells colored blue represent significant downward changes. Abbreviations: same as in Table 2-5.

Table of Transport Parameters and Statistics
Synaptotagmin-GFP

REGION 10

Anterograde

Genotype	A_SV (Mean ± SEM)	A_RL (Mean ± SEM)	A_PF (Mean ± SEM)	A_PD (Mean ± SEM)
Control	0.822 ± 0.035	7.984 ± 0.615	0.017 ± 0.002	0.589 ± 0.079
$khc^{9}/+$	0.700 ± 0.039	4.936 ± 0.479	0.012 ± 0.001	0.589 ± 0.085
$klc^{Bsd4}/+$	0.874 ± 0.038	9.917 ± 0.668	0.012 ± 0.002	0.573 ± 0.099

Compared to Control	A_SV	A_RL	A_PF	A_PD
$khc^{9}/+$	↓	→	→	→
$klc^{Bsd4}/+$	↑↑	↑↑↑	→	→

Retrograde

Genotype	R_SV (Mean ± SEM)	R_RL (Mean ± SEM)	R_PF (Mean ± SEM)	R_PD (Mean ± SEM)
Control	0.659 ± 0.011	4.855 ± 0.180	0.063 ± 0.003	1.855 ± 0.111
$khc^{9}/+$	0.736 ± 0.019	5.400 ± 0.226	0.034 ± 0.002	1.378 ± 0.105
$klc^{Bsd4}/+$	0.689 ± 0.017	6.491 ± 0.299	0.035 ± 0.003	1.307 ± 0.131

Compared to Control	R_SV	R_RL	R_PF	R_PD
$khc^{9}/+$	↑↑↑	↑↑	↓↓↓	↓
$klc^{Bsd4}/+$	↑	↑↑↑	↓↓↓	↓↓↓

Genotype	SF (Mean ± SEM)
Control	0.123 ± 0.018
$khc^{9}/+$	0.094 ± 0.017
$klc^{Bsd4}/+$	0.091 ± 0.018

Compared to Control	SF
$khc^{9}/+$	→
$klc^{Bsd4}/+$	→

REGION 20

Anterograde

Genotype	A_SV (Mean ± SEM)	A_RL (Mean ± SEM)	A_PF (Mean ± SEM)	A_PD (Mean ± SEM)
Control	0.877 ± 0.034	9.823 ± 0.607	0.011 ± 0.001	0.560 ± 0.076
$khc^{9}/+$	1.061 ± 0.061	8.817 ± 0.831	0.009 ± 0.001	0.448 ± 0.081
$klc^{Bsd4}/+$	0.996 ± 0.038	11.689 ± 0.666	0.014 ± 0.002	0.565 ± 0.085

Compared to Control	A_SV	A_RL	A_PF	A_PD
$khc^{9}/+$	→	→	→	→
$klc^{Bsd4}/+$	↑	→	→	→

Retrograde

Genotype	R_SV (Mean ± SEM)	R_RL (Mean ± SEM)	R_PF (Mean ± SEM)	R_PD (Mean ± SEM)
Control	0.689 ± 0.013	6.483 ± 0.218	0.040 ± 0.002	1.553 ± 0.108
$khc^{9}/+$	0.837 ± 0.019	6.336 ± 0.276	0.029 ± 0.002	1.089 ± 0.107
$klc^{Bsd4}/+$	0.694 ± 0.015	6.508 ± 0.266	0.034 ± 0.003	1.382 ± 0.123

Compared to Control	R_SV	R_RL	R_PF	R_PD
$khc^{9}/+$	↑↑↑	→	↓↓	→
$klc^{Bsd4}/+$	→	→	↓	↓

Genotype	SF (Mean ± SEM)
Control	0.087 ± 0.014
$khc^{9}/+$	0.126 ± 0.021
$klc^{Bsd4}/+$	0.101 ± 0.018

Compared to Control	SF
$khc^{9}/+$	→
$klc^{Bsd4}/+$	→

Statistical Significance
↓↓↓ / ↑↑↑ = p<0.001
↓↓ / ↑↑ = p<0.01
↓ / ↑ = p<0.05
→ = p>0.05

Abbreviations	
A = Anterograde	SV = Segmental Velocity (microns/second)
R = Retrograde	RL = Run Length (microns)
	PF = Pause Frequency (pause number/time)
	PD = Pause Duration (seconds)
	SF = Switch Frequency (switch number/trajectory)

Color scheme
Red = up
Blue = down

Table 2-7. Expected and observed findings for axonal transport testable models. The upper part of the table lists expected findings for each model. The bottom part uses observed findings to determine if the data fits the model. If it does, a "YES" is listed under that condition, a general qualification is given, and the cell is colored green. If it does not, a "NO" is listed with the rational underlying it. Most of the predictions made by the standard and tug-of-war models were not supported by our data. Interestingly, many predictions made by the ternary complex model were supported by the data, with some exceptions noted for *dhc/+, dlc/+*, and the kinesin overexpression experiments. For the competition models, the inhibitory-competition model was consistent with most of the data with *dic/+* and kinesin overexpression constituting exceptions. For a more detailed description of each model, refer to the discussion section.

Summary of Models and Supporting Data

Expected Findings (Effects on movement)

Genetic Reduction	Standard Model	Tug-of-war	Ternary complex	Competition inhibitory	Competition activating
Kinesin-1	A = impaired R = no change	A = impaired R = improved	A = impaired R = impaired	A = impaired R = no change	A = impaired R = no change
Cytoplasmic dynein	A = no change R = impaired	A = improved R = impaired	A = impaired R = impaired	A = improved R = impaired	A = impaired R = impaired
Dynactin	A = no change R = impaired	A = improved R = impaired	A = impaired R = impaired	A = impaired R = impaired	A = improved R = impaired
Kinesin-1 overexpression	A = improved R = no change	A = improved R = impaired	A = improved R = improved	A = improved R = no change	A = improved R = no change
DIC overexpression	A = no change R = improved	A = impaired R = improved	A = improved R = improved	A = impaired R = improved	A = improved R = improved
Double reduction (with respect to *grid/+*)	A = no change R = impaired	A = improved R = impaired	A = impaired R = impaired	A = improved R = impaired	A = impaired R = impaired

Observed Findings (Effects on movement)

Genetic manipulation	Standard Model	Tug-of-war	Ternary complex	Competition inhibitory	Competition activating
Kinesin-1	**Kinesin-1**	**Kinesin-1**	**Kinesin-1**	**Kinesin-1**	**Kinesin-1**
KHC reduction	**NO** ASV decreased Retrograde impairment	**NO** Retrograde impairment	**YES** Bi-directional impairment	**YES** Anterograde impairment	**YES** Anterograde impairment
KLC reduction	**NO** ASV decreased Retrograde impairment	**NO** Retrograde impairment	**YES** Bi-directional impairment	**YES** Anterograde impairment	**YES** Anterograde impairment
Cytoplasmic dynein	**Cytoplasmic dynein**	**Cytoplasmic dynein**	**Cytoplasmic dynein**	**Cytoplasmic dynein**	**Cytoplasmic dynein**
DHC reduction	**NO** Anterograde improvement	**YES** Anterograde improvement	**NO** Anterograde improvement	**YES** Anterograde improvement	**NO** Anterograde improvement
DIC reduction	**NO** Anterograde impairment	**NO** Anterograde impairment	**YES** Bi-directional impairment	**NO** Anterograde impairment	**YES** Anterograde impairment
DLC reduction	**NO** Anterograde improvement	**YES** Anterograde improvement	**NO** Anterograde improvement	**YES** Anterograde improvement	**NO** Anterograde improvement
Dynactin	**Dynactin**	**Dynactin**	**Dynactin**	**Dynactin**	**Dynactin**
Arp1 reduction	**NO** Anterograde impairment	**N/A**	**YES** Bi-directional impairment	**YES** Anterograde impairment	**NO** Anterograde impairment
p50 reduction	**NO** Anterograde impairment	**N/A**	**YES** Bi-directional impairment	**YES** Anterograde impairment	**NO** Anterograde impairment
$p150^{Glued}$ reduction	**NO** Anterograde impairment	**N/A**	**YES** Bi-directional impairment	**YES** Anterograde impairment	**NO** Anterograde impairment
Overexpression	**Overexpression**	**Overexpression**	**Overexpression**	**Overexpression**	**Overexpression**
Kinesin overexpression	**NO** Bi-directional impairment	**NO** ASV impairment	**NO** Bi-directional impairment	**NO** Anterograde impairment	**YES** Anterograde impairment
DIC overexpression	**NO** Anterograde improvement	**NO** Anterograde improvement	**YES** Bi-directional improvement	**YES** ↑ ASV Clusters 1 and 3	**YES** Anterograde improvement
Double reduction	**Double reduction**	**Double reduction**	**Double reduction**	**Double reduction**	**Double reduction**
DIC and Arp1 reduction (with respect to *grid/+*)	**NO** Anterograde impairment	**NO** Anterograde impairment	**YES** Bi-directional impairment	**YES** Anterograde improvement	**NO** Anterograde improvement

References

Block, S. M. (1995). "Nanometres and piconewtons: the macromolecular mechanics of kinesin." Trends Cell Biol **5**(4): 169-75.

Block, S. M., L. S. Goldstein, et al. (1990). "Bead movement by single kinesin molecules studied with optical tweezers." Nature **348**(6299): 348-52.

Boylan, K., M. Serr, et al. (2000). "A molecular genetic analysis of the interaction between the cytoplasmic dynein intermediate chain and the glued (dynactin) complex." Mol Biol Cell **11**(11): 3791-803.

Brady, S. T., K. K. Pfister, et al. (1990). "A monoclonal antibody against kinesin inhibits both anterograde and retrograde fast axonal transport in squid axoplasm." Proc Natl Acad Sci U S A **87**(3): 1061-5.

Deacon, S. W., A. S. Serpinskaya, et al. (2003). "Dynactin is required for bidirectional organelle transport." J Cell Biol **160**(3): 297-301.

Gindhart, J. G., Jr., C. J. Desai, et al. (1998). "Kinesin light chains are essential for axonal transport in Drosophila." J Cell Biol **141**(2): 443-54.

Goldstein, L. S. and A. V. Philp (1999). "The road less traveled: emerging principles of kinesin motor utilization." Annu Rev Cell Dev Biol **15**: 141-83.

Gross, S. P. (2004). "Hither and yon: a review of bi-directional microtubule-based transport." Phys Biol **1**(1-2): R1-11.

Gross, S. P., M. A. Welte, et al. (2002). "Coordination of opposite-polarity microtubule motors." J Cell Biol **156**(4): 715-24.

Gunawardena, S. and L. S. Goldstein (2001). "Disruption of axonal transport and neuronal viability by amyloid precursor protein mutations in Drosophila." Neuron **32**(3): 389-401.

Haghnia, M., V. Cavalli, et al. (2007). "Dynactin is required for coordinated bidirectional motility, but not for dynein membrane attachment." Mol Biol Cell **18**(6): 2081-9.

Kamal, A., A. Almenar-Queralt, et al. (2001). "Kinesin-mediated axonal transport of a membrane compartment containing beta-secretase and presenilin-1 requires APP." Nature **414**(6864): 643-8.

Kamal, A., G. B. Stokin, et al. (2000). "Axonal transport of amyloid precursor protein is mediated by direct binding to the kinesin light chain subunit of kinesin-I." Neuron **28**(2): 449-59.

Kim, H., S. C. Ling, et al. (2007). "Microtubule binding by dynactin is required for microtubule organization but not cargo transport." J Cell Biol **176**(5): 641-51.

King, S. J. and T. A. Schroer (2000). "Dynactin increases the processivity of the cytoplasmic dynein motor." Nat Cell Biol **2**(1): 20-4.

Levy, J. R. and E. L. Holzbaur (2006). "Cytoplasmic dynein/dynactin function and dysfunction in motor neurons." Int J Dev Neurosci **24**(2-3): 103-11.

Ligon, L. A., M. Tokito, et al. (2004). "A direct interaction between cytoplasmic dynein and kinesin I may coordinate motor activity." J Biol Chem **279**(18): 19201-8.

Martin, M., S. J. Iyadurai, et al. (1999). "Cytoplasmic dynein, the dynactin complex, and kinesin are interdependent and essential for fast axonal transport." Mol Biol Cell **10**(11): 3717-28.

Morrison, E. E. (2007). "Action and interactions at microtubule ends." Cell Mol Life Sci **64**(3): 307-17.

Popov, S. and M. M. Poo (1992). "Diffusional transport of macromolecules in developing nerve processes." J Neurosci **12**(1): 77-85.

Saxton, W. M., J. Hicks, et al. (1991). "Kinesin heavy chain is essential for viability and neuromuscular functions in Drosophila, but mutants show no defects in mitosis." Cell **64**(6): 1093-102.

Schroer, T. A. (2004). "Dynactin." Annu Rev Cell Dev Biol **20**: 759-79.

Vale, R. D., T. Funatsu, et al. (1996). "Direct observation of single kinesin molecules moving along microtubules." Nature **380**(6573): 451-3.

Vale, R. D., F. Malik, et al. (1992). "Directional instability of microtubule transport in the presence of kinesin and dynein, two opposite polarity motor proteins." J Cell Biol **119**(6): 1589-96.

Yonekawa, Y., A. Harada, et al. (1998). "Defect in synaptic vesicle precursor transport and neuronal cell death in KIF1A motor protein-deficient mice." J Cell Biol **141**(2): 431-41.

Chapter III -

RESCUING AXONAL TRANSPORT PHENOTYPES INDUCED BY APP OVEREXPRESSION

Abstract

Alzheimer's disease (AD) is a devastating neurodegenerative disease for which no effective treatment is currently available. Recently, axonal transport defects have been implicated in the development of AD due to an interaction between the amyloid precursor protein (APP) and the light chain of kinesin-1 (KLC). Several recent reports showed that APP overexpression leads to formation of axonal swellings whose frequency and size increase with kinesin-1 reductions. These swellings are thought to be pathological as they may lead to axonal blockages, transport defects, and activation of neurodegenerative pathways. In the present study, we used both *in vitro* and *in vivo* approaches to test the hypothesis that axonal transport defects can be rescued by genetic manipulations in *Drosophila*. We found that our *in vivo* APPYFP imaging assay provided a more sensitive method for probing this question. Quantitative analysis of APPYFP vesicle movement showed that APP overexpression impaired bi-directional transport though the effect on retrograde movement was much more striking. Interestingly, impairments in transport induced by APP overexpression were significantly rescued by coupling APP overexpression to kinesin-1 overexpression. In addition, cytoplasmic dynein heavy chain reduction had a similar rescuing effect on APPYFP movement. These observations suggest that certain genetic manipulations may help reverse axonal transport defects induced by APP overexpression.

Introduction

Alzheimer's disease is a neurodegenerative disease that affects an estimated 10% of the US population over the age of 65 and 50% of those older than 85. It is a progressive condition that compromises areas of the brain involved in memory, language, and behavior. AD is considered to be the most common neurodegenerative disorder in the world (Bossy-Wetzel, Schwarzenbacher et al. 2004). There are two classical pathological findings in AD: 1) neurofibrillary tangles (NFTs) and 2) amyloid plaques. NFTs are composed of paired helical filaments that accumulate in cell bodies and dendrites. Their formation is attributed to the abnormal phosphorylation of the microtubule-associated protein tau. Amyloid plaques are insoluble aggregates composed of proteolytic fragments of the amyloid precursor protein (APP). These pathological fragments are called amyloid β (Aβ). The proteolytic processing of APP is mediated by a variety of proteins, which include presenilin. It is now known that mutations in both APP and presenilin are associated with familial forms of AD. Given the presumed involvement of APP in AD and previous findings connecting molecular motors to neurodegenerative diseases (LaMonte, Wallace et al. 2002; Reid, Kloos et al. 2002; Puls, Jonnakuty et al. 2003), the question emerged as to whether APP interacts with molecular motor proteins.

Biochemical studies revealed that APP interacts with the light chain of kinesin-1, an observation that gave birth to the idea that APP serves as a receptor for kinesin-1 (Kamal, Stokin et al. 2000). This hypothesis makes a number of unique *in vivo* predictions, which have been tested using both *Drosophila* and mouse models of AD. In *Drosophila*, overexpression of APP induced an axonal phenotype characterized by

swellings with massive accumulation of vesicles, organelles, and motor proteins such as kinesin-1 (Gunawardena and Goldstein 2001). When coupled to reductions in kinesin-1, APP overexpression caused axonal swellings whose frequency and size increase significantly. Not only have these phenotypes been recapitulated in APP transgenic mice but also these animals displayed amyloid plaques whose number was potentiated by KLC reduction (Stokin, Lillo et al. 2005). These results are consistent with the hypothesis that APP interacts with kinesin-1 and titrates it away from the soluble pool required for normal axonal transport. Intriguingly, appearance of swellings was shown to precede the tau pathology characterizing later stages of AD (Stokin, Lillo et al. 2005). Thus, axonal swellings may serve as a precursor for neurodegenerative changes observed in AD.

Surprisingly, reductions in cytoplasmic dynein rescued the axonal phenotype induced by APP overexpression (Gunawardena and Goldstein 2001). However, subsequent work in the Goldstein lab using *in vivo* analysis of movement in single axons of the L3 larvae reported that 50% reduction in ROBL—a gene encoding a dynein light chain in *Drosophila*—combined with a different APP construct—APPYFP—exhibited some axonal swellings. To resolve this discrepancy, we used both *in vitro* and *in vivo* approaches to test the hypothesis that axonal transport defects can be rescued by reduction of cytoplasmic dynein. In addition, we tested the hypothesis that APP induces axonal transport defects via KLC titration by looking at the effects of kinesin-1 overexpression on an APP overexpression background. We found that these genetic manipulations improve bi-directional movement and may

represent a step towards reversal of axonal transport defects induced by APP overexpression.

Methods

Immunohistochemistry and imaging protocol

Drosophila L3 larvae were dissected and immediately fixed in 4% p-formaldehyde for 45 minutes at room temperature. Fixative was then removed and preparations were washed 4 times for 10 minutes each with 0.1% PBT (Tween-20 in PBS). Anti-cysteine string protein (CSP) antibody was then applied at 1:50 dilution in 0.1% PBT samples were kept at 4°C overnight. After 4 washes in 0.1% PBT for 10 minutes each, secondary antibody was applied at 1:100 dilution in 0.1% PBT. Samples were allowed to incubated at room temperature for 1 hour. Next, 4 10-minute washes were conducted in 0.1% PBT to remove excess antibody. Finally, samples were mounted using Vectra Shield, and slides were sealed using nail polish. Slides were allowed to dry overnight for imaging the next day. They were then coded to setup for blind imaging and analysis. Images were then collected using a confocal inverted Nikon microscope, 40X oil objective, and Biorad collection software (Goldstein confocal). On average, three images were taken for each animals beginning at the anterior end of segmental nerves and moving to posterior.

IF image analysis and statistics

Images were analyzed using Image J and a manual thresholding method described as follows. Z-stack collapsed images were first inverted and normalized using 0.02% contrast enhancement. Distances were then calibrated and the thresholding tool was used to manually "fill" swellings. During this crucial thresholding step, special care was taken to prevent individual small vesicles from merging together. If this occurs, clusters of single vesicles would be detected as

swellings. Once distances were calibrated, the analyze function was then used to count particles that were bigger than 1.5 μm^2. This number was set arbitrarily by inspecting many images and determining the total number of pixels present in a typical swelling. The poly-line tool was then used to trace fiber length so results could be expressed as swellings/micron. All images collected for a given animal were averaged together, and animals for a given genotype were pooled for statistics and plotting. Statistics was done using GraphPad and a Student's two-tailed *t* test. Graphs were created using Excel.

Live imaging protocol, data analysis, and statistics

Collection, data analysis, and statistics were done using L3 larvae as described before (see Methods section in chapter II).

Genetics

Drosophila stocks were maintained at room temperature or at 25°C except when crosses were setup for imaging. L3 larvae obtained for either immunohistochemistry (IF) and movement analyses were taken from crosses incubated at 29°C.

For IF, the control group was Oregon R (OR). Only females were used for all conditions. In brief, UAS-APP and UAS-APPYFP overexpression were induced by the panneuronal driver ApplGal4. Virgin APP and OR animals were crossed to ApplGal4, and female animals were selected for dissection and imaging.

To setup for all subsequent experiments, we created an ApplGal4; pin^{88K}/ T(2:3) CyO $TM6B^{Tb}$ stable stock. The chromosome carrying T(2:3) CyO, $TM6B^{Tb}$ is referred to as B3 and carries the dominant markers Hu, Tb, and Cyo. This stable stock

was created by a multi-step cross scheme where 1) ApplGal4 virgins were crossed to *pin*^{88K}/ B3 males; 2) selected ApplGal4/X; B3/+ virgins were crossed to *pin*^{88K}/ B3 males; 3) selected ApplGal4/X; *pin*^{88K}/ B3 were crossed to selected ApplGal4/Y; *pin*^{88K}/ B3; 4) selected ApplGal4; *pin*^{88K}/ B3 virgins were crossed to selected ApplGal4/Y; *pin*^{88K}/ B3.

For IF of kinesin-1 overexpression conditions, we used GEN-KLC/CyO; TM3/TM6B and *sp*/CyO; GEN-KHC stocks. The extra copy of the motor gene in these stocks is also under the control of endogenous regulatory domains present in the wild type condition (Saxton, Hicks et al. 1991; Gindhart, Desai et al. 1998). To achieve overexpression of KLC, we crossed GEN-KLC/CyO; TM3/TM6B to ApplGal4; *pin*^{88K}/B3. We proceeded as follows: 1) ApplGal4; *pin*^{88K}/ B3 virgins were crossed to GEN-KLC/CyO; TM3/TM6B males; 2) ApplGal4/Y; GEN-KLC; TM3/B3 males were selected and crossed to virgin APP695 animals; 3) ApplGal4/X; GEN-KLC/APP695; TM3/+ animals were selected for analysis. For overexpression of KHC experiments, we crossed 1) ApplGal4; *pin*^{88K}/ B3 virgins to *sp*/CyO; GEN-KHC males; 2) ApplGal4/Y; (*sp*; GEN-KHC)/B3 males were selected and crossed to virgin APP695 animals; 3) ApplGal4/X; *sp*/APP695; GEN-KHC/+ animals were selected for analysis. To achieve overexpression of both kinesin-1 subunits, we proceeded as follows: 1) crossed APP695; TM3/TM6B virgins to *sp*/CyO; GEN-KHC males; 2) crossed APP695/CyO; GEN-KHC/TM6B males to *pin*^{88K}/B3 virgins; 3) selected (APP695; GEN-KHC)/B3 animals and established the stable stock APP695; GEN-KHC with B3 floating; 4) crossed ApplGal4; *pin*^{88K}/ B3 virgins to GEN-KLC/CyO; TM3/TM6B males; 5) selected ApplGal4/Y; (GEN-KLC; TM3)/B3 males and crossed

to UAS-APP695; GEN-KHC virgins; 6) selected ApplGal4/X; GEN-KLC/ UAS-APP695; GEN-KHC/TM3 female larvae for the experiment.

For IF of dynein reduction conditions, we crossed 1) ApplGal4; pin^{88K}/ B3 virgins to $robl^{k}$/CyO males; 2) selected ApplGal4; $robl^{k}$/B3 males and crossed to UAS-APP695 virgins; 3) selected ApplGal4; $robl^{k}$/APP695 L3 larvae for the experiment.

For live imaging experiments, the control group was UAS-APPYFP under the control of SG26.1. This group was the same group described in chapter II. As with the IF experiment, only females were used for all conditions.

To examine the effects of APP overexpression on vesicle movement, we first generated an UAS-APPYFP; pin^{88K}/ T(2:3) CyO $TM6B^{Tb}$ stable stock. This stock was created by a multi-step cross scheme where 1) UAS-APPYFP virgins were crossed to pin^{88K}/ B3 males; 2) selected UAS-APPYFP /X; B3/+ virgins were crossed to pin^{88K}/ B3 males; 3) selected UAS-APPYFP /X; pin^{88K}/ B3 were crossed to selected UAS-APPYFP /Y; pin^{88K}/B3; 4) selected UAS-APPYFP; pin^{88K}/B3 virgins were crossed to selected UAS-APPYFP /Y; pin^{88K}/B3. We then created a stock co-expressing 2 copies of UAS-APPYFP and a second stock co-expressing UAS-APPYFP and UAS-APP695. These stocks were generated as follows. For UAS-APPYFP; UAS-APPYFP, we crossed 1) UAS-APPYFP; pin^{88K}/B3 virgins to UAS-APPYFP (2^{nd} chromosome) males; 2) crossed UAS-APPYFP; pin^{88K}/B3 virgins to selected UAS-APPYFP /Y; UAS-APPYFP /B3 males; 3) crossed UAS-APPYFP; UAS-APPYFP /B3 virgins to UAS-APPYFP; UAS-APPYFP /B3 males. This was kept as a stable stock. A similar approach was used to generate the UAS-APPYFP; UAS-APP695 stock: we crossed 1)

UAS-APPYFP; *pin*^{88K}/B3 virgins to UAS-APP695 (2nd chromosome) males; 2) crossed UAS-APPYFP; *pin*^{88K}/ B3 virgins to selected UAS-APPYFP /Y; UAS-APP695/B3 males; 3) crossed UAS-APPYFP; UAS-APP695/B3 virgins to UAS-APPYFP; UAS-APP695/B3 males.

To study the effects of kinesin-1 overexpression in APP overexpression, we followed a scheme that resulted in overexpression of both kinesin-1 subunits in the UAS-APPYFP; UAS-APP695 background. We proceeded as follows. First, we balanced SG26.1: crossed 1) SG26.1 virgins to CyO/*Bl*; TM2/TM6B males; 2) selected CyO/+; SG26.1/TM6B males and crossed them back to CyO/*Bl*; TM2/TM6B; 3) selected CyO/*Bl*; SG26.1/TM6B males and females to establish a stable stock o CyO/*Bl*; SG26.1 with TM6B floating. Second, we created a stock with SG26.1 and GEN-KLC on the same background: we crossed 1) GEN-KLC/CyO; TM3/TM6B females to CyO/*Bl*; SG26.1/TM6B males; 2) selected GEN-KLC/CyO; SG26.1/TM6B female virgins and males to establish a stable stock with CyO and TM6B floating. Third, we took advantage of the UAS-APP695; GEN-KHC stock established for the IF experiments and crossed to UAS-APPYFP; *pin*^{88K}/B3 virgins to generate UAS-APPYFP /Y; (UAS-APP695; GEN-KHC)/B3. Fourth, we cross GEN-KLC; SG26-1 virgins to UAS-APPYFP /Y; (UAS-APP695; GEN-KHC)/B3 males and selected UAS-APPYFP /X; UAS-APP695/GEN-KLC; SG26-1/GEN-KHC non-tubby female larvae for imaging.

To study the effects of dynein reductions in APP overexpression, we proceeded as follows. For ROBL, we crossed 1) CyO/*Bl*; SG26.1 virgins to *robl*^{k}/B3 males; 2) selected *robl*^{k}/CyO; SG26.1/+ males and crossed to *pin*^{88K}/B3 virgins; 3)

selected (*robl*^{k}; SG26.1)/B3 animals to establish a stable stock; 4) crossed UAS-APPYFP; UAS-APP695 virgins to (*robl*^{k}; SG26.1)/B3 males and selected UAS-APPYFP /X; UAS-APP695/*robl*^{k}; SG26.1/+ non-tubby female larvae for imaging.

To study the effects of DHC reduction on APP overexpression, we crossed 1) UAS-APP695; TM2/TM6B virgins to *dhc64c*$^{4-19}$/TM6B males; 2) selected UAS-APP695/+; *dhc64c*$^{4-19}$/TM6B males were then crossed to *pin*^{88K}/B3 virgins; 3) (UAS-APP695; *dhc64c*$^{4-19}$)/B3 males and females were then selected to form stable stock; 4) UAS-APPYFP; *pin*^{88K}/B3 virgins were then selected and crossed to SG26.1 males; 5) UAS-APPYFP; SG26.1/B3 males were then crossed to (UAS-APP695; *dhc64c*$^{4-19}$)/B3 virgins; 6) UAS-APPYFP /+; UAS-APP695/+; *dhc64c*$^{4-19}$/SG26.1 non-tubby female larvae were selected for imaging.

Results

Effects of APP695 overexpression on axonal morphology

Previous experiments reported that APP695 overexpression induces axonal swellings in segmental nerves of L3 *Drosophila* larvae (Gunawardena and Goldstein 2001). However, axonal swellings are only rarely observed when movement of APP tagged with YFP (APPYFP) is visualized *in vivo*. Two possible explanations for this are that these constructs express at different levels in *Drosophila* or that fundamental differences exist between the *in vitro* and *in vivo* assays. To rule out the second possibility, we used IF to determine swelling number in APPYFP as compared to APP695. We found that swelling number in APP695 animals was significantly increased as compared to control whereas no statistical difference was found for APPYFP (Figure 3-1). This suggests that no discrepancies exist between the two assays.

Effects of cytoplasmic dynein reduction on APP-induced axonal swellings

Next, we tested whether DLC reductions rescued APP695-induced swellings by quantifying swelling number in a *robl*^{k}/+; APP695 overexpression background. This genetic manipulation has been previously reported to rescue the number of swellings in APP695 animals (Gunawardena and Goldstein 2001). We were surprised to find that 50% reduction in DLC failed to rescue axonal swellings in many cases (Figure 3-2A). However, we also noted a large variability in the outcome with some experiments showing rescue but others not. Polymerase chain reaction (PCR) analysis of working stocks confirmed deletion of the ROBL gene, ruling out obvious genetic errors (data not shown). After quantification of images collected in two independent

robl^{k}/+ experiments, we found that on average DLC reduction failed to rescue swellings induced by APP695 overexpression (Figure 3-2B).

Effects of kinesin-1 increases on APP-induced axonal swellings

The interaction between APP and KLC makes *in vivo* predictions, which have been tested in both *Drosophila* and mouse models (Gunawardena and Goldstein 2001; Stokin, Lillo et al. 2005). If APP overexpression leads to axonal swellings by titrating kinesin-1 away from an essential cellular pool, we wondered whether increases in kinesin-1 would rescue the phenotype. To test this possibility we conducted three experiments designed to differentiate between effects of APP overexpression on KLC alone or on the KLC-KHC complex. If APP binding to KLC occurs before association of KLC with KHC, then overexpression of KLC alone would be sufficient to rescue. On the other hand, if binding to KLC occurs after KLC has formed a complex with KHC, overexpression of both KHC and KLC would be necessary for rescue. Thus, we tested three kinesin-1 overexpression conditions: (1) GEN-KLC, (2) GEN-KHC, and (3) GEN-KLC + GEN-KHC (GEN-Kinesin). We were surprised to find that none of the conditions tested had a significant rescuing effect on APP695-induced swellings (Figure 3-3). However, as with the DLC reduction experiments described above, we found a large degree of variability in the behavior. This made us wonder if the IF assay might be insufficient to generate definitive conclusions in these experiments. Though useful for fast phenotypic screenings, this assay might not be sufficiently consistent for detecting subtle changes in behavior. Thus, we turned to the *in vivo* assay, which is much more powerful than the IF method since it allows study of vesicle dynamics.

Effects of APP overexpression on APPYFP movement

Development of the *in vivo* APPYFP imaging assay described in chapter II provided a great tool for further testing of whether kinesin-1 overexpression or dynein reduction rescue phenotypes induced by APP overexpression. As stated above, not only is this method more sensitive it also yields much more valuable information on transport of single vesicles.

We began by looking at how APP overexpression impaired transport in two backgrounds: (1) a background containing 2 copies of APPYFP and (2) a background containing 1 copy of APPYFP and 1 copy of APP695. Because Western blot analysis showed that expression of UAS-APP695 is many-fold higher than that of UAS-APPYFP, we posited these two overexpression backgrounds would provide us with a graded effect on transport. Indeed, we observed that APP overexpression led to the appearance of axonal swellings in both overexpression backgrounds. In addition, our analysis of cargo populations showed a significant increase in the percentage of stationary cargoes for both UAS-APPYFP; UAS-APPYFP and UAS-APPYFP; UAS-APP695 (Figure 3-4A; Table 3-1). As expected from the protein analysis, APPYFP; APP695 showed a stronger phenotype than UAS-APPYFP; UAS-APPYFP with increases in stationary percentage being accompanied by significant decreases in all moving populations. Interestingly, the only change in moving percentage for APPYFP; APPYFP was a decrease in reversing. No significant change in A/R ratio was observed for either background (Table 3-1, right).

A possible outcome for APP overexpression is increased APP loading on vesicles. This could lead to increased recruitment of kinesin-1 motor to vesicles via

APP-KLC binding. Alternatively, APP overexpression might not change kinesin-1 motor number on vesicles but instead might increase APPYFP flux. To differentiate between these possibilities we looked at flux and vesicle intensity parameters. For APPYFP; APPYFP, we observed a significant decrease in retrograde flux but no change in anterograde (Table 3-1); mean fluorescence intensity showed a significant increase for both anterograde and retrograde cargoes (Figure 3-6). APPYFP; APP695 had a similar effect, except for additional impairment in anterograde flux (Table 3-1; Figure 3-6). This is consistent with the idea that APP overexpression leads to increased APP loading in vesicles. This may lead to kinesin-1 motor number increases on the surface of vesicles.

If APP overexpression increased kinesin-1 number on vesicles, we should see evidence for this in the analysis of APPYFP movement. For instance, increases in kinesin-1 motor number might translate into increases in anterograde run length (ARL). Indeed, we observed a significant increase in ARL for region 10 of APPYFP; APPYFP (Figure 3-4B; Table 3-2). Interestingly, no change in anterograde segmental velocity (ASV), anterograde pause frequency (APF), and anterograde pause duration (APD) were observed. In addition, no increase in ARL was observed for APPYFP; APP695. The only significant change in this condition was a significant decrease in ASV (Figure 3-4B; Table 3-2). These differences might relate to differential levels of expression for APPYFP and APP695.

Surprisingly, APP overexpression had a dramatic effect on retrograde behavior. Both backgrounds showed a significant decrease in retrograde segmental velocity (RSV) and retrograde run length (RRL) (Figure 3-5A; Table 3-2). In

addition, APPYFP; APP695 also showed a significant increase in retrograde pause frequency (RPF) and retrograde pause duration (RPD) (Figure 3-5B; Table 3-2). Taken together these experiments suggest the intriguing possibility that APP overexpression may lead to increased kinesin-1 motor on the surface of vesicles. This may lead to displacement of cytoplasmic dynein from vesicle surfaces, setting up an imbalance in motor protein ratios required for optimal transport.

Effects of kinesin-1 overexpression on APPYFP movement in an APP695 overexpression background

In the IF experiments, we observed that kinesin-1 overexpression failed to rescue axonal swellings induced by APP695 overexpression (Figure 3-3). We wondered if this would also be the case in the *in vivo* assay. To test this, we overexpressed both subunits of kinesin-1 (GEN-kinesin) and looked to see how this affected APPYFP movement in the APP695 overexpression background. The increase in stationary percentage observed in APPYFP; APP695; GEN-kinesin as compared to APPYFP; APP695 suggested that transport was further impaired by kinesin-1 overexpression (Figure 3-7A; Table 3-1). Not only was stationary percentage increased significantly in GEN-kinesin but also there was a significant decrease in all moving percentages. In agreement with these observations, bi-directional flux was significantly decreased (Table 3-1, right). Interestingly, we noted a significant decrease in mean vesicle intensity for GEN-kinesin (Figure 3-6). This suggested that kinesin-1 overexpression might lead to decreased APPYFP loading on vesicles. Alternatively, it might indicate fewer vesicles clustering together in swellings—an indirect indication that swelling size decreased.

Because we observed a dramatic decrease in bi-directional flux, we expected that transport parameters would also be impaired in APPYFP; APP695; GEN-kinesin as compared to APPYFP; APP695. Surprisingly, this was not the case as ASV and ARL increased and APF and APD decreased significantly (Figure 3-7B and C; Table 3-2). In addition, we observed a significant enhancement in RRL, which was accompanied by significant decreases in RPF and RPD (Figure 3-8; Table 3-2). RSV, however, decreased significantly (Figure 3-8A; Table 3-2), which was counterintuitive. Thus, there was a rescuing effect by GEN-kinesin on APPYFP; APP695.

Effects of cytoplasmic dynein reductions on APPYFP movement in an APP695 overexpression background

Next, we tested if cytoplasmic dynein reduction would also rescue APP695 overexpression using the *in vivo* assay. Thus, we conducted two experiments in which DHC or DLC would be reduced by 50% in an APP695 overexpression background. Our analysis of moving populations showed no significant change in stationary percentages for both DHC and DLC (Figure 3-7A; Table 3-1). In addition, we observed further decrease in retrograde and reversing percentages for DHC. For DLC, the only significant change was increase in anterograde percentage as compared to APPYFP; APP695. Consistent with these findings, a bi-directional reduction in flux was observed for DHC. Only retrograde flux decreased significantly for DLC (Table 3-1, right). Interestingly, both DHC and DLC groups showed a significant decrease in mean vesicle intensity as compared to APPYFP; APP695 (Figure 3-6).

We then turned to analysis of movement parameters to see if reduction in DHC or DLC would improve movement as compared to APPYFP; APP695. Remarkably, DHC reduction led to a significant increase in ASV and ARL (Figure 3-7B; Table 3-2). Significant decreases in APF and APD were also observed (Figure 3-7C; Table 3-2). However, DLC reductions had little rescuing effect on APPYFP; APP695 and showed a decrease in ASV being observed (Figure 3-7B; Table 3-2).

Interestingly, the effect of DHC reduction on RL was bi-directional, with DHC reduction leading to a significant increase in RRL (Figure 3-8A; Table 3-2). This was accompanied by a significant decrease in RPF and RPD as compared to APPYFP; APP695 (Figure 3-8B; Table 3-2). However, RSV decreased significantly (Figure 3-8A; Table 3-2). Similarly, DLC reduction showed a significant enhancement in RRL but decreases in RSV, RPF, and RPD (Figure 3-8; Table 3-2). Thus, reductions in cytoplasmic dynein showed a rescuing effect on movement as compared to APPYFP; APP695.

Discussion

We set out to test whether kinesin-1 overexpression or cytoplasmic dynein reductions rescue transport defects induced by APP695 overexpression. As with previous reports, we found that APP695 overexpression leads to the formation of axonal swellings characterized by accumulation of vesicular proteins such as CSP. However, DLC reduction on average failed to rescue the APP695-induced phenotype in the present study. We speculate that this discrepancy arises from improvements in imaging and quantification methods used here. Not only did we analyze all Z-stack images in the present study but also set a 1.5 μm^2 size threshold for swellings. In addition, we measured fiber length and expressed the results as swellings/mm. Though this approach constitutes a major improvement over previously available methods, swelling quantification can still be improved by implementing a more standardized computerized system to the detection of swellings. Such approach would benefit from local thresholding, which would help smooth out variations in staining intensity across the specimen.

As to the variability observed in the IF assay, we were surprised to find such high degree of variability in the APP695 overexpression phenotype. In several cases, little difference existed between APP695 and controls. We wonder if this behavior constitutes the reason why so much variability was also observed for DLC rescuing. Because we do not have a before and after comparison in the same animal, it is impossible to tell whether a given animal presented swellings to begin with. This problem certainly plagued our genomic kinesin-1 experiments as well though an important difference exists between the two backgrounds. Whereas 50% reduction in

DLC showed no increase in axonal swellings as compared to ApplGal4 controls, increases in kinesin-1 were not completely benign. In several cases, kinesin-1 overexpression resulted in axonal accumulations of CSP. Thus, it seems as if changes in kinesin-1—either reduced or increased levels—may be more deterministic than cytoplasmic dynein as to pathological changes in the axon.

Live imaging of vesicle movement in axons has provided us with a much more powerful tool to study axonal transport as compared with the IF static system. For one, live imaging of APPYFP vesicles clearly shows that not all axonal swellings constitute blockages. Indeed, the majority of swellings seem to be dynamic structures allowing vesicles to course through them. Thus, it is not accurate to refer to all axonal swellings as "axonal clogs." Of course, we have observed several cases where axonal swellings appear to be clogs, but these tend to occur much less frequently and only for considerably large swellings. It would be interesting to know how swellings change in the long-term to see if these structures are dynamic or not. If swellings indeed represent a starting point in the neurodegeneration cascade, this should be evident in long-term studies. In addition, it would be interesting to know if swellings change the autocorrelation behavior of moving particles. Though smaller swellings do not seem to do so, this would be an excellent question to explore further. To this end, we have collected several streams flanking swellings that can provide a starting point.

One major limitation of our current analysis package for live imaging is its inability to accurately deal with larger particles, or blobs. Visual inspection of swellings in our movies shows that several vesicles are clustered in these structures. However, we cannot accurately resolve these particles to determine how many

vesicles exist in a particular swelling. Advances in a "blob tracker" algorithm recently developed by our collaborators may help us gain a better understanding of phenomena localized to swellings. Thus, probing for rescuing effects of APP overexpression in the present study relied more on changes to movement than an in-depth analysis of swellings. It should be noted, however, that changes in intensity might be an indirect indicator for swelling size since greater accumulation of vesicles in these structures seem to increase their brightness. Interestingly, both kinesin-1 overexpression and dynein reduction led to decreases in mean fluorescence intensity as compared to APPYFP; APP695 (Figure 3-6). Still, utilization of the blob tracker for better analysis of swelling parameters should help strengthen this point.

In broad terms, inspection of stationary percentage and flux should give an indication as to the degree of movement in a system. In previous experiments, we observed that increases in stationary percentage correlate well with bi-directional impairment in transport. Flux analysis has also correlated well with the degree of movement, with increases in directional flux often translating into improved directional movement. Viewed through this lens, neither kinesin-1 overexpression nor cytoplasmic dynein reductions rescued transport impairment induced by APP overexpression. Nevertheless, we have also observed some striking changes in movement, which must be taken into account.

The bi-directional improvement in RL observed in kinesin-1 overexpression as compared to APPYFP; APP695 suggests that kinesin-1 overexpression rescues movement. This certainly fits with the idea of APP overexpression acting as a titrating factor for kinesin-1. The activating effect on RRL is also consistent with our idea that

kinesin-1 acts as a processivity factor for cytoplasmic dynein. Thus, even if stationary percentages increased in the kinesin-1 overexpression group, vesicle movement improved.

As with the kinesin-1 overexpression experiment, cytoplasmic reduction showed phenotypic rescuing. DHC reduction, for instance, led to a significant increase in ASV and ARL as compared to APPYFP; APP695. Interestingly, it also led to improvement in retrograde movement showing that improvements to anterograde movement often benefit retrograde. Thus, cytoplasmic dynein reduction can rescue vesicle movement in an APP overexpression background.

In conclusion, the findings reported here suggest that both kinesin-1 overexpression and cytoplasmic dynein reduction can rescue movement in APP overexpression phenotypes. While stationary cargo percentage did not appear to change with our genetic manipulations, mean fluorescence intensity analysis suggests that swellings comprised fewer vesicle aggregates. These findings suggest that manipulations to genetic pathways may provide a mechanism for reversing neurodegenerative changes seen in APP overexpression pathways.

Chapter 3 will also be submitted for publication: Reis GR and Goldstein LSB. "Kinesin-1 overexpression and cytoplasmic dynein reduction improve transport in an APP overexpression background." The dissertation author was the primary author and investigator of this paper.

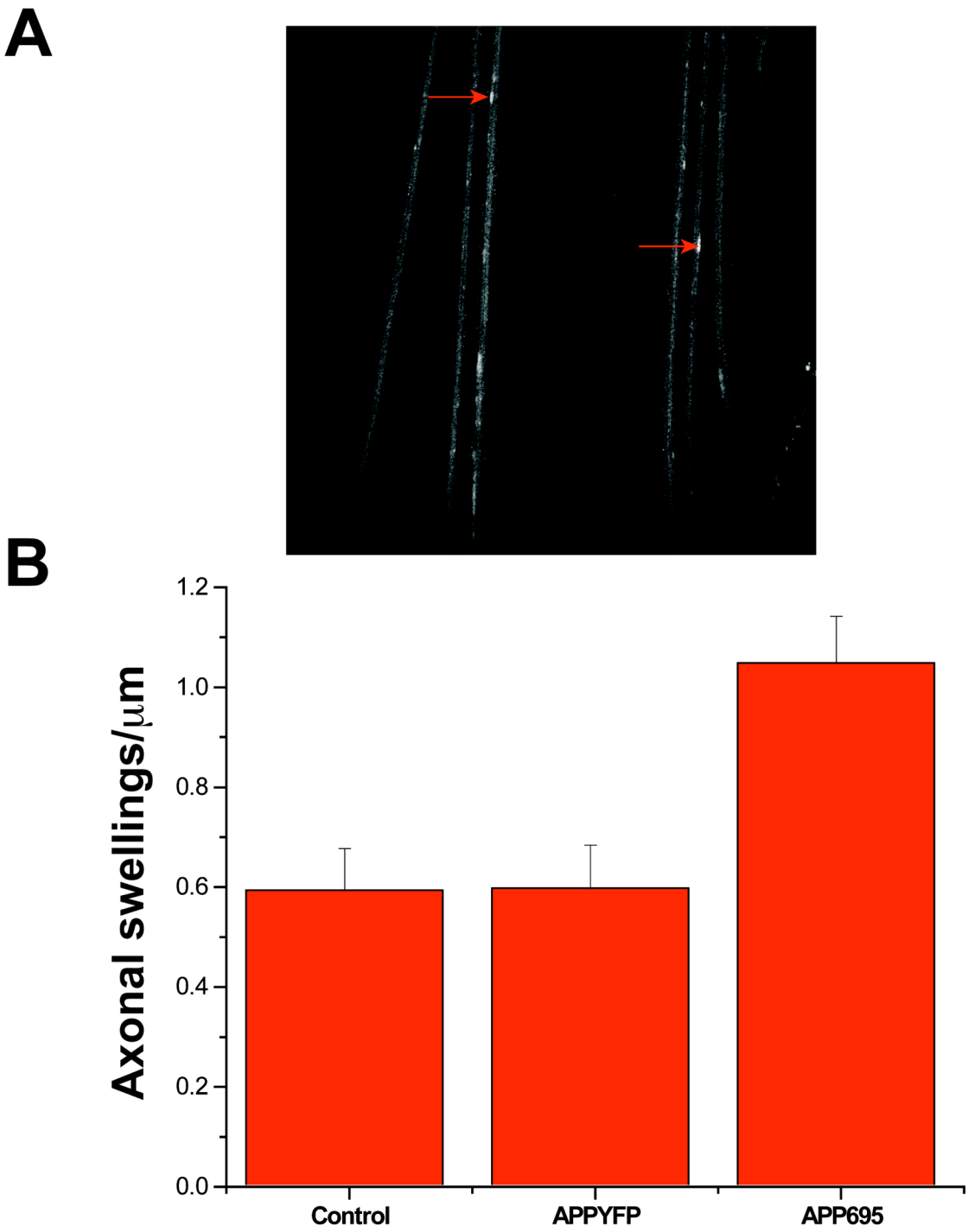

Figure 3-1. APP695 overexpression induces axonal swelling formation. A) Anti-cysteine string protein immunostaining showing axonal swellings in ApplGal4/X; APP695/+ (red arrows point to swellings). B) Quantification of axonal swellings induced by APPYFP (N=10) and APP695 (N=10) showing a statistically significant increase above control (N=10) in swelling number for APP695 (Student's t test; $P < 0.001$). The control group was Oregon R.

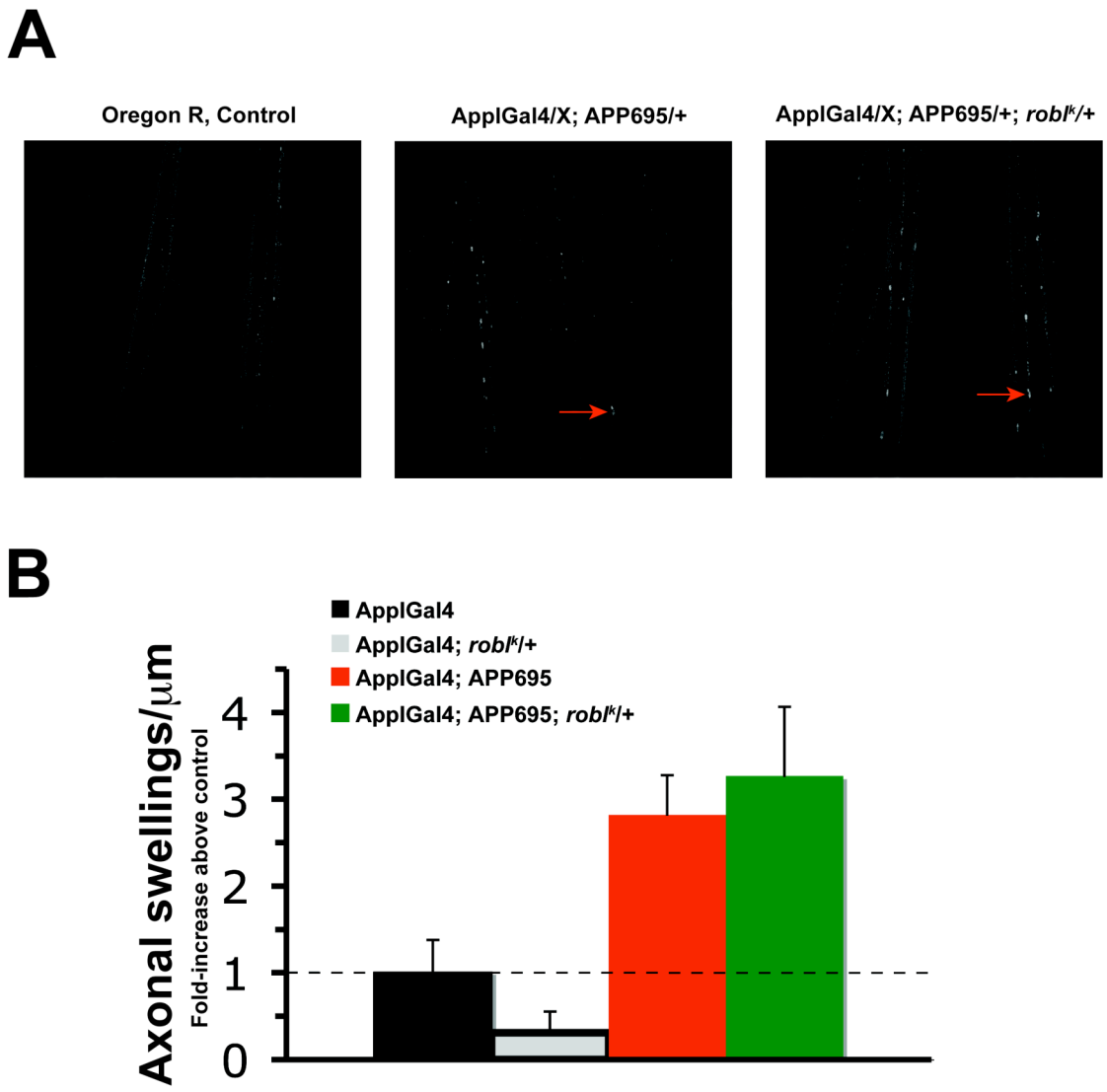

Figure 3-2. DLC reduction does not rescue swellings induced by APP695 overexpression A) Anti-cysteine string protein immunostaining showing axonal swellings in both ApplGal4/X; APP695/+ as well as ApplGal4/X; APP695/+; roblk//+ (red arrow points to a swelling in each image). B) Quantification of axonal swellings induced by ApplGal4; APP695 (N=12) were significantly increased above the ApplGal4 control (N=6). Mean swelling number in controls was 1.9 swellings/mm. Student's t test showed no significant difference between ApplGal4; APP695 and ApplGal4; APP695; roblk (N=15) groups [P, N.S.]. Two sets of experiments were combined in the ApplGal4; APP695; roblk/+ group. Analysis of ApplGal4; roblk/+ animals (N=4) showed no significant change in swelling number, suggesting that 50% reduction in ROBL does not cause swellings. All N values refer to animal numbers.

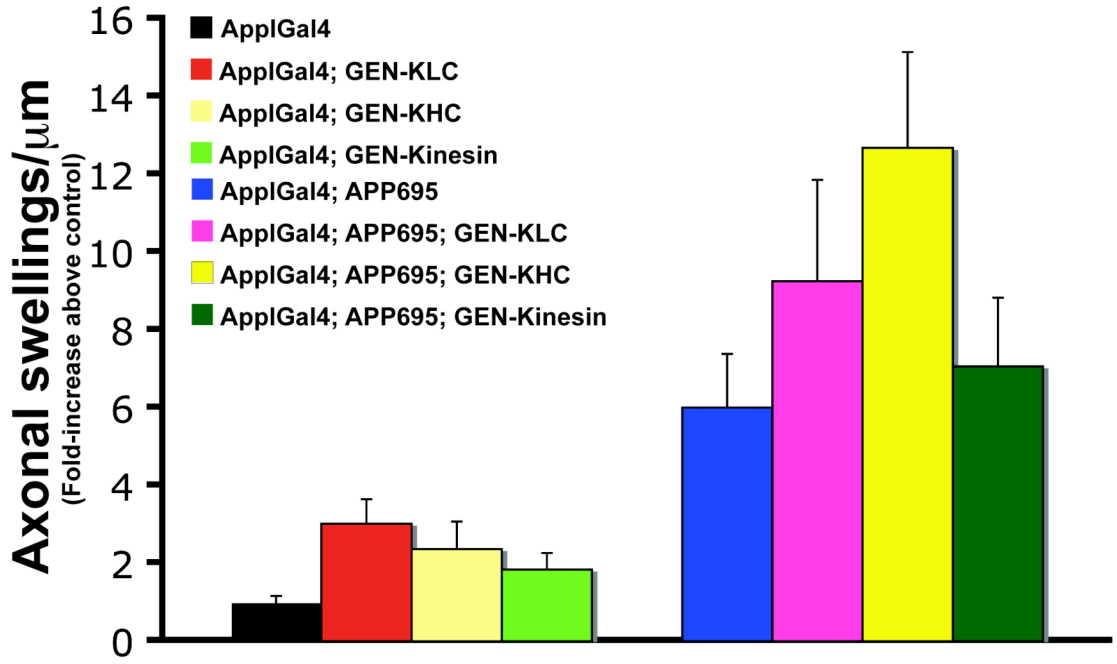

Figure 3-3. Kinesin-1 overexpression does not rescue swellings induced by APP695 overexpression. Graphical representation for quantification of swellings in control vs. APP overexpression genotypes. The Y-axis refers to fold-increases above control. UAS expression was under control of the panneuronal driver ApplGal4. GEN-Kinesin refers the presence of both GEN-KLC and GEN-KHC in the same background. Three individual sets of experiments were pooled for this analysis, resulting in a large number of animals per condition: ApplGal4 (N=38); ApplGal4; GEN-KLC (N=21); ApplGal4; GEN-KHC (N=28); ApplGal4; GEN-Kinesin (N=27); ApplGal4; APP695; GEN-KLC (N=44); ApplGal4; APP695; GEN-KHC (N=51); ApplGal4; APP695; GEN-KHC (N=54); ApplGal4; APP695; GEN-Kinesin (N=37). N values represent number of animals per condition. On average, 3 images were collected for each animal, and quantification for each image was then averaged to yield one value per animal (see Methods). Student's t test showed P [N.S.] for pairwise comparisons between any condition in the APP overexpression groups.

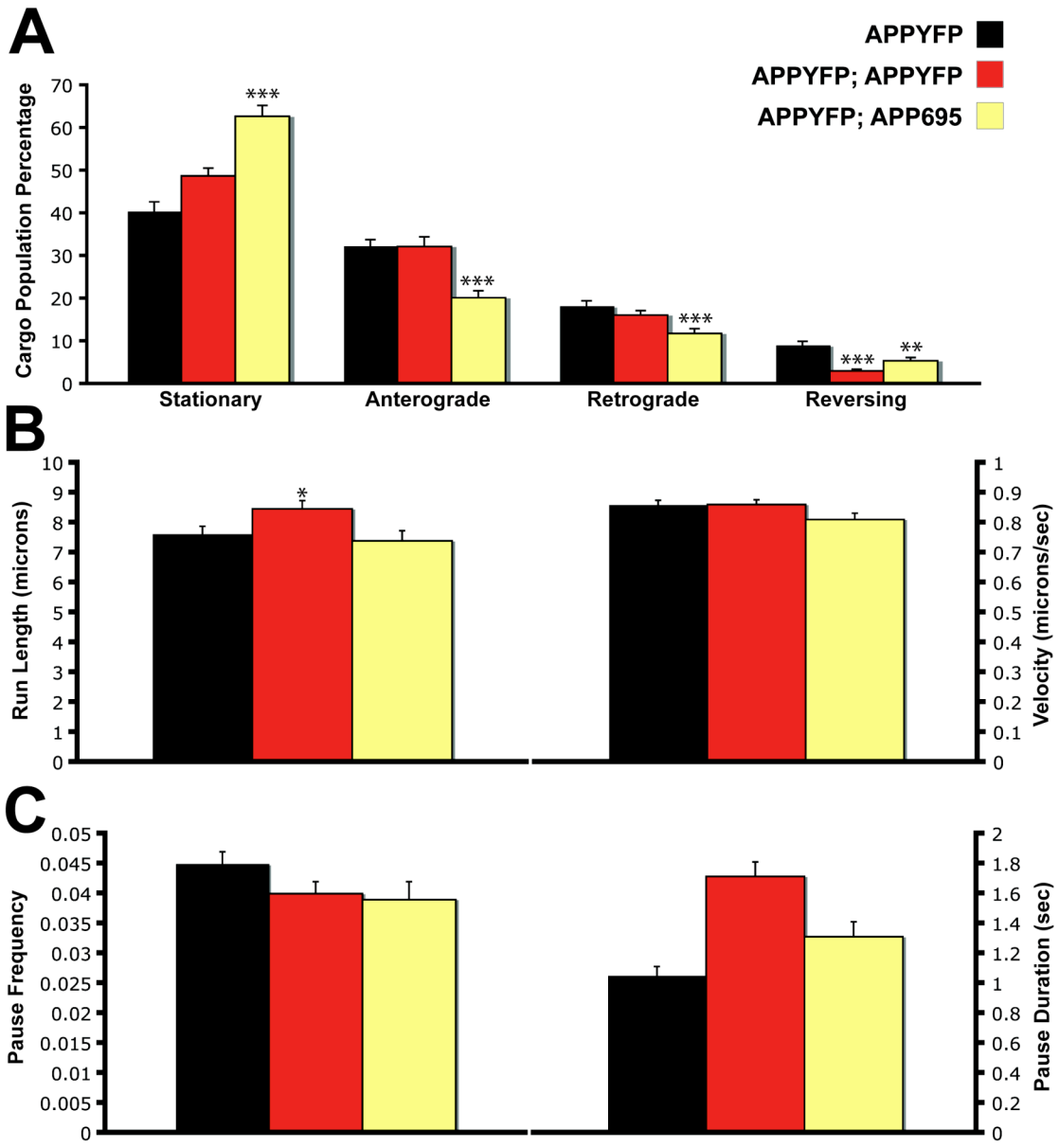

Figure 3-4. Effects of APP overexpression on anterograde APPYFP movement for region 10. A) Cargo population analysis showing a significant increase in stationary percentage for APPYFP; APP695 at the expense of decreases in moving populations. Only reversing percentage decreased significantly for APPYFP; APPYFP. Refer to Table 3-1 for population percentage values. B) APP overexpression had only a mild effect on anterograde behavior with APPYFP; APPYFP leading to a significant increase in ARL (Left). No significant changes were observed in ASV for either overexpression background (Right). C) APF (Left) and APD (Right) did not change significantly in either overexpression background. Statistical significance for all parameters was determined using a Wilcoxon rank-sum test, except for segmental velocity where the Kolmogorov-Smirnov test was used: * = $P < 0.05$; ** = $P < 0.01$; *** = $P < 0.001$. Refer to Table 2-1 for ARL, ASV, APF, and APD mean values.

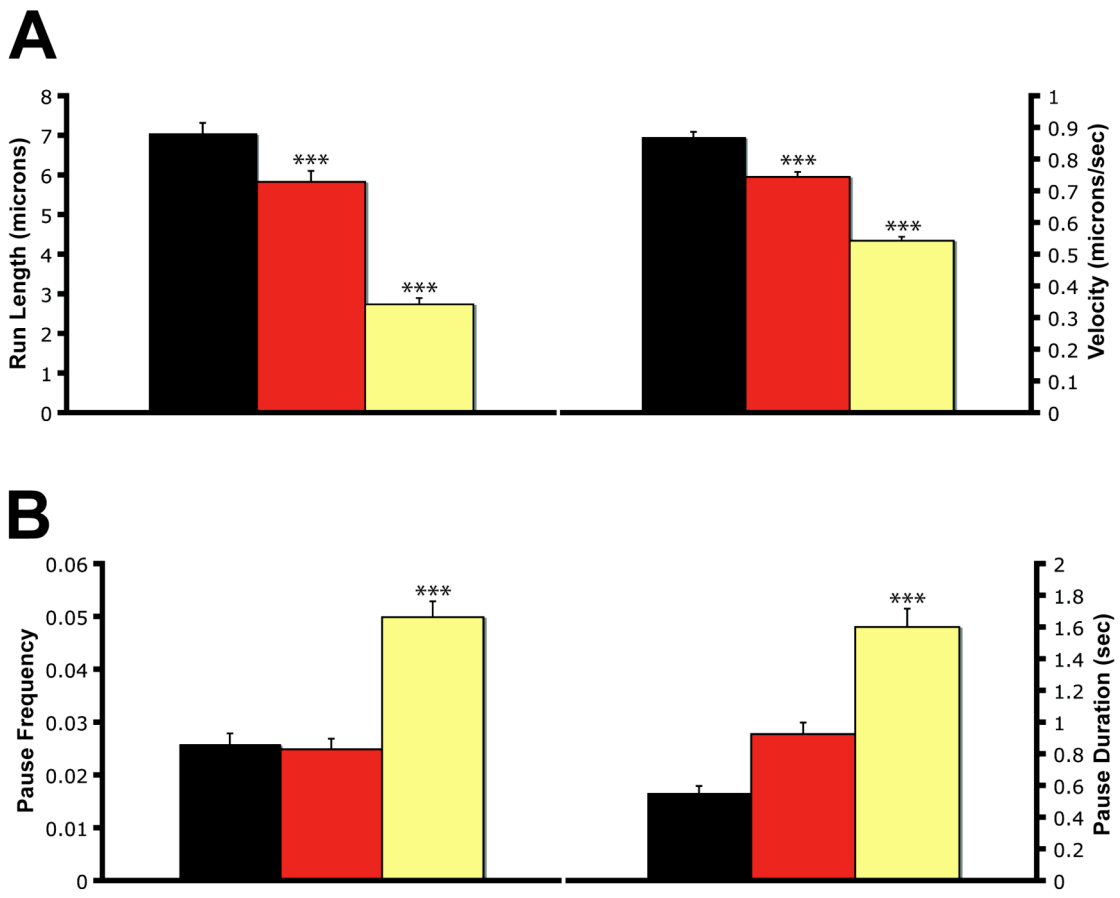

Figure 3-5. Effects of APP overexpression on retrograde APPYFP movement in region 10. A) RRL (Left) and RSV (Right) decreased significantly in both APP overexpression backgrounds. B) RPF (Left) increased significantly only for APPYFP; APP695, and RPD (Right) increased significantly in both APP overexpression backgrounds. Statistical significance: * = $P < 0.05$; ** = $P < 0.01$; *** = $P < 0.001$. Refer to Table 2-2 for RRL, RSV, RPF, and RPD mean values. See Methods for a detailed definition of each parameter.

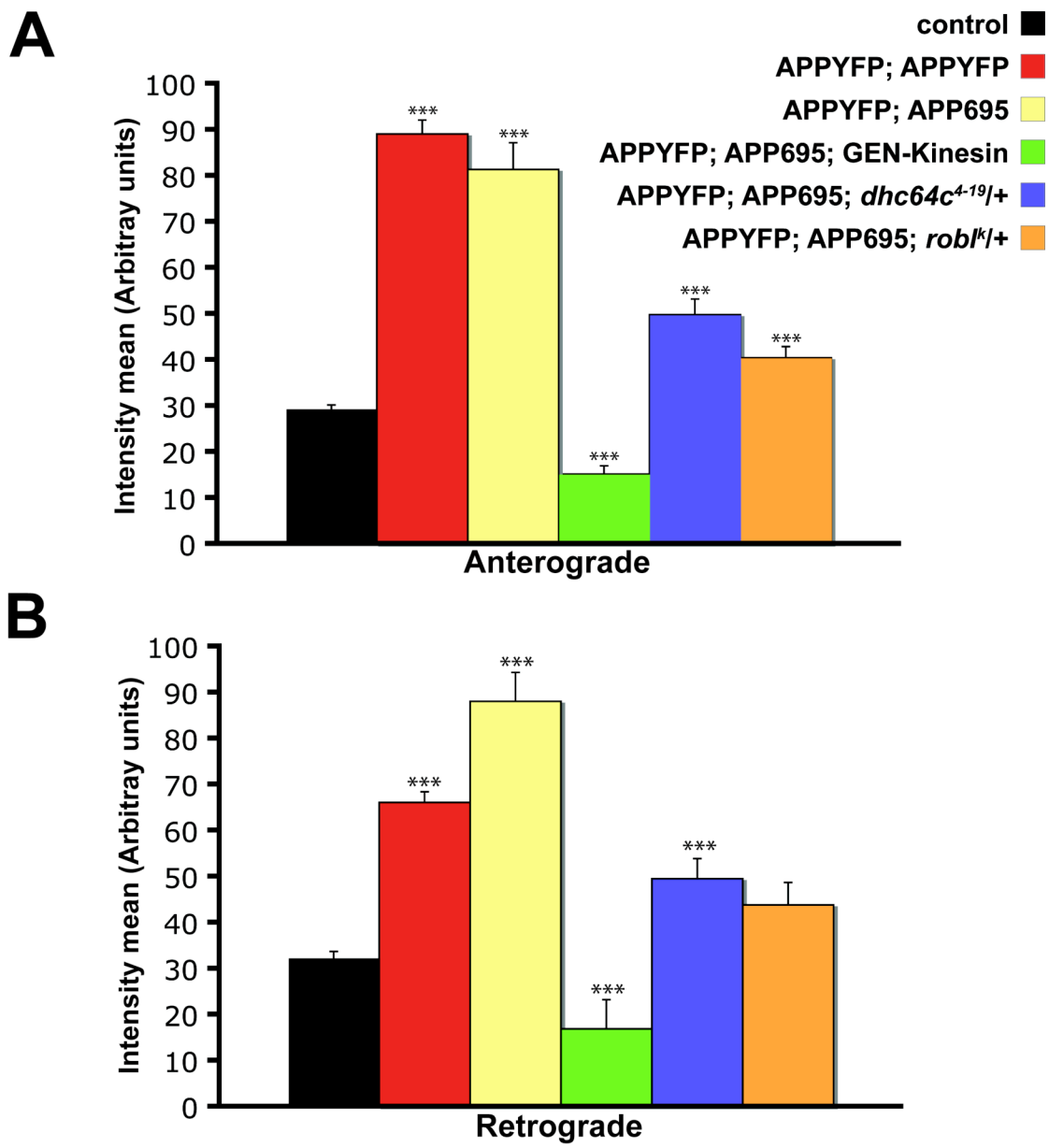

Figure 3-6. Intensity analysis for APP overexpression and rescue experiments in region 10. A) Effects on anterograde and B) retrograde vesicle populations. APP overexpression leads to a significant increase in bi-directional mean intensity fluorescence as compared to control [$P < 0.001$ for all comparisons]. Interestingly, kinesin-1 overexpression led to a significant bi-directional decrease in mean intensity as compared to control [$P < 0.001$; this is also true for comparisons between APP overexpression groups and GEN-Kinesin]. We also observed a significant decrease in bi-directional mean intensity for the dynein reduction groups as compared to APPYFP; APP695 [$P < 0.001$]. *** = $P < 0.001$ and represents pairwise comparisons to control.

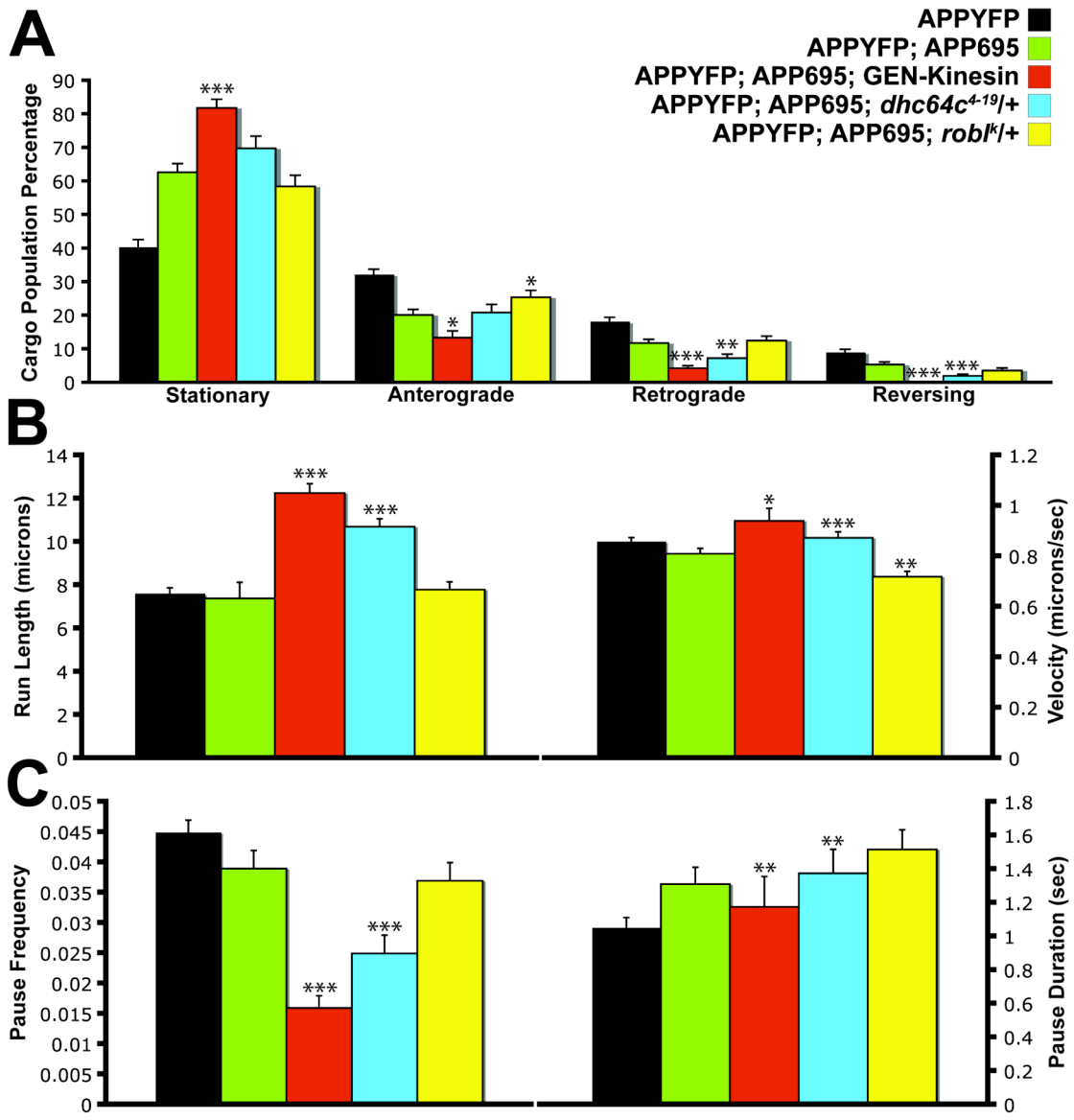

Figure 3-7. Effects of kinesin-1 overexpression and cytoplasmic dynein reductions on APPYFP vesicle movement in an APP695 overexpression background (region 10). A) Cargo population analysis showing a significant increase in stationary percentage for the kinesin-1 overexpression condition (GEN-Kinesin) at the expense of decreases in moving populations. DHC reduction led to a significant decrease in retrograde and reversing percentage, and DLC reduction led to a significant increase in anterograde percentage. All pairwise comparisons made to APPYFP; APP695. Refer to Table 3-1 for population percentage values. B) (Left) ARL increased significantly in GEN-Kinesin and dhc/+ groups; (Right) ASV increased significantly in GEN-Kinesin and dhc/+ groups but decreased significantly in the dlc/+ group as compared to APPYFP; APP695. C) (Left) APF decreased significant in GEN-Kinesin and dhc/+ groups but not in dlc/+; (Right) APD was significantly reduced in GEN-Kinesin but increased in the dhc/+ group. Significance: * = $P < 0.05$; ** = $P < 0.01$; *** = $P < 0.001$.

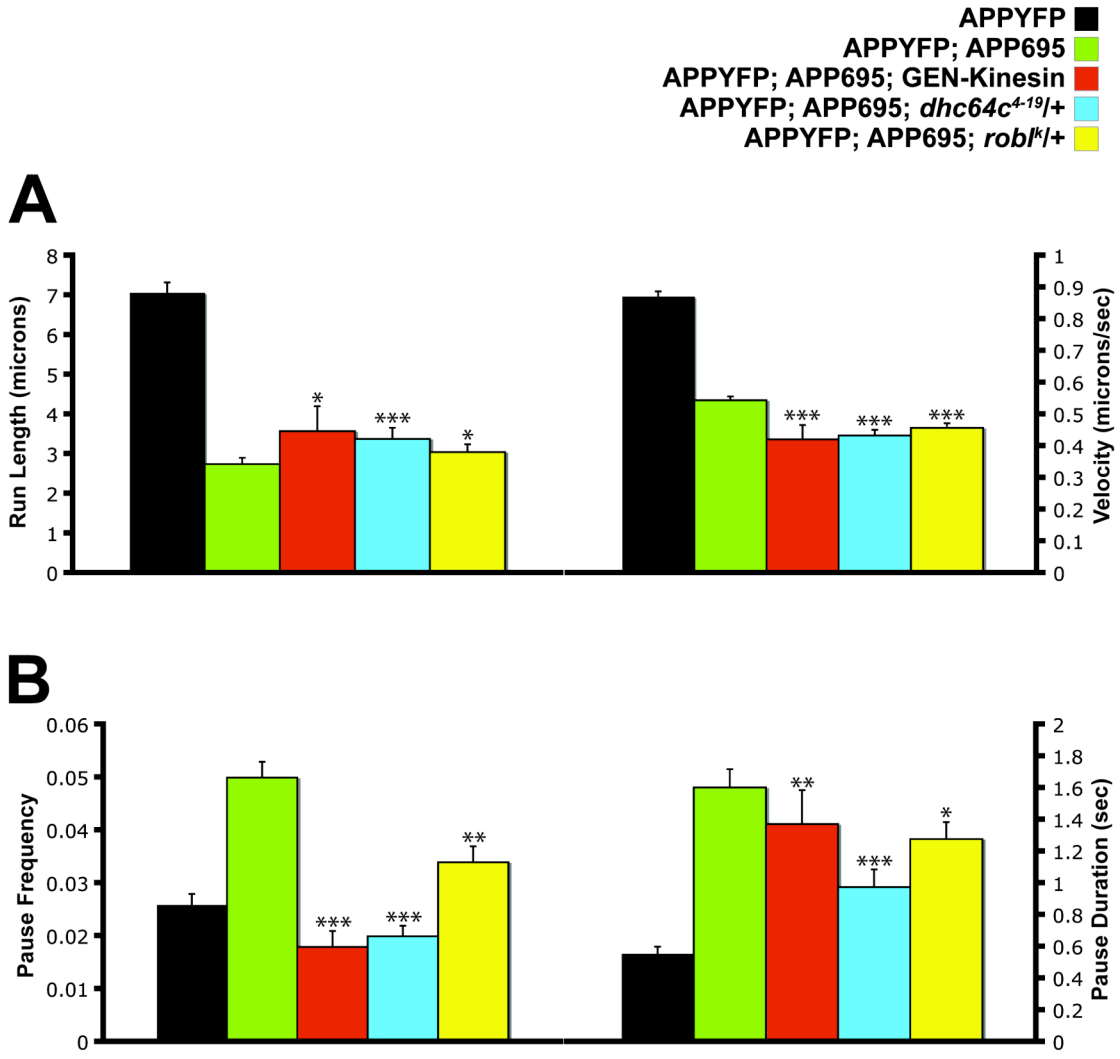

Figure 3-8. Effects of kinesin-1 overexpression and cytoplasmic dynein reductions on retrograde APPYFP vesicle movement in an APP695 overexpression background (region 10). A) RRL (Left) increased and RSV (Right) decreased significantly in GEN-Kinesin and dynein reductions as compared to APPYFP; APP695. B) RPF (Left) and RPD (Right) decreased significantly in both GEN-Kinesin and dynein reductions as compared to APPYFP; APP695. Statistical significance was determined from pairwise comparisons to APPYFP; APP695: * = $P < 0.05$; ** = $P < 0.01$; *** = $P < 0.001$. Refer to Table 2-2 for RRL, RSV, RPF, and RPD mean values. See Methods for a detailed definition of each parameter.

Table 3-1. Cargo population and flux analysis for APPYFP vesicle movement in axonal region 10. Statistical significance on means was accessed by using a Wilcoxon rank-sum test. Cells colored red denote significant increases above the APPYFP control mean, with 1 arrow signifying $p<0.05$, 2 arrows $p<0.01$, and 3 arrows $p<0.001$. Cells colored blue represent significant downward changes with the number of arrows representing the level of p value significance as described for red cells. Abbreviations: A, anterograde; R, retrograde. See Methods for detailed information on how these parameters were defined.

Cargo Population and Flux Analysis
APP OVEREXPRESSION – REGION 10

Mean Percentage

Genotype	Stationary Percentage (Mean ± SEM)	Anterograde Percentage (Mean ± SEM)	Retrograde Percentage (Mean ± SEM)	Reversing Percentage (Mean ± SEM)
APPYFP	40.42 ± 2.22	32.29 ± 1.49	18.23 ± 1.20	9.058 ± 0.88
APPYFP; APPYFP	48.73 ± 1.81	32.18 ± 2.29	16.11 ± 1.03	2.99 ± 0.41
APPYFP; APP695	62.69 ± 2.58	20.14 ± 1.66	11.79 ± 1.10	5.38 ± 0.77
GENKHC; GENKLC	81.87 ± 2.57	13.42 ± 2.01	4.29 ± 0.73	0.43 ± 0.22
APPYFP; APP695; (dhc64c^{k-19}/+)	69.80 ± 2.31	20.88 ± 2.44	7.32 ± 1.13	2.00 ± 0.46
APPYFP; APP695; (rab^{5}/+)	58.46 ± 3.32	25.42 ± 2.05	12.52 ± 1.35	3.61 ± 0.73
Compared to APPYFP (rank-sum)	**Stationary**	**Anterograde**	**Retrograde**	**Reversing**
APPYFP; APPYFP	↑ ↑	→	→	↓ ↓ ↓
APPYFP; APP695	↑ ↑ ↑	↓ ↓ ↓	↓ ↓ ↓	↓ ↓
GENKHC; GENKLC	↑ ↑ ↑	↓ ↓ ↓	↓ ↓ ↓	↓ ↓ ↓
APPYFP; APP695; (dhc64c^{k-19}/+)	↑ ↑ ↑	↓ ↓ ↓	↓ ↓ ↓	↓ ↓ ↓
APPYFP; APP695; (rab^{5}/+)	↑ ↑ ↑	↓ ↓	↓ ↓	↓ ↓ ↓
Compared to APPYFP; APP695 (rank-sum)	**Stationary**	**Anterograde**	**Retrograde**	**Reversing**
GENKHC; GENKLC	↑ ↑ ↑	↓	↓ ↓ ↓	↓ ↓ ↓
APPYFP; APP695; (dhc64c^{k-19}/+)	→	→	↓ ↓	↓ ↓ ↓
APPYFP; APP695; (rab^{5}/+)	→	↑	→	→
Statistical Significance				**Color scheme**
↓↓↓ / ↑↑↑ = p<0.001				Red = up
↓↓ / ↑↑ = p<0.01				Blue = down
↓ / ↑ = p<0.05				
→ = p>0.05				

A/R

A:R Ratio
2.19 ± 0.21
3.85 ± 1.00
2.30 ± 0.42
2.52 ± 0.31
3.58 ± 0.50
2.61 ± 0.40
Compared to APPYFP (rank-sum)
→
→
→
↑ ↑
→
Compared to APPYFP; APP695 (rank-sum)
→
→
→

Flux Analysis

Genotype	Anterograde (Mean ± SEM)	Retrograde (Mean ± SEM)
APPYFP	11.16 ± 2.02	6.42 ± 1.32
APPYFP; APPYFP	10.33 ± 2.15	4.25 ± 0.95
APPYFP; APP695	5.75 ± 1.17	1.80 ± 0.51
GENKHC; GENKLC	2.48 ± 0.74	0.32 ± 0.23
APPYFP; APP695; (dhc64c^{k-19}/+)	4.66 ± 1.07	0.78 ± 0.28
APPYFP; APP695; (rab^{5}/+)	5.18 ± 1.22	1.31 ± 0.46
Compared to Control (rank-sum)	**Anterograde**	**Retrograde**
APPYFP; APPYFP	→	↓ ↓ ↓
APPYFP; APP695	↓ ↓ ↓	↓ ↓ ↓
GENKHC; GENKLC	↓ ↓ ↓	↓ ↓ ↓
APPYFP; APP695; (dhc64c^{k-19}/+)	↓ ↓ ↓	↓ ↓ ↓
APPYFP; APP695; (rab^{5}/+)	↓ ↓ ↓	↓ ↓ ↓
Compared to APPYFP; APP695 (rank-sum)	**Anterograde**	**Retrograde**
GENKHC; GENKLC	↓ ↓ ↓	↓ ↓ ↓
APPYFP; APP695; (dhc64c^{k-19}/+)	↓	↓ ↓ ↓
APPYFP; APP695; (rab^{5}/+)	→	↓
Statistical Significance		
↓↓↓ / ↑↑↑ = p<0.001		
↓↓ / ↑↑ = p<0.01		
↓ / ↑ = p<0.05		
→ = p>0.05		

Table 3-2. Summary of transport parameters for APPYFP vesicle movement in APP overexpression backgrounds (axonal region 10). Statistical significance on mean segmental velocities was accessed using the Kolmogorov-Smirnov test. For all other parameters, the Wilcoxon rank-sum test was used. Cells colored red denote significant increases above the control mean; cells colored blue represent significant downward changes as in Table 3-1. Abbreviations: A, anterograde; R, retrograde; SV, segmental velocity (microns/second); RL, run length (microns); PF, pause frequency (number of pauses/15 seconds); PD, pause duration (seconds); SF, switch frequency (number of switches/trajectory). See Methods for a detailed definition of each parameter.

Table of Transport Parameters and Statistics
APP OVEREXPRESSION – REGION 10

Anterograde

Genotype	A_SV (Mean ± SEM)	A_RL (Mean ± SEM)	A_PF (Mean ± SEM)	A_PD (Mean ± SEM)
APPYFP	0.86 ± 0.015	7.628 ± 0.256	0.045 ± 0.002	1.053 ± 0.06
APPYFP; APPYFP	0.861 ± 0.016	8.463 ± 0.277	0.040 ± 0.002	1.715 ± 0.097
APPYFP; APP695	0.811 ± 0.021	7.397 ± 0.337	0.039 ± 0.003	1.312 ± 0.100
GENKHC; GENKLC	0.941 ± 0.050	12.265 ± 0.743	0.016 ± 0.002	1.177 ± 0.180
APPYFP; APP695; (dhc64c$^{6-19}$/+)	0.874 ± 0.024	10.713 ± 0.431	0.025 ± 0.003	1.376 ± 0.143
APPYFP; APP695; (rob^{P}/+)	0.72 ± 0.021	7.801 ± 0.362	0.037 ± 0.003	1.518 ± 0.117

Compared to APPYFP	A_SV (Mean ± SEM)	A_RL (Mean ± SEM)	A_PF (Mean ± SEM)	A_PD (Mean ± SEM)
APPYFP; APPYFP	→	↑↑↑	→	→
APPYFP; APP695	↓↓	→	→	→
GENKHC; GENKLC	↑↑	↑↑↑	↓↓↓	↑↑
APPYFP; APP695; (dhc64c$^{6-19}$/+)	↑↑↑	↑↑↑	↓↓↓	↑
APPYFP; APP695; (rob^{P}/+)	↓↓↓	→	→	→

Compared to APPYFP; APP695	A_SV (Mean ± SEM)	A_RL (Mean ± SEM)	A_PF (Mean ± SEM)	A_PD (Mean ± SEM)
GENKHC; GENKLC	↑	↑↑↑	↓↓↓	↓↓
APPYFP; APP695; (dhc64c$^{6-19}$/+)	↑↑↑	↑↑↑	↓↓↓	↑↑
APPYFP; APP695; (rob^{P}/+)	↓↓	→	→	→

Retrograde

Genotype	R_SV (Mean ± SEM)	R_RL (Mean ± SEM)	R_PF (Mean ± SEM)	R_PD (Mean ± SEM)
APPYFP	0.873 ± 0.015	7.076 ± 0.246	0.026 ± 0.002	0.559 ± 0.042
APPYFP; APPYFP	0.746 ± 0.017	5.844 ± 0.256	0.025 ± 0.002	0.929 ± 0.073
APPYFP; APP695	0.545 ± 0.012	2.753 ± 0.156	0.050 ± 0.003	1.605 ± 0.115
GENKHC; GENKLC	0.422 ± 0.045	3.581 ± 0.632	0.018 ± 0.003	1.374 ± 0.214
APPYFP; APP695; (dhc64c$^{6-19}$/+)	0.434 ± 0.018	3.388 ± 0.279	0.020 ± 0.002	0.977 ± 0.111
APPYFP; APP695; (rob^{P}/+)	0.458 ± 0.015	3.054 ± 0.199	0.034 ± 0.003	1.280 ± 0.106

Compared to APPYFP	R_SV (Mean ± SEM)	R_RL (Mean ± SEM)	R_PF (Mean ± SEM)	R_PD (Mean ± SEM)
APPYFP; APPYFP	↓↓↓	↓↓	→	→
APPYFP; APP695	↓↓↓	↓↓↓	↑↑↑	↑↑↑
GENKHC; GENKLC	↓↓↓	↓↓↓	→	→
APPYFP; APP695; (dhc64c$^{6-19}$/+)	↓↓↓	↓↓↓	→	→
APPYFP; APP695; (rob^{P}/+)	↓↓↓	↓↓↓	↑↑	↑↑↑

Compared to APPYFP; APP695	R_SV (Mean ± SEM)	R_RL (Mean ± SEM)	R_PF (Mean ± SEM)	R_PD (Mean ± SEM)
GENKHC; GENKLC	↓↓↓	↑	↓↓↓	↓↓
APPYFP; APP695; (dhc64c$^{6-19}$/+)	↓↓↓	↑↑↑	↓↓↓	↓↓↓
APPYFP; APP695; (rob^{P}/+)	↓↓↓	↑	↓↓	↓

Genotype	SF (Mean ± SEM)
APPYFP	0.235 ± 0.019
APPYFP; APPYFP	0.086 ± 0.012
APPYFP; APP695	0.195 ± 0.021
GENKHC; GENKLC	0.023 ± 0.010
APPYFP; APP695; (dhc64c$^{6-19}$/+)	0.086 ± 0.016
APPYFP; APP695; (rob^{P}/+)	0.107 ± 0.017

Compared to APPYFP	SF
APPYFP; APPYFP	↓↓↓
APPYFP; APP695	→
GENKHC; GENKLC	↓↓↓
APPYFP; APP695; (dhc64c$^{6-19}$/+)	↓↓↓
APPYFP; APP695; (rob^{P}/+)	↓↓↓

Compared to APPYFP; APP695	SF
GENKHC; GENKLC	↓↓↓
APPYFP; APP695; (dhc64c$^{6-19}$/+)	↓↓↓
APPYFP; APP695; (rob^{P}/+)	↓↓↓

Statistical Significance
↓↓↓ / ↑↑↑ = p<0.001
↓↓ / ↑↑ = p<0.01
↓ / ↑ = p<0.05
→ = p>0.05

Abbreviations
A = Anterograde
R = Retrograde
SV = Segmental Velocity (microns/second)
RL = Run Length (microns)
PF = Pause Frequency (pause number/time)
PD = Pause Duration (seconds)
SF = Switch Frequency (switch number/trajectory)

Color scheme
Red = up
Blue = down

References

Bossy-Wetzel, E., R. Schwarzenbacher, et al. (2004). "Molecular pathways to neurodegeneration." Nat Med **10 Suppl**: S2-9.

Gindhart, J. G., Jr., C. J. Desai, et al. (1998). "Kinesin light chains are essential for axonal transport in Drosophila." J Cell Biol **141**(2): 443-54.

Gunawardena, S. and L. S. Goldstein (2001). "Disruption of axonal transport and neuronal viability by amyloid precursor protein mutations in Drosophila." Neuron **32**(3): 389-401.

Kamal, A., G. B. Stokin, et al. (2000). "Axonal transport of amyloid precursor protein is mediated by direct binding to the kinesin light chain subunit of kinesin-I." Neuron **28**(2): 449-59.

LaMonte, B. H., K. E. Wallace, et al. (2002). "Disruption of dynein/dynactin inhibits axonal transport in motor neurons causing late-onset progressive degeneration." Neuron **34**(5): 715-27.

Puls, I., C. Jonnakuty, et al. (2003). "Mutant dynactin in motor neuron disease." Nat Genet **33**(4): 455-6.

Reid, E., M. Kloos, et al. (2002). "A kinesin heavy chain (KIF5A) mutation in hereditary spastic paraplegia (SPG10)." Am J Hum Genet **71**(5): 1189-94.

Saxton, W. M., J. Hicks, et al. (1991). "Kinesin heavy chain is essential for viability and neuromuscular functions in Drosophila, but mutants show no defects in mitosis." Cell **64**(6): 1093-102.

Stokin, G. B., C. Lillo, et al. (2005). "Axonopathy and transport deficits early in the pathogenesis of Alzheimer's disease." Science **307**(5713): 1282-8.